Spring 2019

Amplitude-preserved processing of the Blackfoot 10 Hz seismic data

Bader Mohammed A Algarni

Department:

AMPLITUDE-PRESERVED PROCESSING OF THE BLACKFOOT 10 HZ SEISMIC DATA

by

BADER MOHAMMED A ALGARNI

A THESIS

Presented to the Faculty of the Graduate School of the

MISSOURI UNIVERSITY OF SCIENCE AND TECHNOLOGY

In Partial Fulfillment of the Requirements for the Degree

MASTER OF SCIENCE

IN

GEOLOGY AND GEOPHYSICS

2019

Approved by:

Dr. Kelly Liu, Advisor

Dr. Stephen Gao

Dr. Neil Anderson

ABSTRACT

The broadband 3C-2D seismic survey was acquired in the Blackfoot Field in southern Alberta. The single-component 10 Hz geophone data were reprocessed to increase vertical resolution and provide a better seismic image of the incised valley channel fill deposits in the Glauconitic Formation. The amplitude-preserved seismic processing of the data was followed by the Kirchhoff prestack time migration. The processing parameters and algorithms used were based on parameter optimization approach. Elevation statics and surface consistent residual statics were utilized to remove near surface delays in the data. Seismic noise, such as ground roll and air blast, were attenuated effectively by various algorithms. Amplitude and phase distortions due to near surface conditions were corrected by processing of the surface consistent deconvolution and amplitude balancing. The Kirchhoff prestack time migration was applied to the data to obtain a migrated section that adequately characterizes the subsurface structure. The final stacked seismic section shows a better image of the incised valley of the Glauconitic Formation than the legacy seismic section. Log data from Well 14-09 were utilized to generate synthetic seismogram, establish seismic-to-well tying, and interpret key seismic horizons.

ACKNOWLEDGMENTS

I would like to express my very great appreciation to Dr. Kelly Liu for her continuous support, guidance, and motivation throughout this research. I would also like to extend my appreciation to the rest of my thesis committee: Dr. Stephen Gao and Dr. Neil Anderson, for their insightful comments and encouragement.

I am very grateful to my sponsor, Saudi Aramco, for giving me this opportunity to pursue my graduate studies in the geology and geophysics program at Missouri University of Science and Technology.

The Paradigm Echos system was utilized for the seismic processing in this study, and the IHS Markit Kingdom was used for seismic interpretation. I thank both Paradigm and IHS Markit for their generous donations.

I am thankful to my family for their endless support and inspiration. Thank you to my parents and to my brothers and sisters for supporting me in all my life.

TABLE OF CONTENTS

Page

LIST OF ILLUSTRATIONS

Page

LIST OF TABLES

Page

NOMENCLATURE

Symbol	Description
3C	Three-component
2D	Two-dimensional
CREWES	Consortium for Research in Elastic Wave Exploration Seismology
CMP	Common midpoint
MMbbls	Million barrels
BCF	Billion cubic feet
AGC	Automatic gain control
dB	Decibel
NMO	Normal moveout
AVO	Amplitude versus offset
SEG	Society of Exploration Geophysicists
RMS	Root-mean-square
TWT	Two way traveltime
RMS	Root-mean-square
CVS	Constant velocity stack
FVS	Function velocity stack

1. INTRODUCTION

The broadband 3C-2D seismic datasets utilized in this research were acquired in the summer of 1995 by the Consortium for Research in Elastic Wave Exploration Seismology (CREWES) in the Blackfoot Field in southern Alberta. The survey area is positioned 15 km southeast of Strathmore, which is situated east of Calgary (Figure 1.1). Encana Petroleum Ltd. owns and develops the Blackfoot Field (Lu and Maier, 2009).

The main objectives of the project were to 1) examine and analyze the application of 3C geophones in broadband seismic exploration, 2) acquire broadband seismic data from 0.5 Hz to 100 Hz, 3) compare the arrays of vertical geophones with the 10 Hz strings, and 4) seismically differentiate between sand and shale lithology at the target zone.

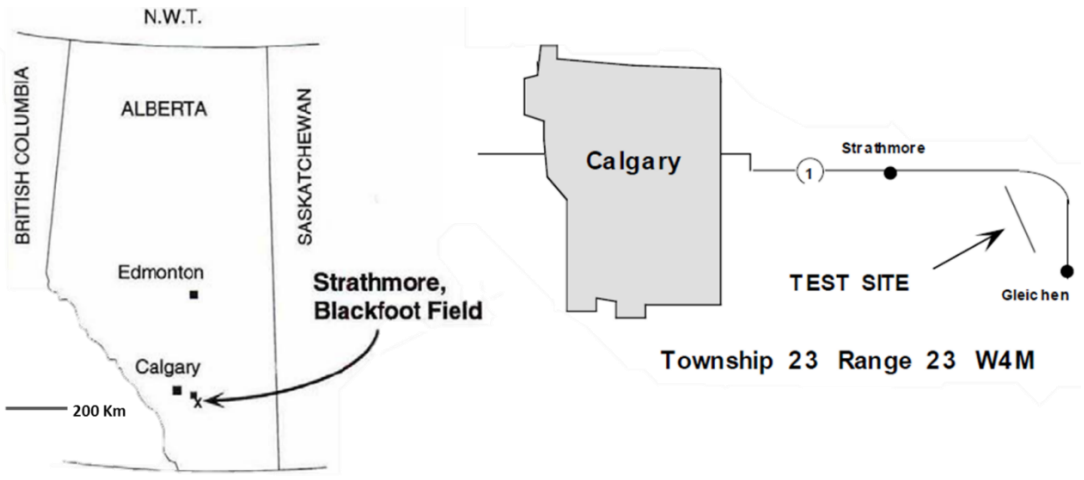

Figure 1.1. Map showing the location of the study area (Gallant et al., 1995).

The survey was acquired using four different geophones which include 3C 2 Hz, 3C 4.5 Hz, 3C 10 Hz, and single-component 10 Hz, resulting in four lines of 2D vertical and 3C seismic datasets. Each seismic profile is deployed one meter apart from the others. The total length of the profile is about 4 km with SSE-NNW orientation. Each line has a total of 200 receiver and shot stations with a 20 m spacing interval. The seismic shooting was carried out using 6 kg dynamite for each shot buried at a depth of 18 m. The amount of explosive was higher than a typical acquisition in order to broaden the frequency spectrum of the signal. All receiver stations were active for the shots in a fixed receiver spread. The area contains 16 drilled wells, which include both density and sonic logs. Well 14-09 intersects the survey profile at CMP 312, and will be used in the seismic-to-well tying and seismic data interpretation in this study (Figure 1.2).

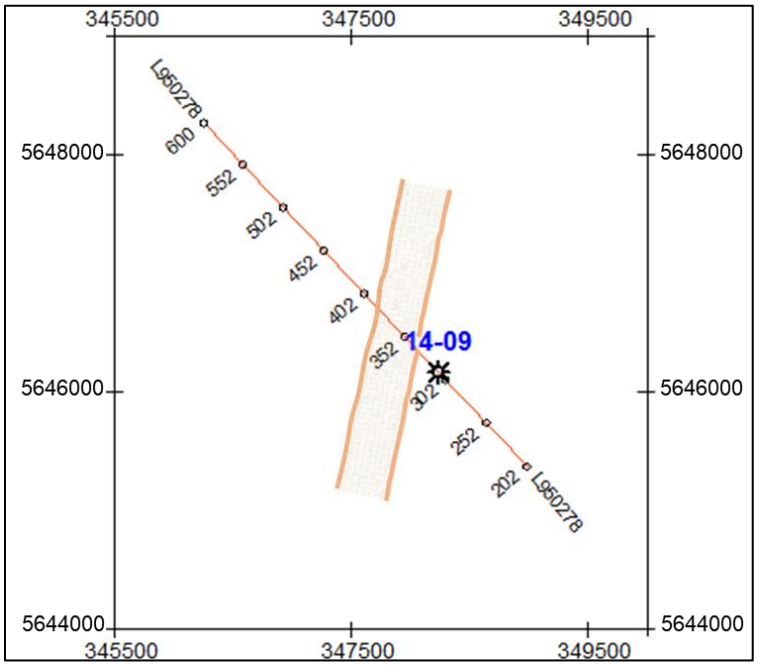

Figure 1.2. Location map of the 2D seismic line 950278 and Well 14-09. The outline indicates the extent of the incised valley.

Previous processing results of the Blackfoot 3C-2D seismic data indicate that the 10 Hz vertical string data has a better imaging of the subsurface than the 3C geophones data (Lu and Maier, 2009). The primary objective of this study is to utilize the most recent processing algorithms to better image the Glauconitic Sandstone of the Lower Cretaceous. The target reservoir at a depth of 1500 m is between 1100 ms and 1200 ms (Stewart, 1995), and is characterized as an incised valley channel fill deposit that truncates underlying regional markers of the Ostracod Formation (Mawdsley et al., 1996) (Figure 1.3). Hence, imaging of the target reservoir is limited by the thickness of the channel and the seismic resolution. Reprocessing of the data in this study focuses on increasing the seismic resolution and enhancing the signal-to-noise ratio for the target formation.

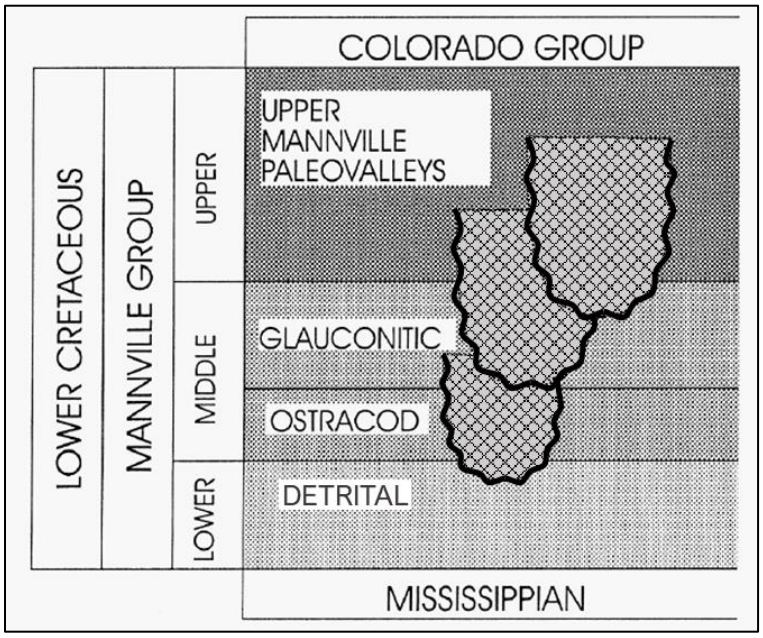

Figure 1.3. Internal stratigraphy of the Mannville Group in the Blackfoot Field, southern Alberta (Hopkins and Mayer, 2001).

1.1. GEOLOGICAL BACKGROUND

The Blackfoot Field is located in the Alberta Basin, a part of the western Canadian sedimentary basin (Wright et al., 1994). The Alberta Basin extends in a northwest direction and is bounded by the thrust belt of the Rocky Mountain to the west, the Williston Basin to the southeast, and the Precambrian Shield to the northeast (Figure 1.4). The basin consists of Mesozoic and Paleozoic sedimentary rocks that dip westward and unconformably overlay the Precambrian Canadian Shield rocks (Connolly et al., 1990).

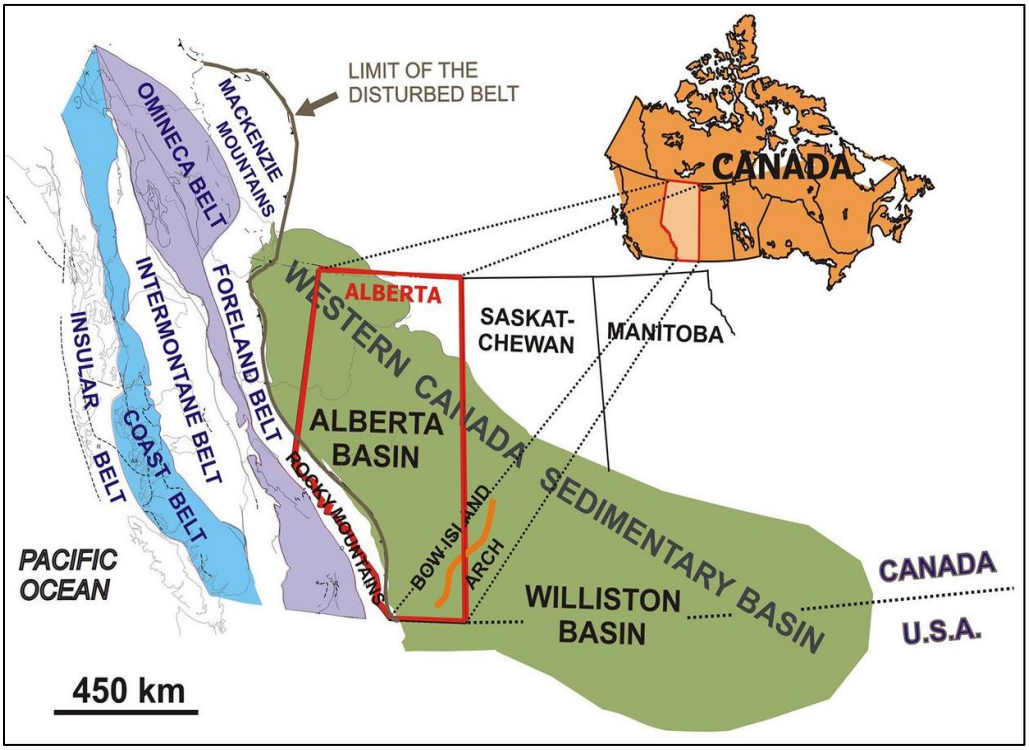

Figure 1.4. Map showing the location of the Alberta Basin (Machel et al., 2012).

The Mannville Group, which is part of the Lower Cretaceous sedimentary rock, is comprised of the Upper, Middle, and Lower Mannville units (Hopkins and Meyer, 2001) (Figure 1.3). The Glauconitic Formation in the area, a part of the Middle Mannville unit, is characterized by high porosity, permeable quartz, and chert-rich sandstone. The formation was deposited during the maximum transgression of the Boreal Sea forming a low-sinuosity incised-valley system (Zailtlin et al., 1995). This incised-valley system has truncated the underlying regional Glauconitic, Ostracod, and Detrital Formations (Dufour et al., 2002).

The Glauconitic Sandstone contains productive reservoirs. The cumulative production in the target zone has reached more than 200 MMbbls of oil and 400 BCF of gas (Miller et al., 1995). The target zone can reach up to 45 m in thickness and is encountered at a depth of 1500 m (Dufour et al., 2002).

1.2. SURVEY ACQUISITION

The Blackfoot 3C-2D survey was conducted using four types of geophones (3C 2 Hz, 3C 4.5 Hz, 3C 10 Hz, and single-component 10 Hz) with dynamite as a source charge. The main objectives of the survey are to differentiate between sand and shale channel fills at the target zone and to compare the geophone ability for recording broadband seismic data.

The seismic profile used in this study was obtained by utilizing six Oyo GS-30CT 10 Hz vertical geophones in each string as a receiver station (Figure 1.5). The spacing of geophones within receiver array is 4 meters. The recorded seismic traces are stacked within each receiver station to suppress ground roll and random noises and attain a better

signal-to-noise ratio. The receiver and shot stations were evenly positioned with 20 m spacing interval. The geophones were attached to planting poles to improve ground coupling (Gallant et al., 1995).

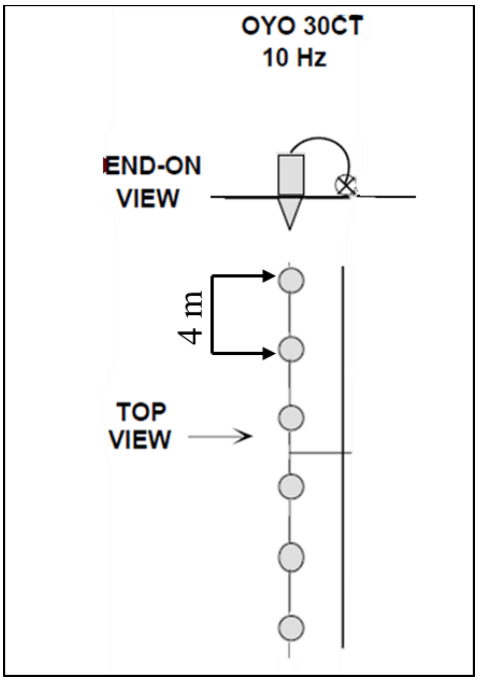

Figure 1.5. Field layout of vertical 10 Hz geophones and cable at each receiver station (Gallant et al., 1995).

The ARAM-24 seismic recording system was used to deliver maximum recording range. The 24-bit dynamic range instrument was necessary to be able to extract the signal given the presence of significant ground roll noise and the single configuration of the 3C geophones (Gallant et al.,1995).

The seismic profile used in this study comprises 200 shot records. In each shot record, all 200 receiver stations were alive and recording. The shooting direction is from

southeast to northwest starting at shot point #101 and ending at shot point #300. The station interval is 20 m for both source and receiver. The maximum offset reaches 3980 m (Table 1.1). The fixed spread of the receiver stations in the survey resulted in a unique fold profile that is equal to one at the edge of the profile and increases towards the middle of the line. The first and last shot records exhibit end-on spread geometries, while shot records in the middle of the profile have symmetrical split-spread geometries. Similarly, the maximum offset varies from 4 km at the edges of the profile to 2 km towards the center.

Table 1.1. The acquisition parameters for the seismic profile used in this study.

Line length	4 km
Source type	Dynamite
Source interval	20 m
Source depth	18 m
Number of shots	200
Receiver type	Oyo GS-30CT 10 Hz
Receiver interval	20 m
Number of receivers	200
Number of channels	200
Recording length	6 s
Maximum Offset	3980 m
Sampling interval	1 ms

1.3. SURVEY CONDITIONS AND DATA QUALITY

The acquisition of the survey was conducted in a rolling steppe area. The seismic profile crosses over several croplands and cattle pastures as well as two small roads with

insignificant traffic. Wind and rain were moderate during the acquisition of the survey, causing most of the recorded noise (Gallant et al., 1995).

Representative field records including first, middle, and last shot gathers from the vertical 10 Hz array seismic profile illustrate the quality of the field recording (Figure 1.6). The raw data exhibit strong-amplitude ground roll noise with distinctive dispersion patterns. At near offsets, the seismic traces are contaminated by source generated noise that masks seismic reflections. In addition, 60 Hz noise, DC component noise, and ambient noise are present. Automatic Gain Control (AGC) was applied as a display function on raw data of the same field records to reveal obscure seismic amplitudes at later arrival times (Figure 1.7). The seismic reflections are displayed clearly on the resulting shot gathers.

The spectral analysis of shot gathers 105, 198, and 262 provides a preliminary evaluation of the frequency content of the signal (Figure 1.8). The frequency bandwidth extends from 5 Hz to approximately 75 Hz at a given threshold of -20 dB. The seismic data have a dominant frequency of 20 Hz and a roll-off trend of -10 dB per octave at higher frequencies. Furthermore, a slight increase in the amplitude values is detected below the geophone natural frequency of 10 Hz.

The processing of the seismic data in this study followed the approach of parameter optimization. First, different processing parameters were applied and analyzed on a selected subset of the prestack data. Subsequently, the same analyses were applied to all of the data to examine the stacked seismic section. The combined analyses of the prestack and poststack domains provided a better assessment for parameter optimization.

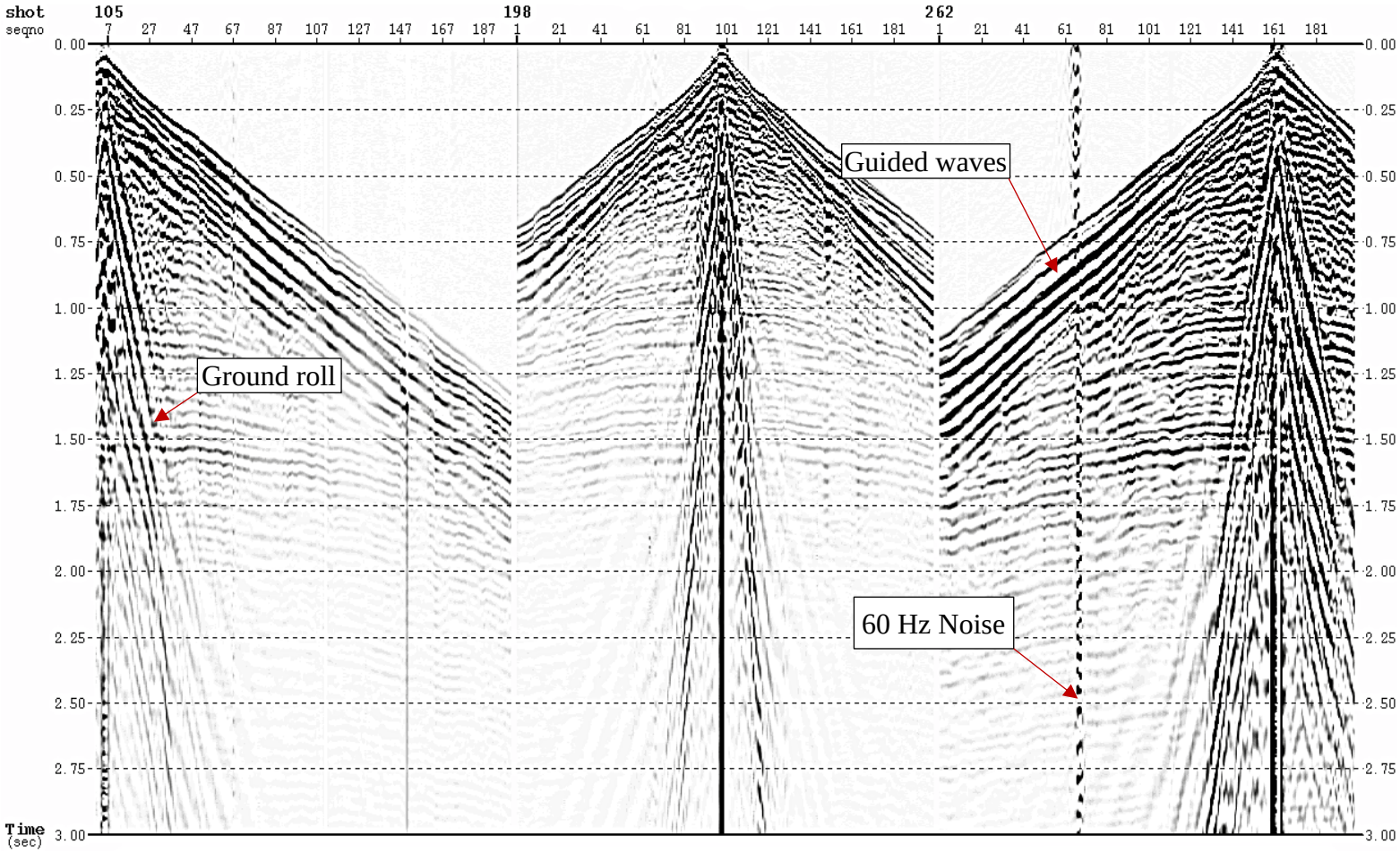

Figure 1.6. Raw seismic data from shot gathers 105, 198, and 262. The strong amplitude ground roll, guided waves, and power line noises are indicated.

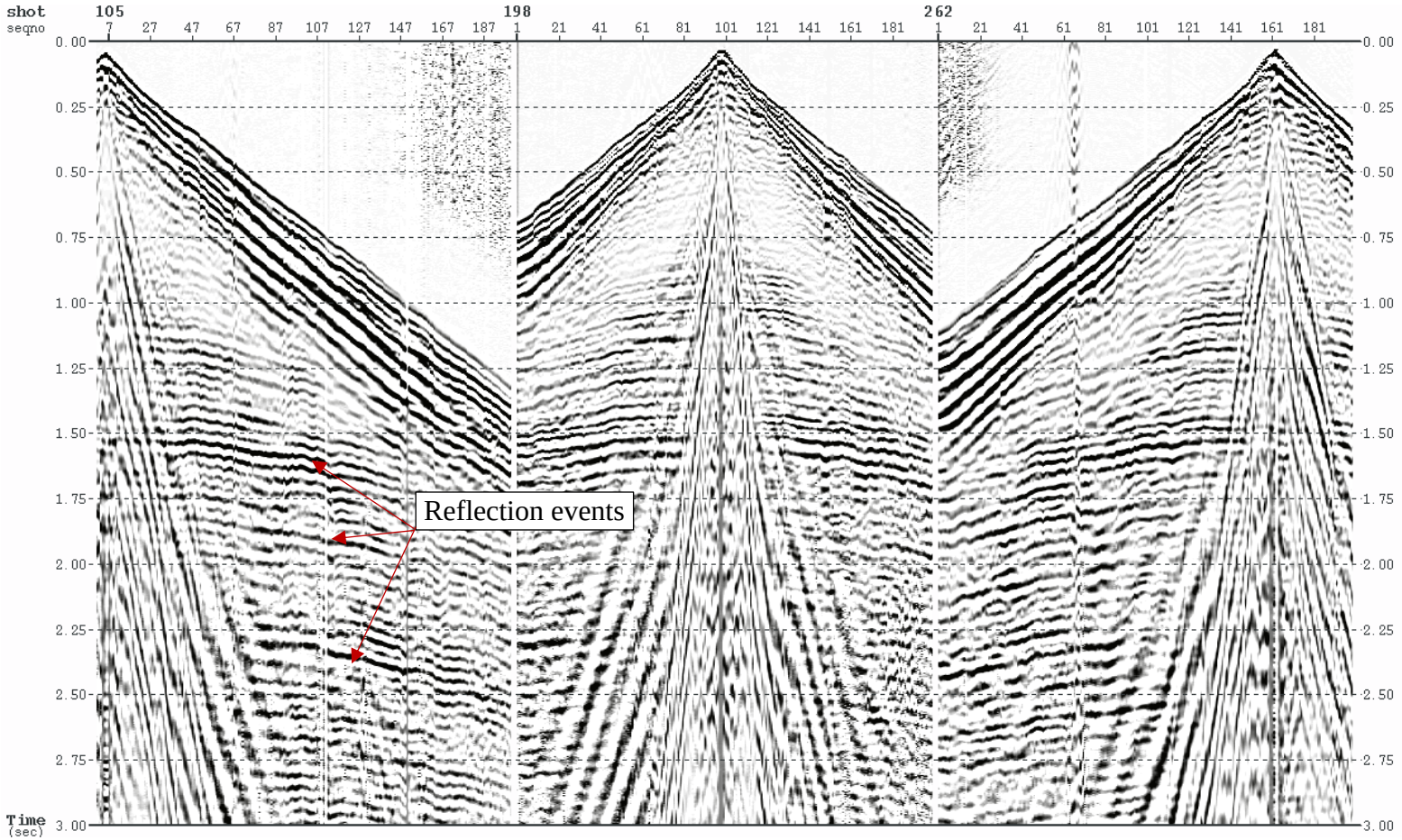

Figure 1.7. Shot gathers 105, 198, and 262 after applying AGC. Seismic reflection events are observable after the AGC processing.

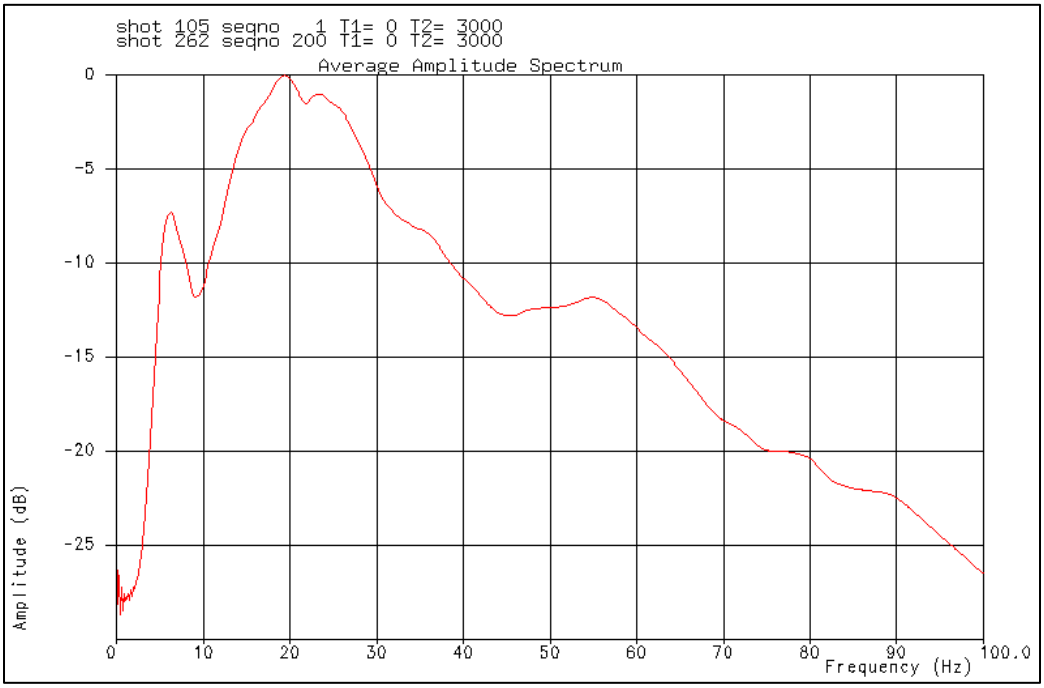

Figure 1.8. The average amplitude spectrum of shots 105, 198, and 262.

1.4. OBJECTIVES

The single-component 10 Hz geophone is less sensitive to noise than the corresponding 3C geophones and showed a better resolution of the target zone in previous processing (Lu and Maier, 2009). Different types of noise in the data, such as ground roll and source-generated noises, present challenges and require various algorithms to reduce noise. The primary objective of this study is to reprocess the single-component 10 Hz geophone data to increase vertical resolution and provide a better seismic image of the incised valley channel fill of the Glauconitic Formation. The reprocessing of the data implements amplitude-preserved seismic processing followed by prestack time migration. The resulting common image gathers and the computed seismic velocity field provide the foundation for further steps such as AVO analysis, acoustic

impedance prestack inversion, and lithology discrimination. The focus of the reprocessing is targeted at a time interval from 1000 ms to 1500 ms.

Another objective is to utilize the available log data from Well 14-09 to establish seismic-to-well tie by the generation of synthetic seismogram. Seismic interpretations are conducted using the calibrated seismic and well data.

2. METHODOLOGY

The seismic data in this study were processed using Echos, an interactive seismic data processing software provided by Paradigm. Different processing algorithms and parameters were tested and optimized on a selected subset of the prestack data. In addition, these parameters were tested on the entire data to analyze the stacked seismic section. The resulting seismic section from each processing step is considered a byproduct. The combination of prestack and poststack analyses for each processing step is found to be beneficial in optimizing the parameters.

The data were processed using the workflow outlined in Figure 2.1. Ground roll and source-generated noises strongly contaminate the signal at near offsets and introduce a challenge to achieve high signal-to-noise ratios. Different types of noise attenuation algorithms were tested on the data to retain signal in near-offset traces. The surface consistent deconvolution improved temporal resolution by removing the undesirable source and receiver effects and whitening the frequency spectrum. The iterations of velocity analysis and normal moveout (NMO) correction and residual static correction improved the stacking of reflection events. Prestack Kirchhoff migration was applied to the data to obtain a migrated seismic section that adequately characterizes the subsurface structures.

The established workflow in this study aims to preserve relative trace-to-trace amplitudes for further amplitude variations with offset (AVO) analysis, which provides valuable information for lithology discrimination and fluid modeling to differentiate between shale and sand valley-fills in the target reservoir. The noise attenuation applied

to the data was performed with caution to prevent any distortion in the lateral variations of reflection amplitudes and yet improve signal-to-noise ratios.

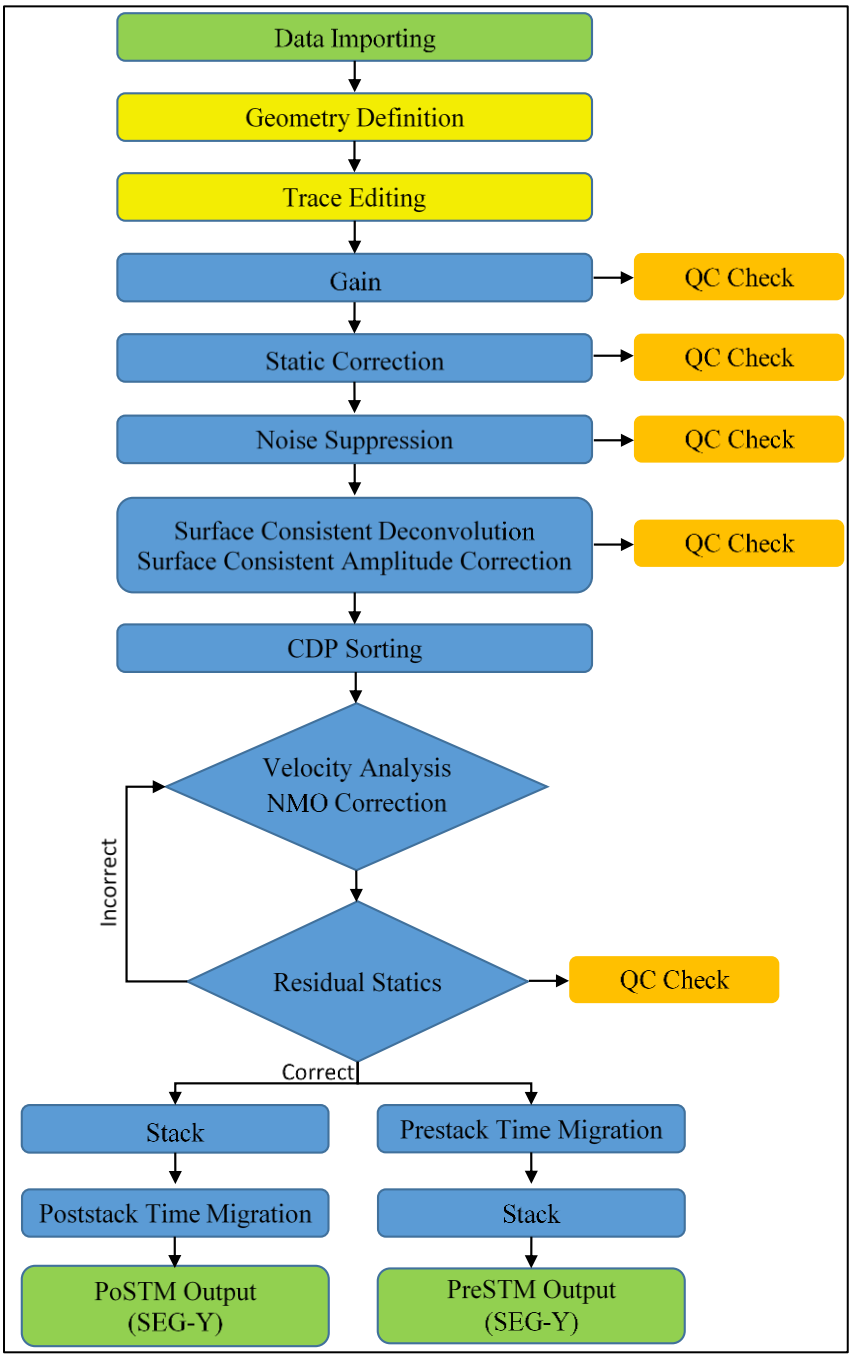

Figure 2.1. 2D seismic data processing workflow used in this study.

2.1. DATA IMPORTING

The data were stored as IBM floating point numbers in a SEGY standard rev. 0 format (Barry et al., 1975). Most of the trace headers follow this standard with few exceptions. For instance, first breaks and station number information adhere to ProMAX standards (Maier et al., 2009). The SEGY text header contains information about non-standard header words. Consequently, the software headers were amended based on the seismic trace headers. The data were converted from SEGY to internal disco format during the loading process.

2.2. GEOMETRY DEFINITION

The survey geometry information was retrieved from the seismic trace headers, which include the coordinates, elevation, and other information of each seismic trace (Figure 2.2). Elevation profiles of source and receiver stations are shown in Figure 2.3. Numerous multi-trace processes such as frequency-wavenumber (F-K) rely on the defined geometry. Hence, geometry information plays a crucial role in the processing of seismic data.

Since the survey was acquired in a fixed receiver layout, the fold coverage is reduced to one at the edges of the seismic profile and increases gradually towards the center to reach the maximum fold of 82. The fixed receiver layout provides a challenge when stacking CMP gathers to obtain a balanced seismic section. For instance, signal-to-noise ratios are reduced laterally towards the edges of the profile due to fewer traces being summed in a single CMP gather.

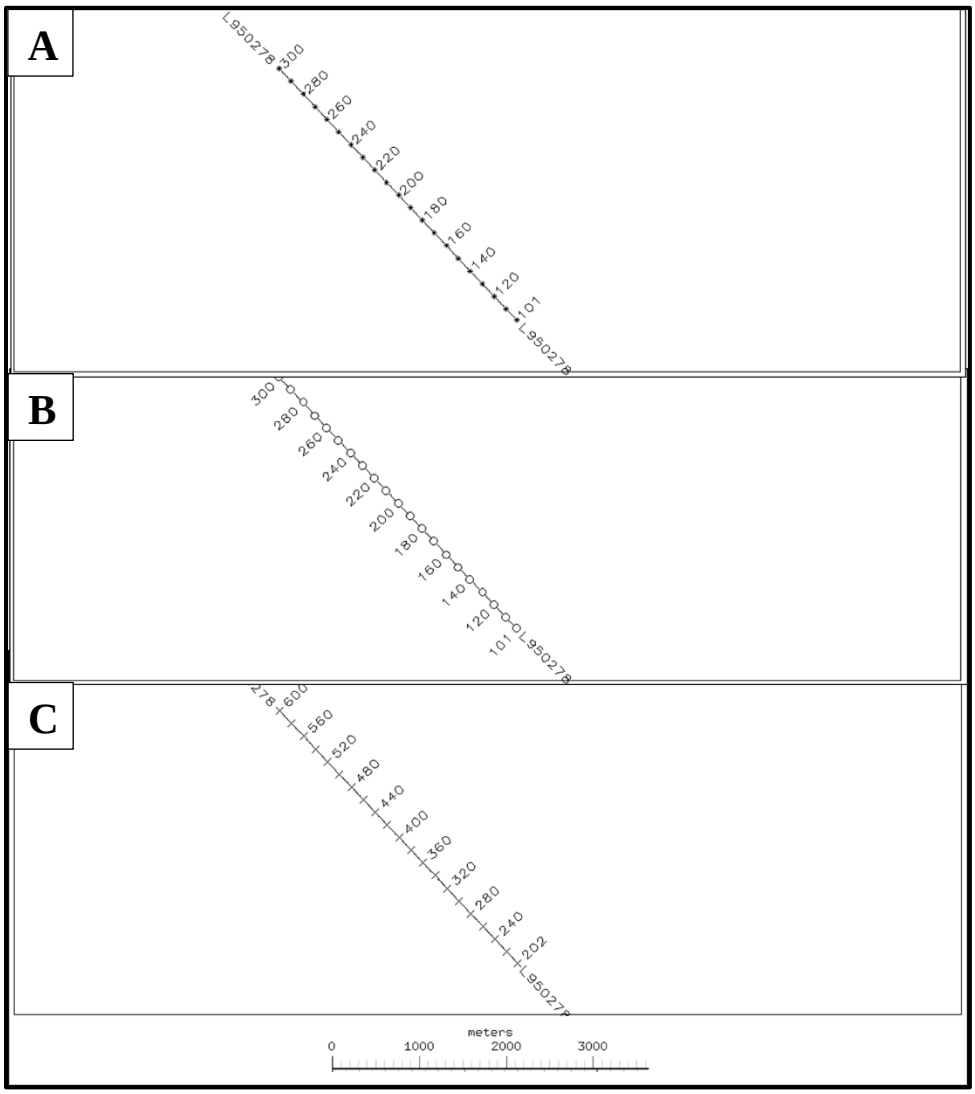

Figure 2.2. Basemap of the survey geometry. A, B, and C are the shot, receiver, and CMP stations, respectively.

The geometry definitions were further validated by examining the offset header of each trace. The horizontal distance from the source to the receiver defines the offset of the seismic trace. Figure 2.4 shows the resulting offset pattern of the traces in selected shot gathers.

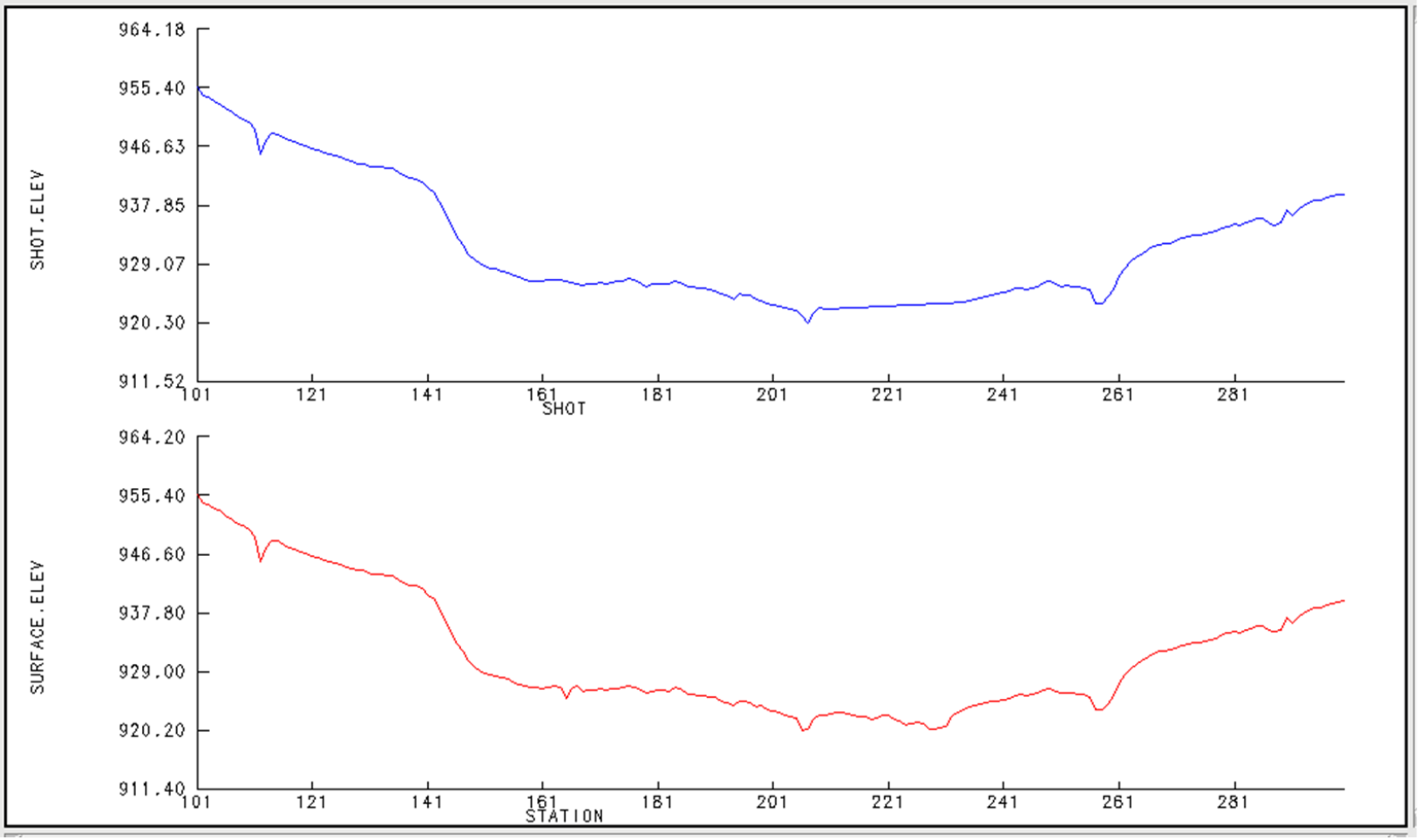

Figure 2.3. Elevation profile of source (top) and receiver (bottom) stations.

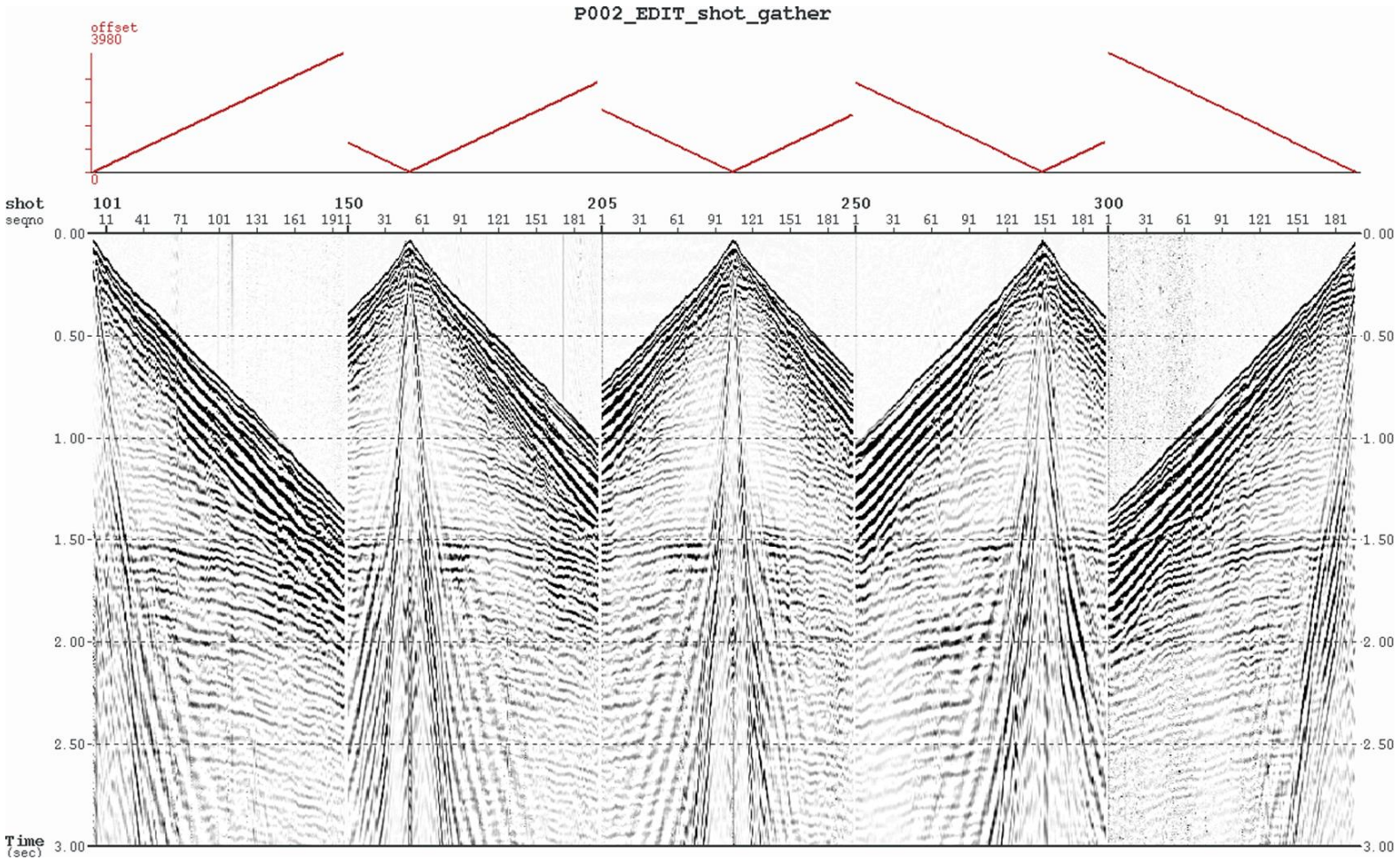

Figure 2.4. Displayed offset header for shot gathers 101, 150, 205, 250, and 300. The offset pattern indicates the source-receiver distance for each trace.

2.3. TRACE EDITING

One of the preprocessing steps of the Blackfoot seismic data is trace editing. Seismic data often include traces that are contaminated by unpredictable high-amplitude noises. These traces degrade seismic data quality and need to be removed before other processing steps such as noise attenuation and residual static correction. The editing process includes omission of test shots, noisy, and dead traces from the data.

The observer logs were used to identify test shots and bad field records. Shots 166, 167, 199, 240, 253, and 288 were skipped during the survey acquisition due to land access restrictions. The first and last three shots were test shots and were removed from the data.

Some noisy traces were not omitted during trace editing stage, such as traces with DC component noise (Figure 2.5). These noisy traces were processed by the noise attenuation algorithms in the next processing step. However, some traces are dominated by unpredictable high-amplitude noise, which overwhelms the stacked section (Figure 2.6). These noise bursts lie in the same frequency bandwidth of the signal. Therefore, frequency filtering of the noise leads to signal loss. Consequently, bad traces dominated by strong noise bursts were omitted.

The manual editing of bad traces can be a time-consuming process and, therefore, an automated trace editing technique was used. The root-mean-square (RMS) amplitude was calculated for each input trace within a specified time gate. The design of the time gate is from 2000 ms to 3000 ms, where reflection amplitudes are considerably weaker than the noise burst amplitudes (Figure 2.6). Then, traces that contain noise bursts were

flagged using an amplitude threshold. Subsequently, flagged traces were omitted from the data (Figure 2.7).

2.4. SPHERICAL DIVERGENCE CORRECTION

Seismic wave field spreads out spherically from a source point which causes the divergence of wavefront and amplitudes decay. Hence, spherical divergence correction is required to restore reflection amplitudes. Geometrical spreading of reflection waves depends mainly on the two-way traveltime (TWT) and the source-receiver distance (Wang et al., 1989). As velocity increases with depth, seismic amplitudes decay further due to the effect of refraction (Newman, 1973). Therefore, offset-dependent spherical divergence correction, defined by (Ursin, 1990), was applied to the data (Figure 2.8). The resulting amplitudes are balanced in the time and offset axes. Reflection amplitudes at later traveltime are restored. Recovered amplitudes from shot gather 205 were examined using gain analysis function in the processing software (Figure 2.9). The obtained gain curves reflect amplitudes recovery of the data.

2.5. FIELD STATIC CORRECTION

Elevation differences of source and receiver stations and variations in weathering thickness and velocity affect the arrival time of seismic reflection waves by introducing irregular time delays (Figure 2.10). These time delays alter reflection alignment within a CMP gather to be out of phase. As a result, the stacking of seismic traces becomes a destructive summing of reflection amplitudes and diminishes the reflection events of the

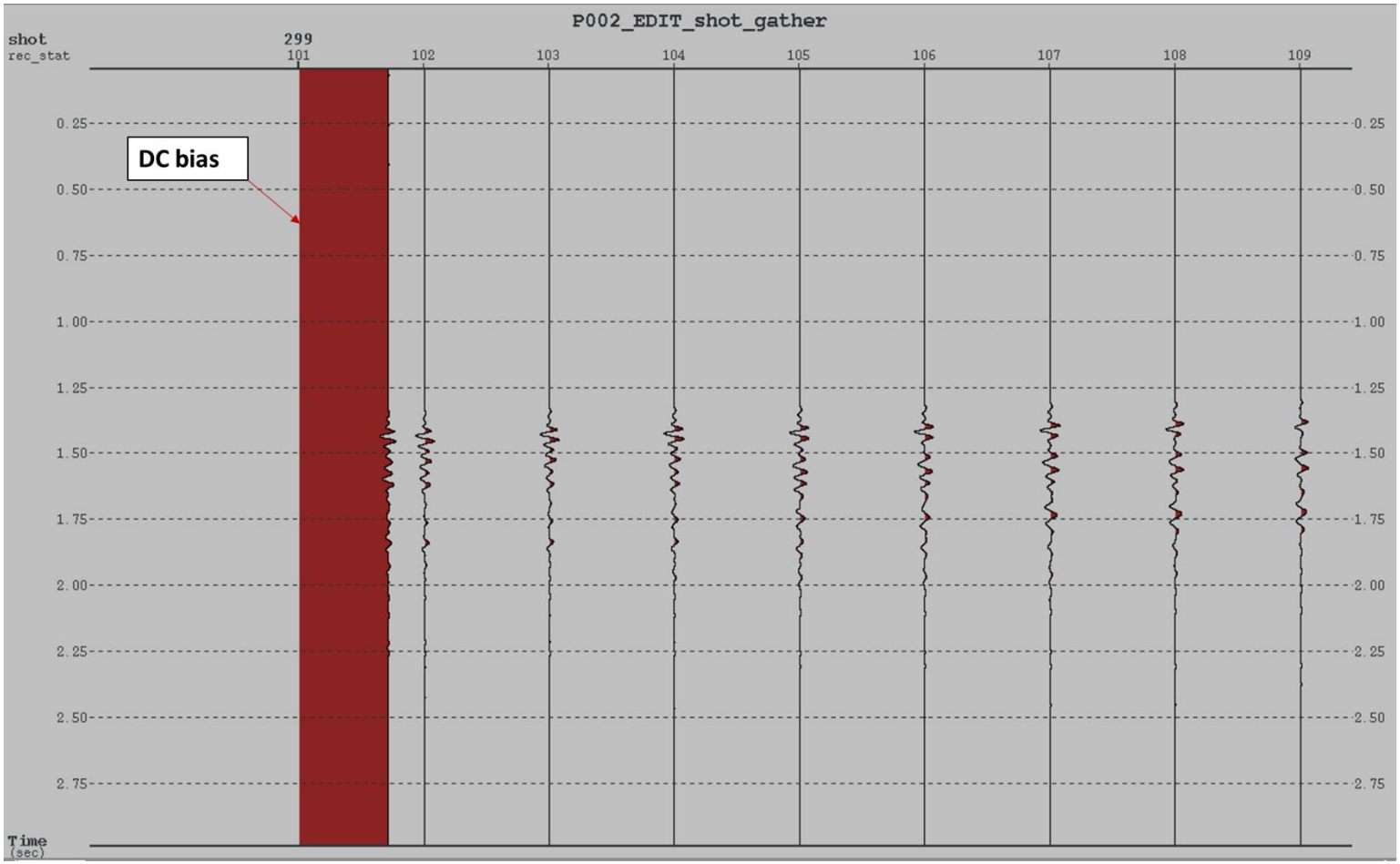

Figure 2.5. Traces dominated by DC component noise in shot gather 299.

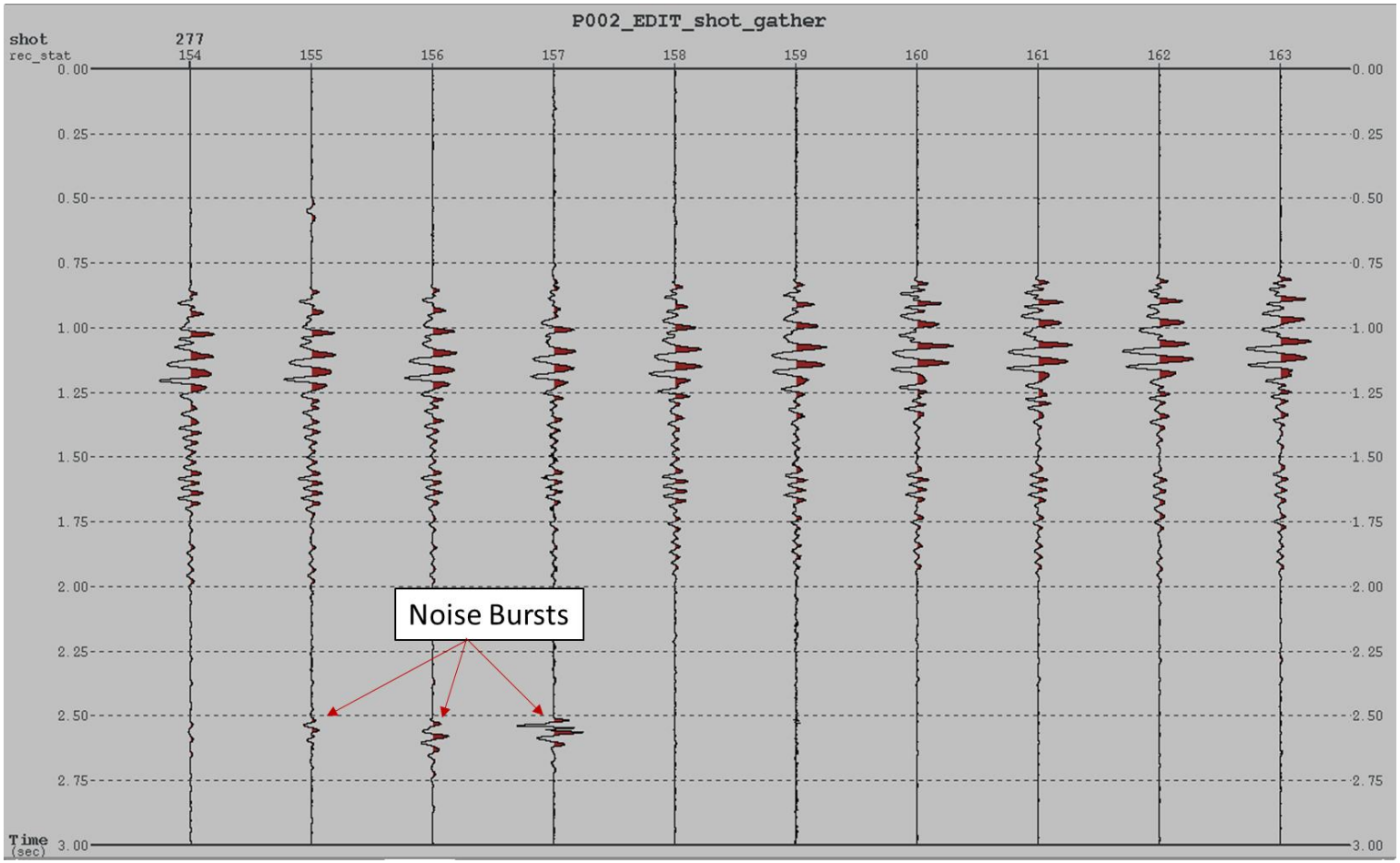

Figure 2.6. Traces contaminated by strong noise bursts from shot gather 277.

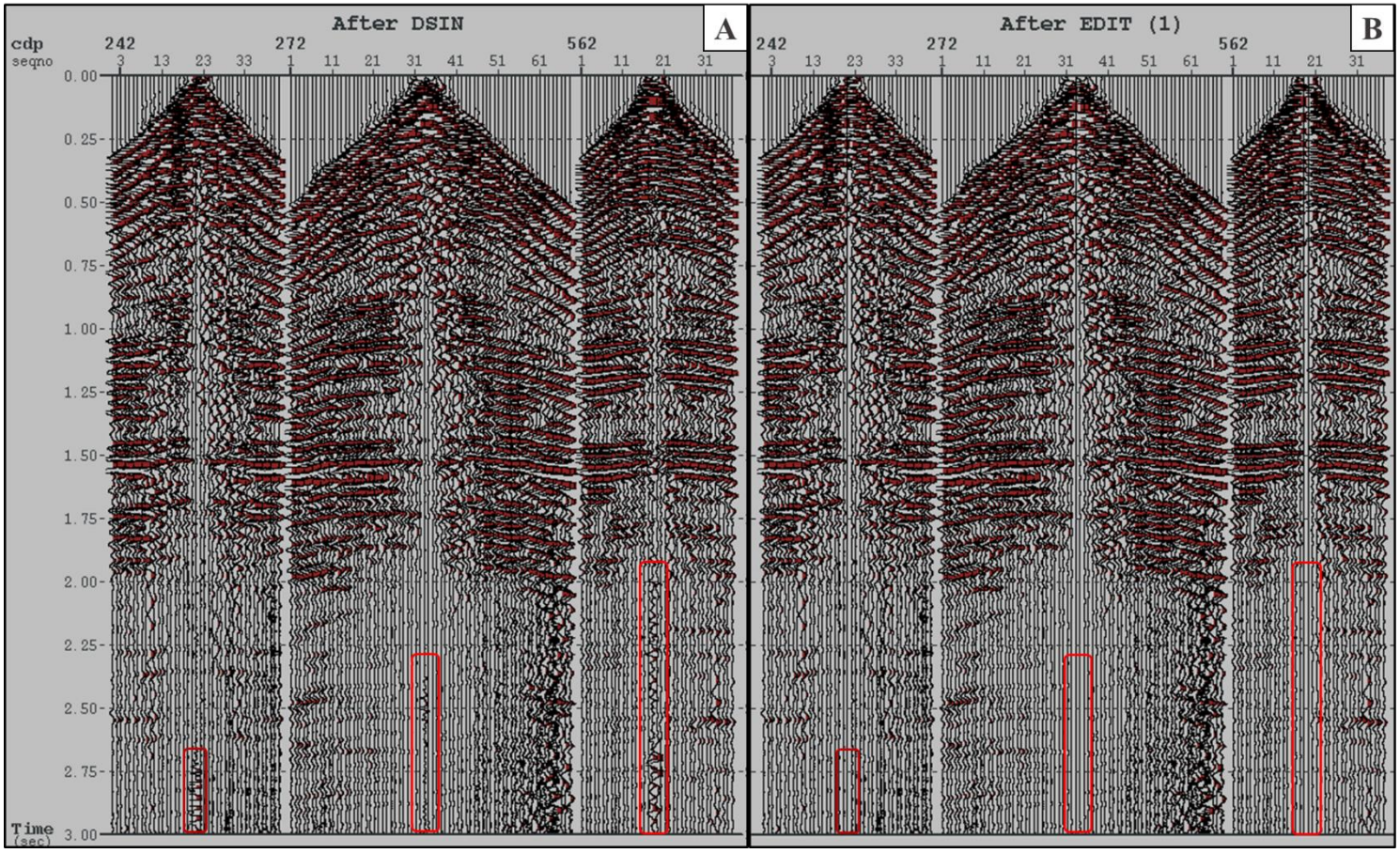

Figure 2.7. CMP gathers 242, 272, and 562. A) Before automatic trace editing. B) After automatic trace editing. The noisy traces were removed.

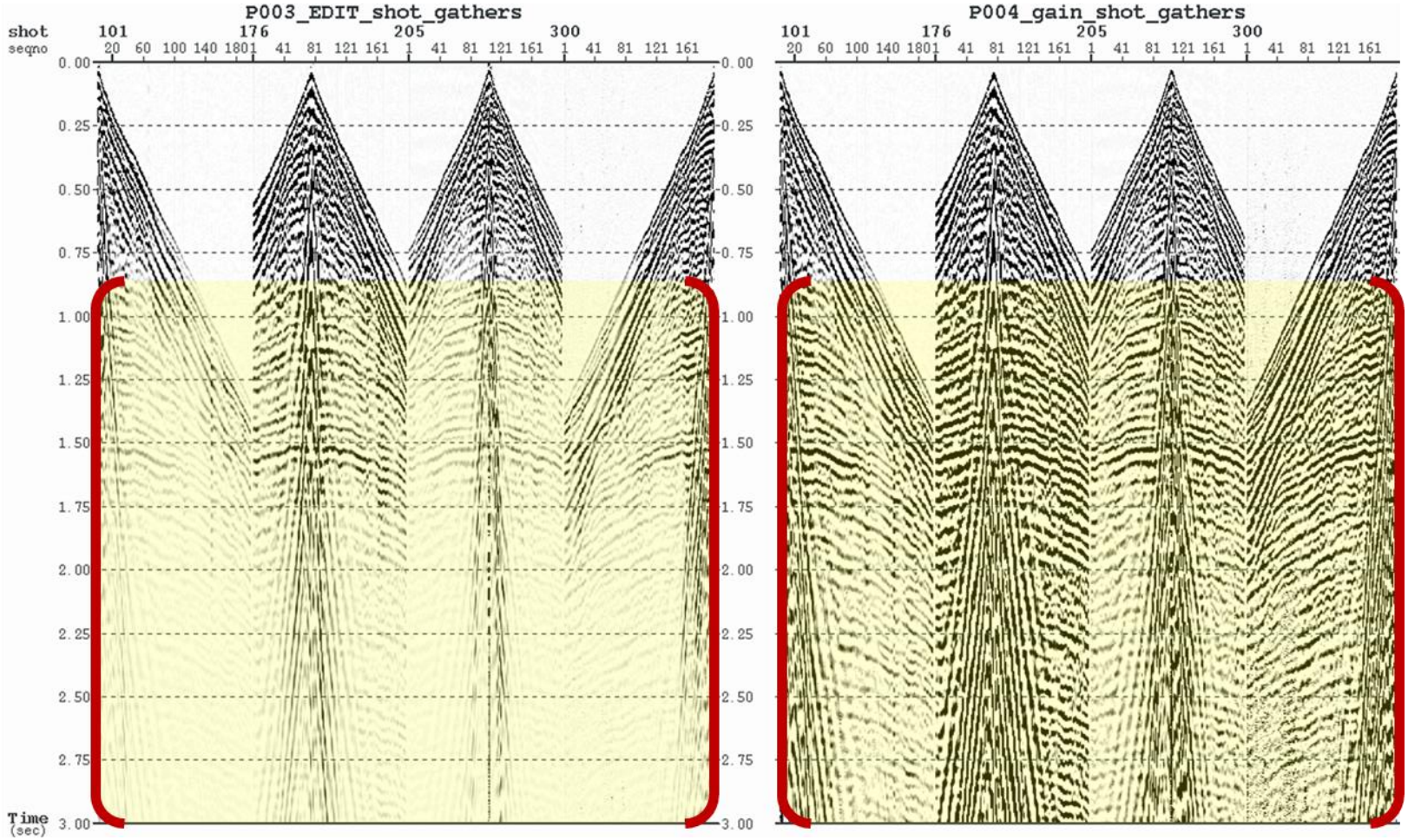

Figure 2.8. Shot gathers 101, 176, 205, and 300. A) Before spherical divergence correction. B) After spherical divergence correction. Decayed amplitudes were restored.

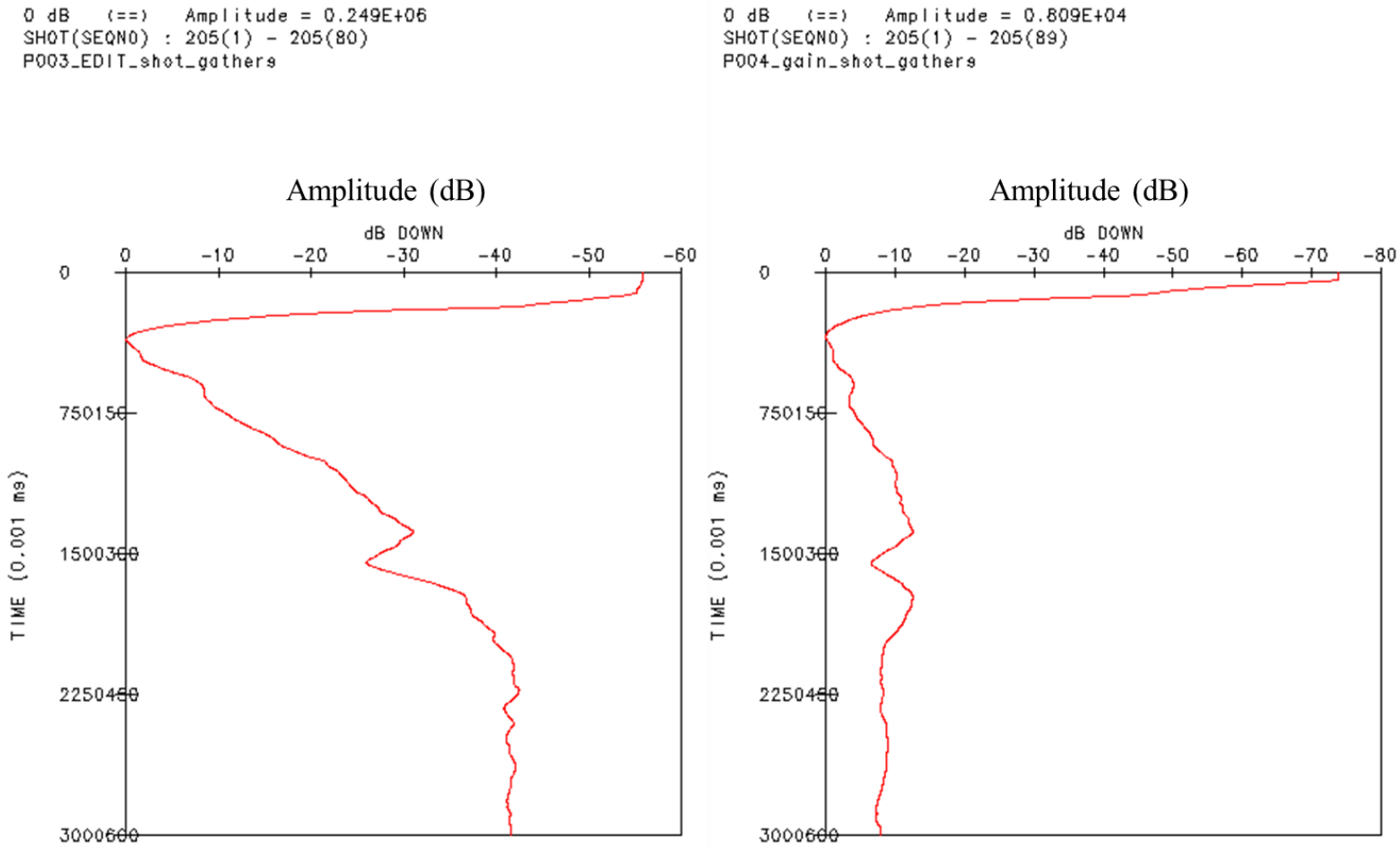

Figure 2.9. Gain analysis of shot gather 205. The RMS amplitudes are displayed in dB. A) Before spherical divergence correction. B) After spherical divergence correction.

produced stacked section. Hence, static corrections are applied to each seismic trace to improve the seismic imaging of the subsurface.

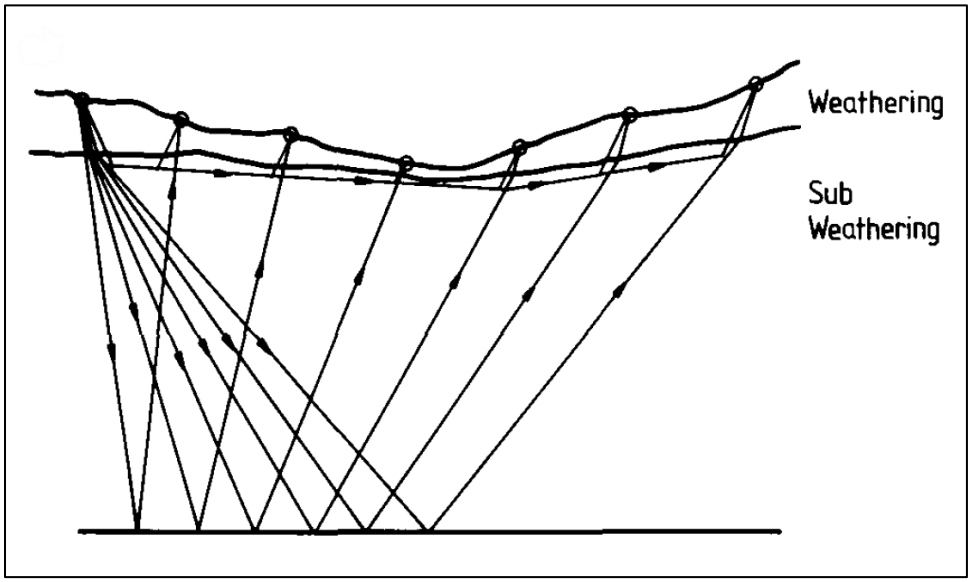

Figure 2.10. Diagram showing the raypath of reflection waves through weathered layer and the bedrock below (Hatherly et al., 1994).

Static corrections consist of elevation correction, i.e., datum statics, which counts for the variations in elevation of the source and receiver stations, and the weathering correction. The elevation correction is given by Equation (1):

$$t_e = \frac{E - E_d}{V_{subW}}, \tag{1}$$

where E and E_d are the station and datum elevations, respectively, and V_{subW} is the subweathering velocity. The datum elevation was set to 900 m above sea level for the processing of this dataset. The refraction velocity moveout application (RVMO) module was used to test a set of refraction velocities on shot gather 101 (Figure 2.11). The

resulting horizontal first arrivals determine the correct subweathering velocity. Due to limited knowledge of the thickness and velocity variations of the weathering zone, the weathering velocity and thickness are assumed to be constant along the seismic profile. The weathering correction was calculated by estimating a 10 m thickness and velocity of 1600 m/s. Figures 2.12 and 2.13 shows the calculated static corrections for source and receiver stations, respectively.

2.6. NOISE SUPPRESSION

Noise attenuation is a key step in the seismic data processing workflow. The data used in this study are contaminated by noises such as guided waves, ground roll, and source-generated noises. The removal of noise is essential for several factors. Processing steps such as deconvolution and prestack time migration algorithms are sensitive to noise. Furthermore, the imaging quality of the subsurface depends on the signal-to-noise ratios, which are significantly reduced by the presence of noise. In addition, future studies, such as AVO inversions and lithology discrimination, rely on effective noise attenuation.

The first step in noise suppression is to analyze noise in the field records. Noise sources are categorized as coherent and incoherent (random) noise (Yilmaz, 2001). Three types of coherent noise are present in the data, which include ground roll, guided waves, and air blast.

Ground roll, i.e., Rayleigh wave, is characterized by high amplitudes, low frequencies, and frequency dispersion. Ground roll noise in the study area is associated with a velocity close to 900 m/s (Figure 2.14). In the F-K domain, ground roll noise is

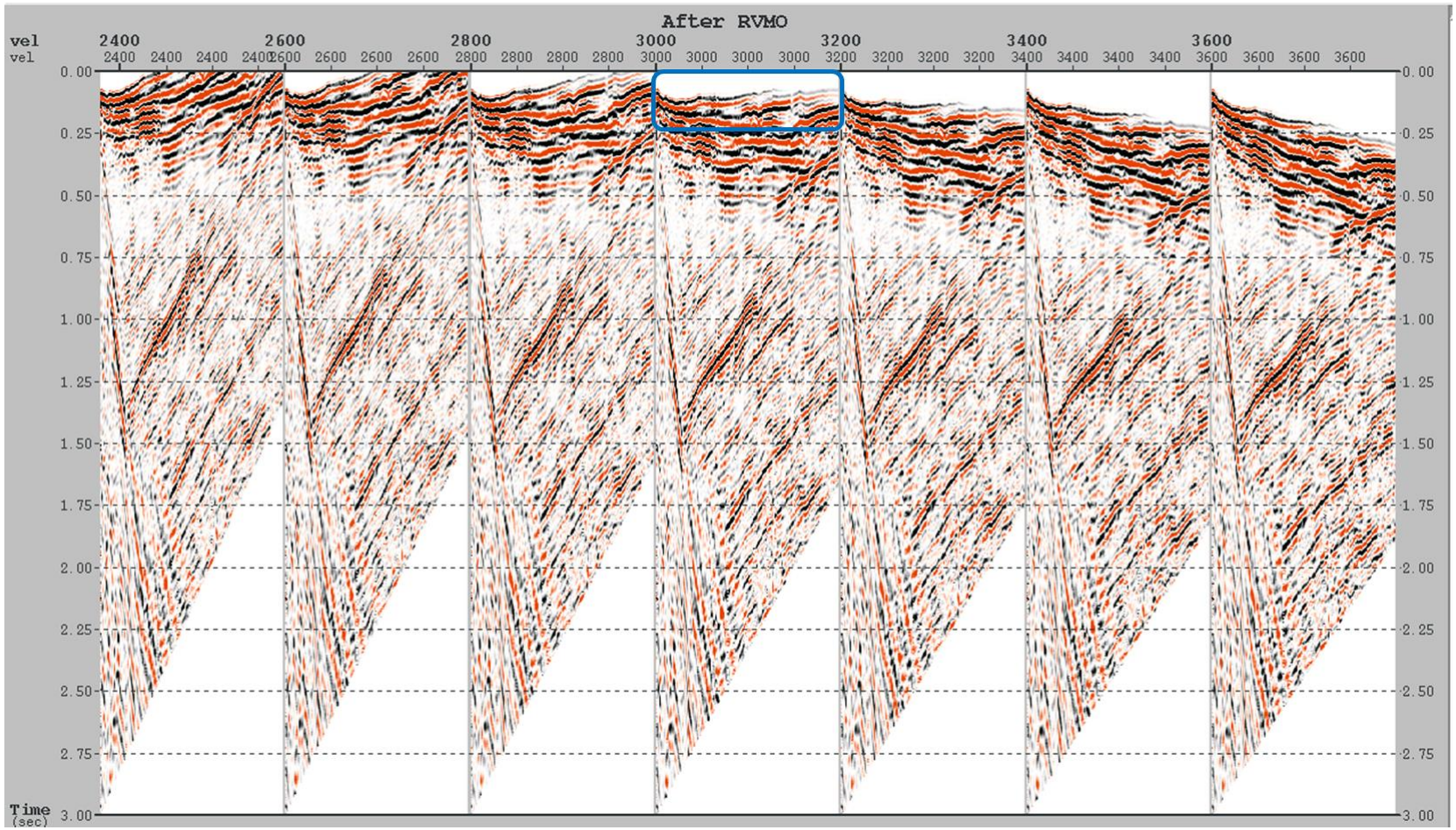

Figure 2.11. Velocity test results for shot gather 101. The direct arrivals are horizontal at a refraction velocity of 3000 m/s.

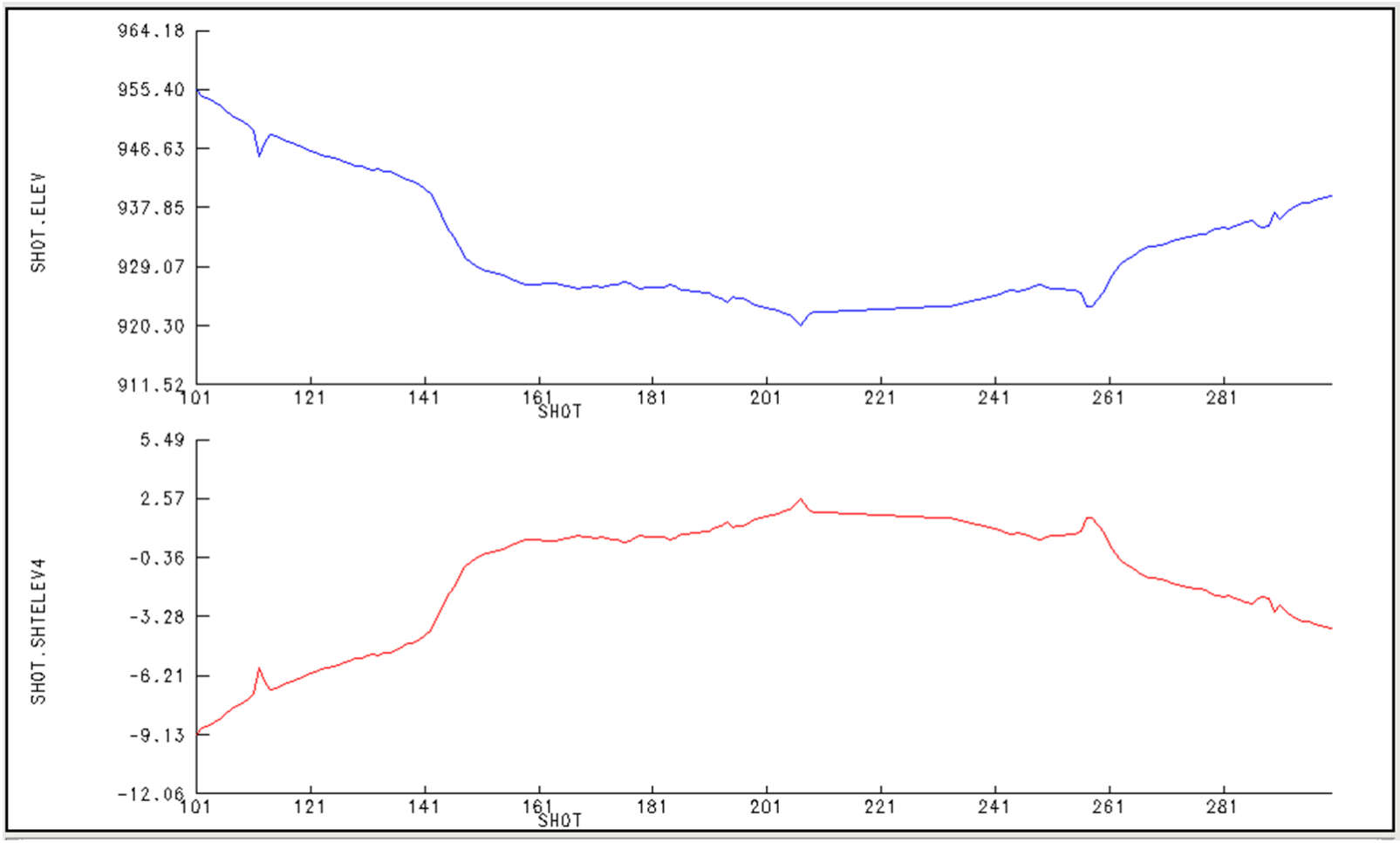

Figure 2.12. Elevation profile (top) and calculated static correction (bottom) for the source stations. Few source stations are associated with positive value statics as they are placed below the seismic datum.

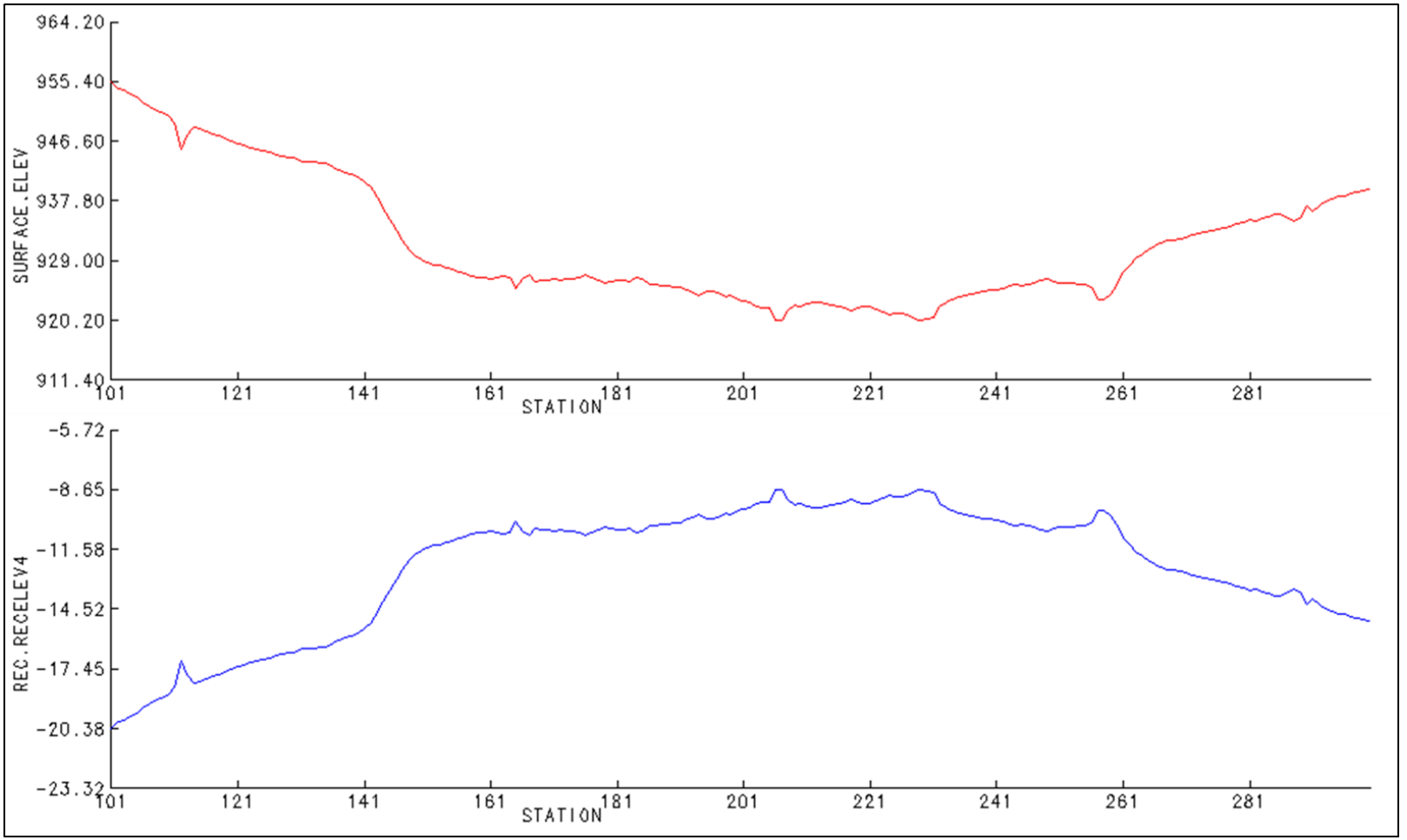

Figure 2.13. Elevation profile (top) and calculated static correction (bottom) for the receiver stations.

separated from seismic reflection events because of its distinctive linear moveout and dispersive character.

Guided waves, which are less frequent in land data than ground roll, propagate horizontally in a low-velocity shallow bed. The first arrivals are dominated by these dispersive waves. In this study, guided waves were removed from the data simply by muting.

Air blast heavily contaminates the near-offset traces and are associated with a low velocity of 340 m/s. Since air blast noise lies in the same frequency range as the signal, frequency bandpass filtering is not effective in removing this type of noise. In order to retain reflection amplitudes, a filter was designed in the F-K domain and applied to the data.

The low frequency array filtering (LFAF) module was used to attenuate ground roll and air blast noise (Oppenheim and Schafer, 1989; Robinson and Treitel, 1980). This filter is designed in the F-K domain by specifying a range of frequencies from 1 Hz to 25 Hz and maximum surface velocity of 1500 m/s. While the LFAF module greatly eliminated ground roll and air blast noise, near-offset traces contain residual noise characterized by low-frequency amplitudes (Figure 2.15). These remaining amplitudes were not filtered due to the lack of separation in the F-K domain between reflection events and linear noise at lower frequencies. Figure 2.16 shows the F-K analysis of the obtained results. Reflection amplitudes in the F-K domain were obscured by the linear noise of guided waves and ground roll before applying LFAF module. Subsequently, the removal of linear noise revealed reflection amplitudes near zero wavenumber.

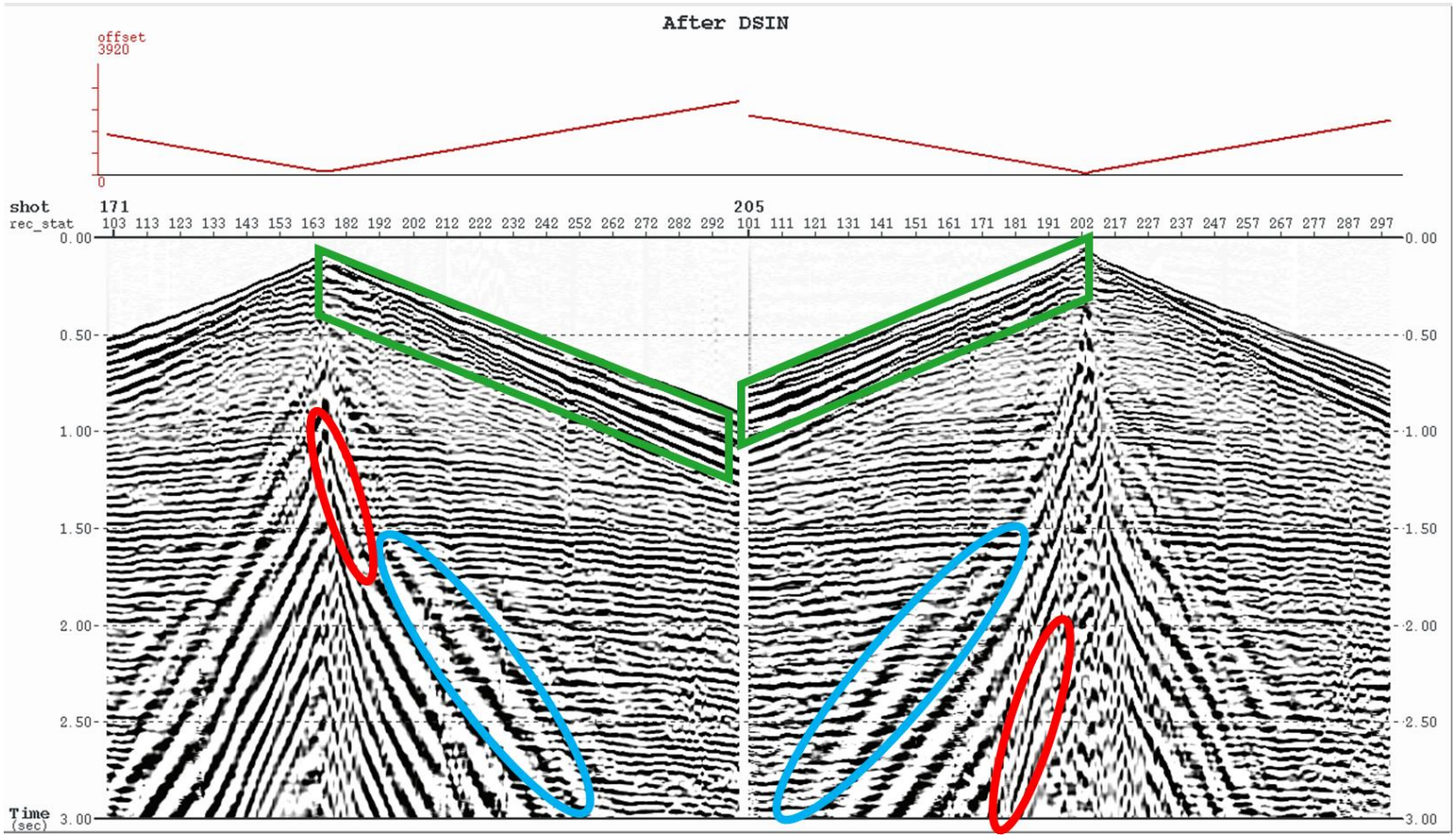

Figure 2.14. Shot gathers 171 and 205 with AGC applied. Guided waves, ground roll, and air blast noises are indicated by the green, blue, and red outlines, respectively.

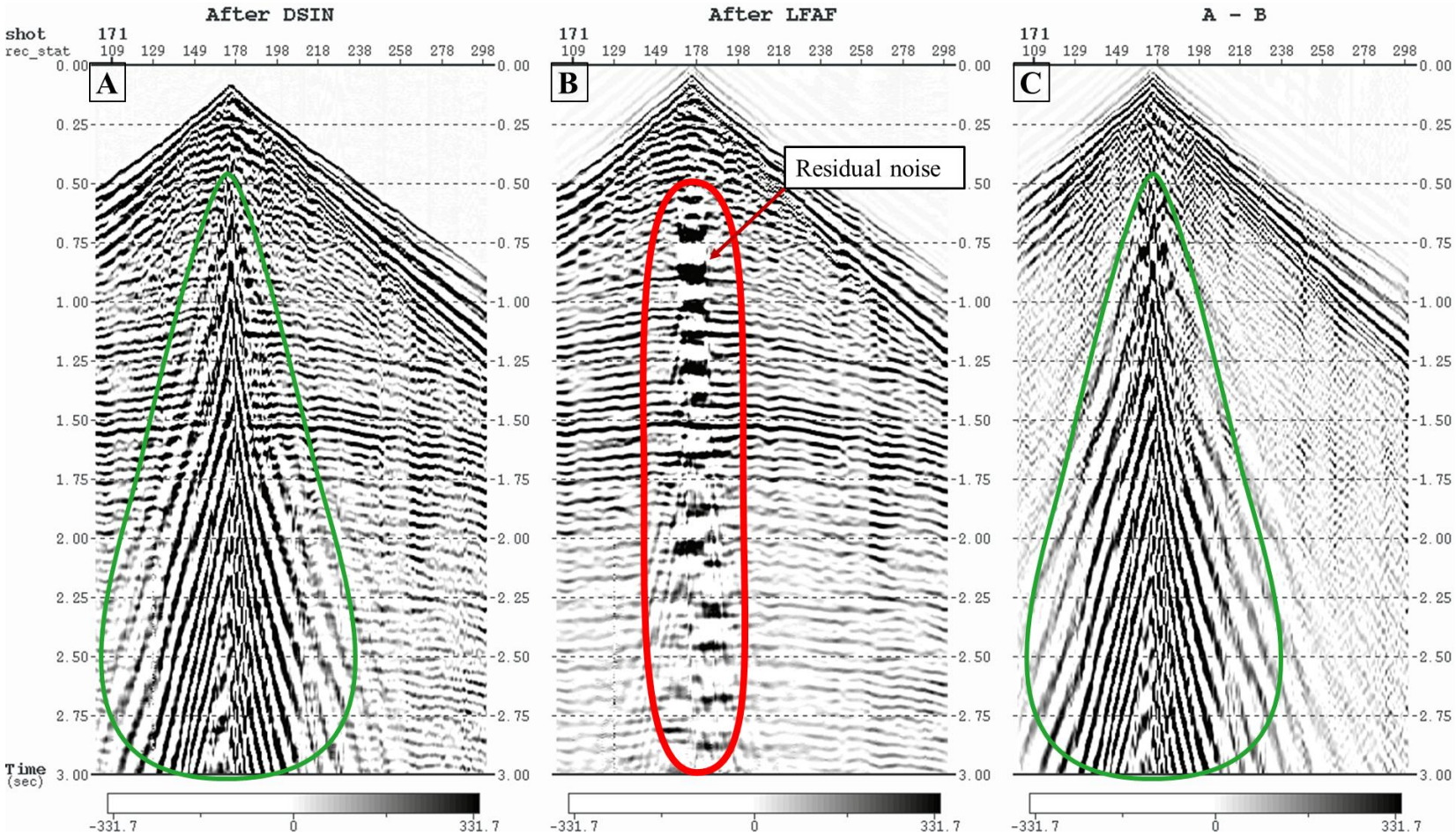

Figure 2.15. Shot gather 171. A) Before LFAF application. B) After LFAF application. C) The difference between A and B. Ground roll and air blast noise were significantly suppressed.

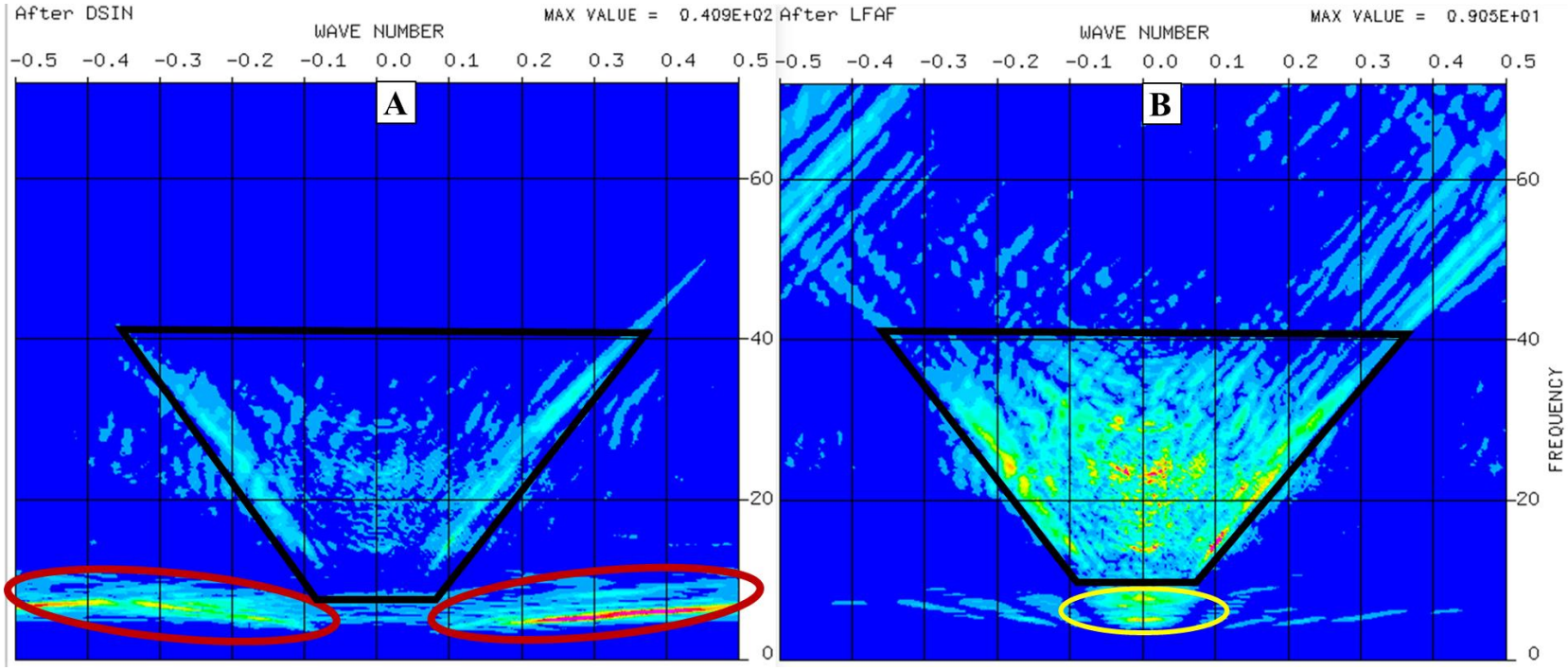

Figure 2.16. F-K analysis of shot gather 171. A) Before LFAF application. B) After LFAF application. Reflection events, ground roll, and residual noise are outlines in black, red, and yellow, respectively.

Bandpass filters operate in the frequency domain by passing only the desired range of frequencies. Hence, seismic noise that has a frequency range different from that of the signal can be filtered by rejecting the amplitudes of those frequencies. A band-pass filter from 10 Hz to 72 Hz was applied to the data (Figure 2.17). By rejecting the amplitudes of frequencies below 10 Hz, the residual low-frequency noise was notably suppressed (Figure 2.18). In addition, noise that is associated with frequencies above 72 Hz was removed from the data. As a result, reflection amplitudes are more visible and, the signal-to-noise ratio has been improved.

The time-frequency noise suppression (TFCLEAN) module was applied to the data to attenuate noise bursts in the seismic records (Goupillaud et al., 1983; Taner et al., 1979). Each seismic shot gather is transformed into the time-frequency domain using fast Fourier transform (FFT). The transformed data are decomposed into different frequency sub-bands. Next, a noise threshold is defined to detect noise bursts, where any amplitude sample above the threshold is scaled to the computed median value and amplitudes below the threshold are passed unaltered. Subsequently, the unchanged phase information and the balanced amplitude information for all frequency bands are combined and transformed into the spacetime domain using inverse FFT. The obtained results from TFCLEAN are shown in Figure 2.19. The difference before and after applying TFCLEAN shows the removed random noise. The coherency of reflection events is improved in the resulting shot gathers.

Various noise attenuation algorithms were tested on the data. Parameters were optimized to attain higher signal-to-noise ratios and remove noise effectively. Guided

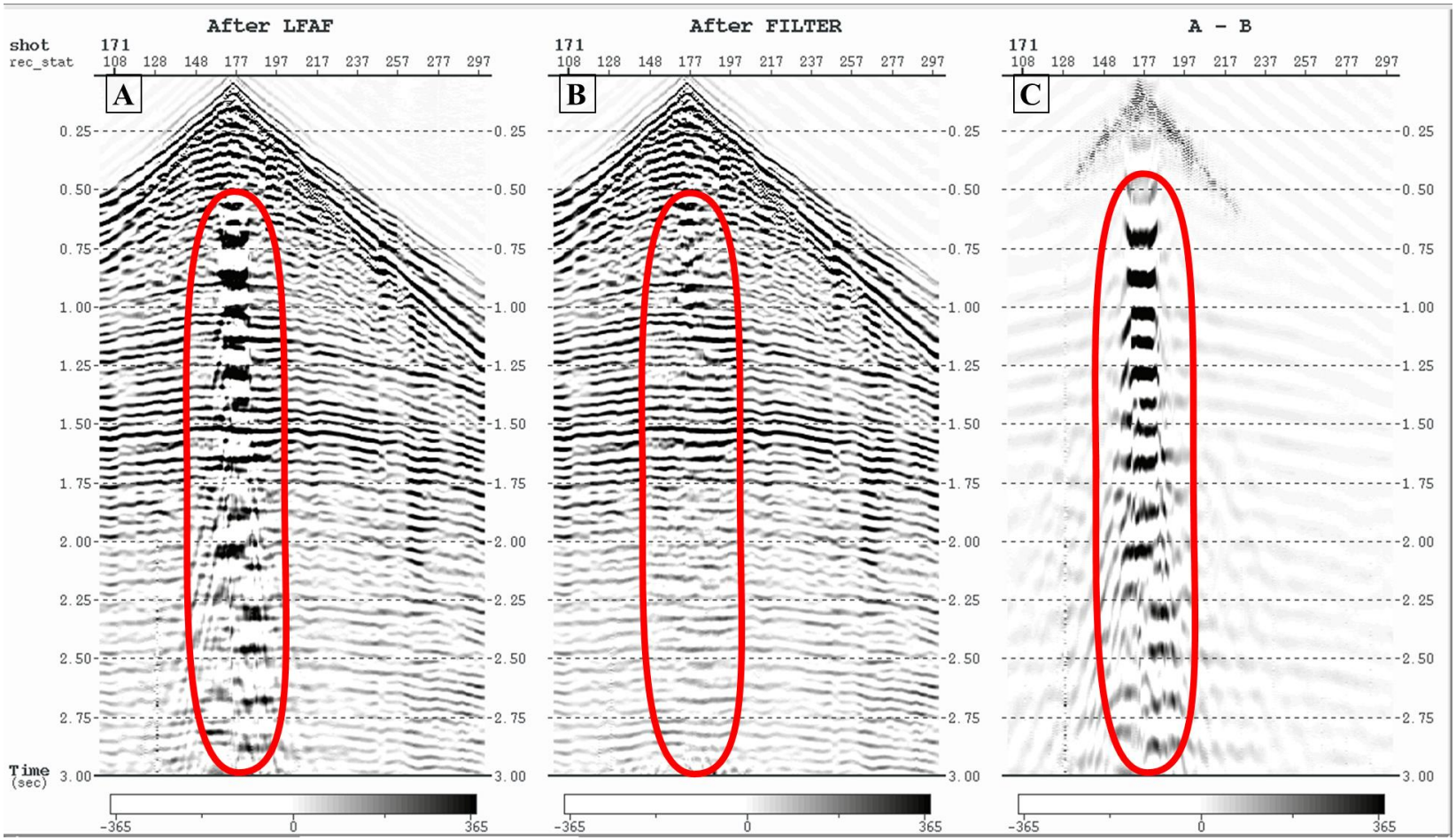

Figure 2.17. Shot gather 171. A) Before band-pass filtering. B) After band-pass filtering. C) The difference between A and B.

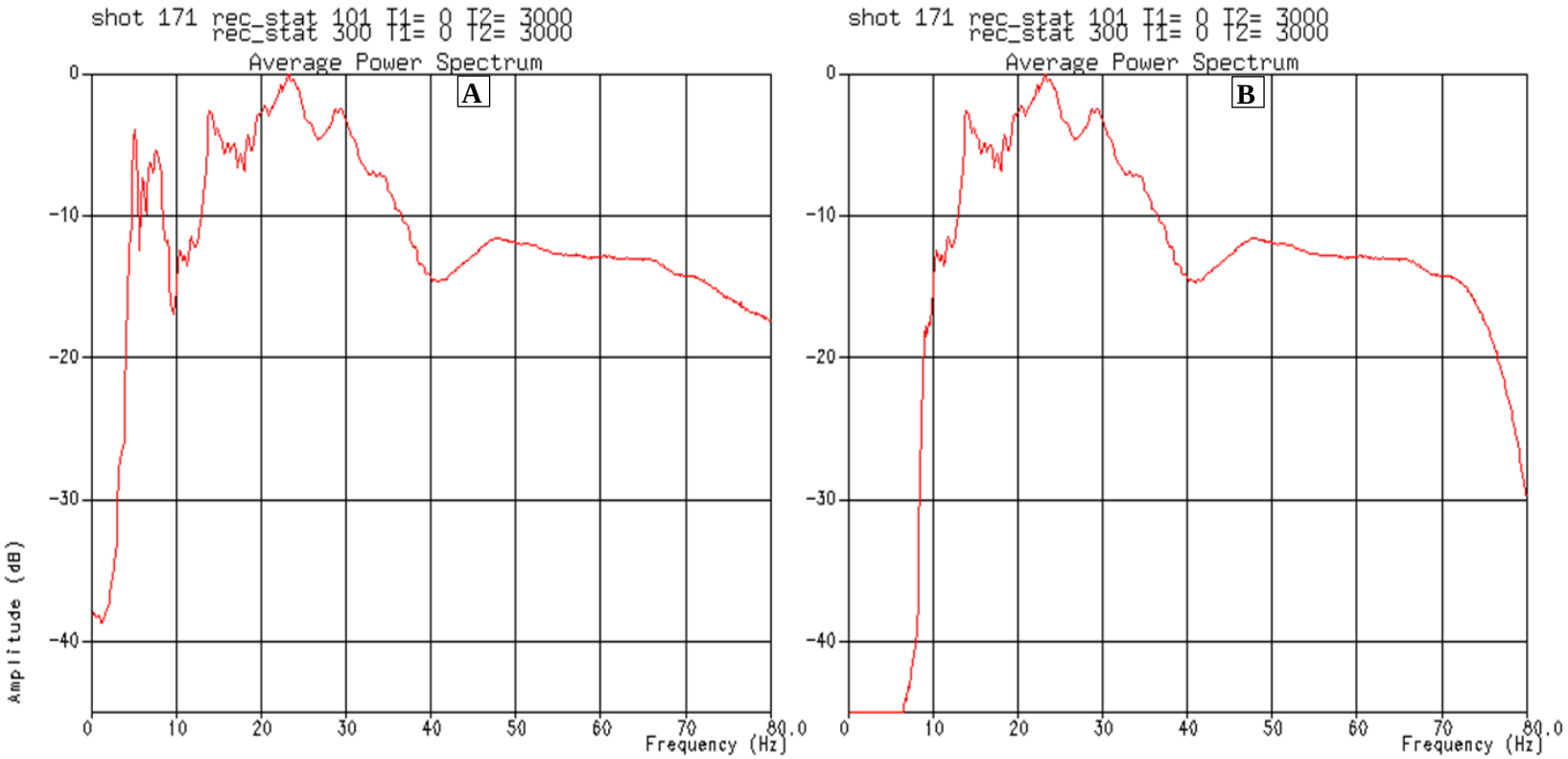

Figure 2.18. The average power spectrum of shot gather 171. A) Before band-pass filtering. B) After band-pass filtering.

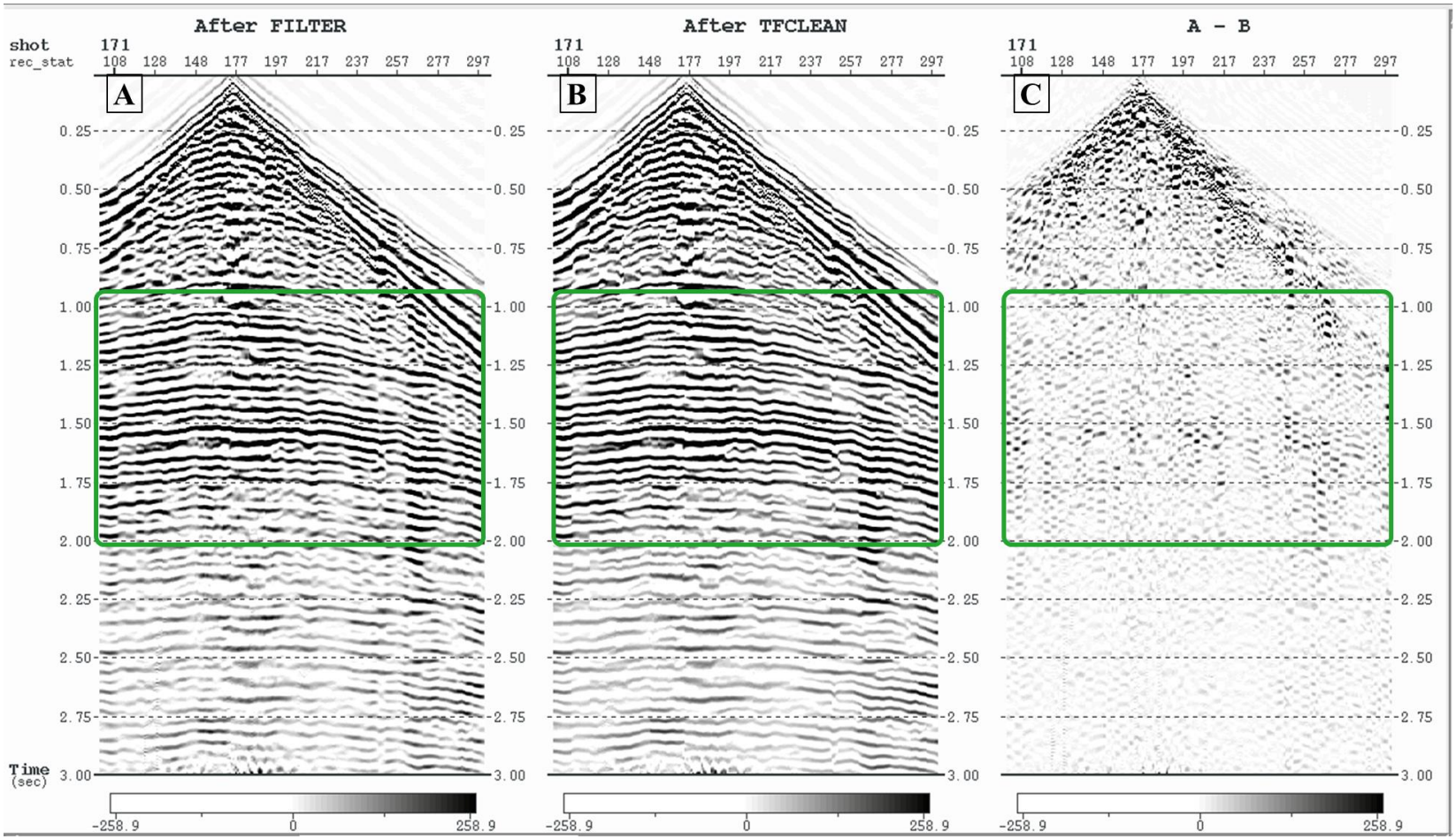

Figure 2.19. Shot gather 171. A) Before TFCLEAN application. B) After TFCLEAN application. C) The difference between A and B.

waves, ground roll, and air blast noises were analyzed and attenuated by different applications. The final results from the noise attenuation processing are shown in Figures 2.20 and 2.21. Reflection events are more observable and coherent.

2.7. DECONVOLUTION

The seismic trace is commonly modeled as a result of the convolution of the seismic wavelet and the reflectivity function of the earth (Arya and Holden, 1978). Deconvolution, an essential step in prestack seismic data processing, compresses the seismic wavelet and removes short-period multiples from the data. Therefore, it increases temporal resolution and improves the seismic section.

Deconvolution is generally attained by applying an inverse filter to remove undesirable effects on the seismic records. Types of deconvolution include spiking, predictive (gap), and surface-consistent deconvolutions. Each type is based on certain assumptions and has a different objective. Since the aims of the study are to improve vertical resolution and preserve relative amplitudes, spiking deconvolution and surface-consistent deconvolution were performed in this study.

The basic convolutional model of the seismic trace in the frequency domain is given by Equation (2):

$$S(f) = R(f)\ x\ W(f), \tag{2}$$

where S(f) is the seismic trace, R(f) is the reflectivity function of the earth, and W(f) is the seismic wavelet.

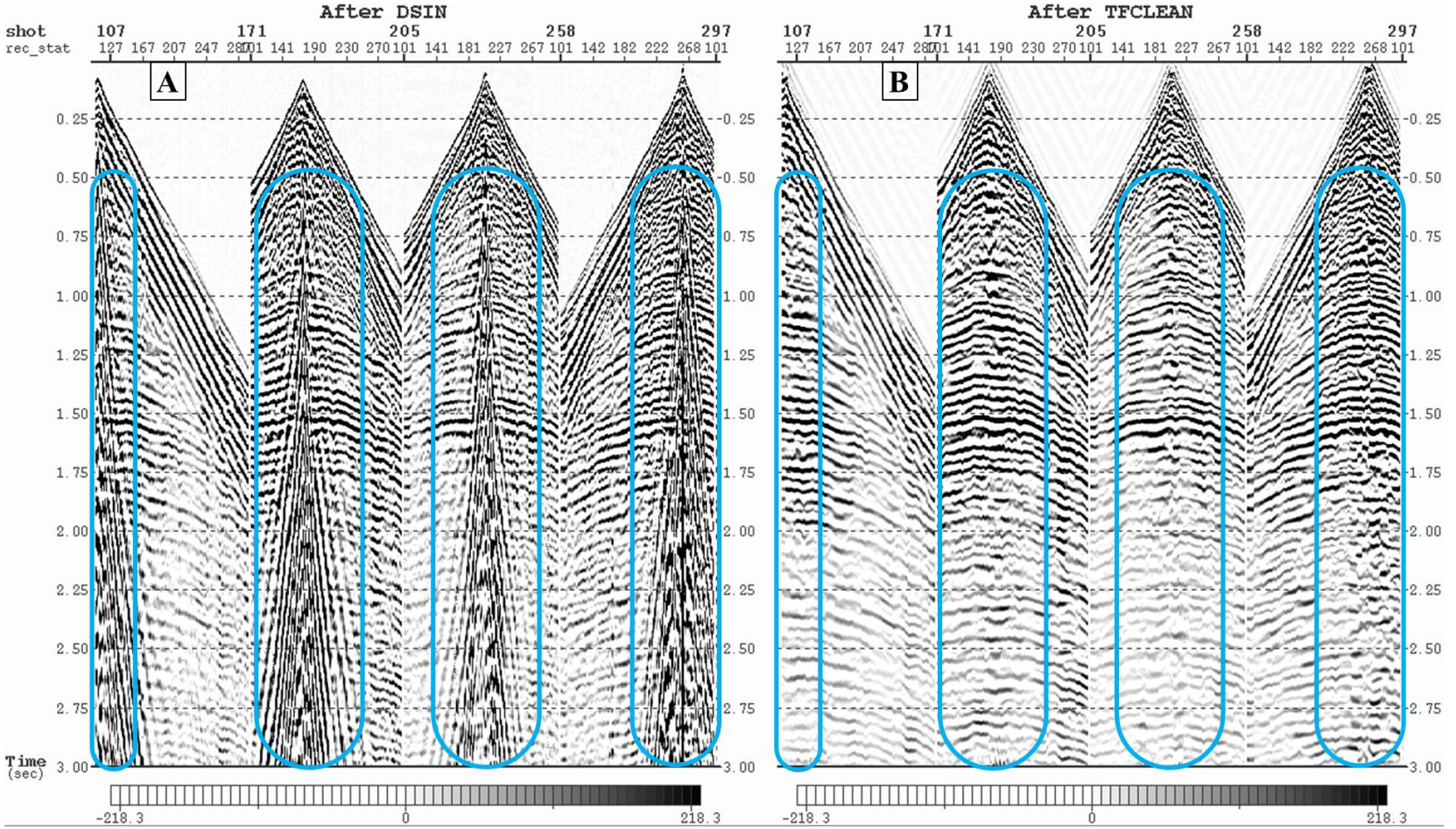

Figure 2.20. Shot gathers 107, 171, 205, 258, and 297. A) Before the noise attenuation processing. B) After the noise attenuation processing.

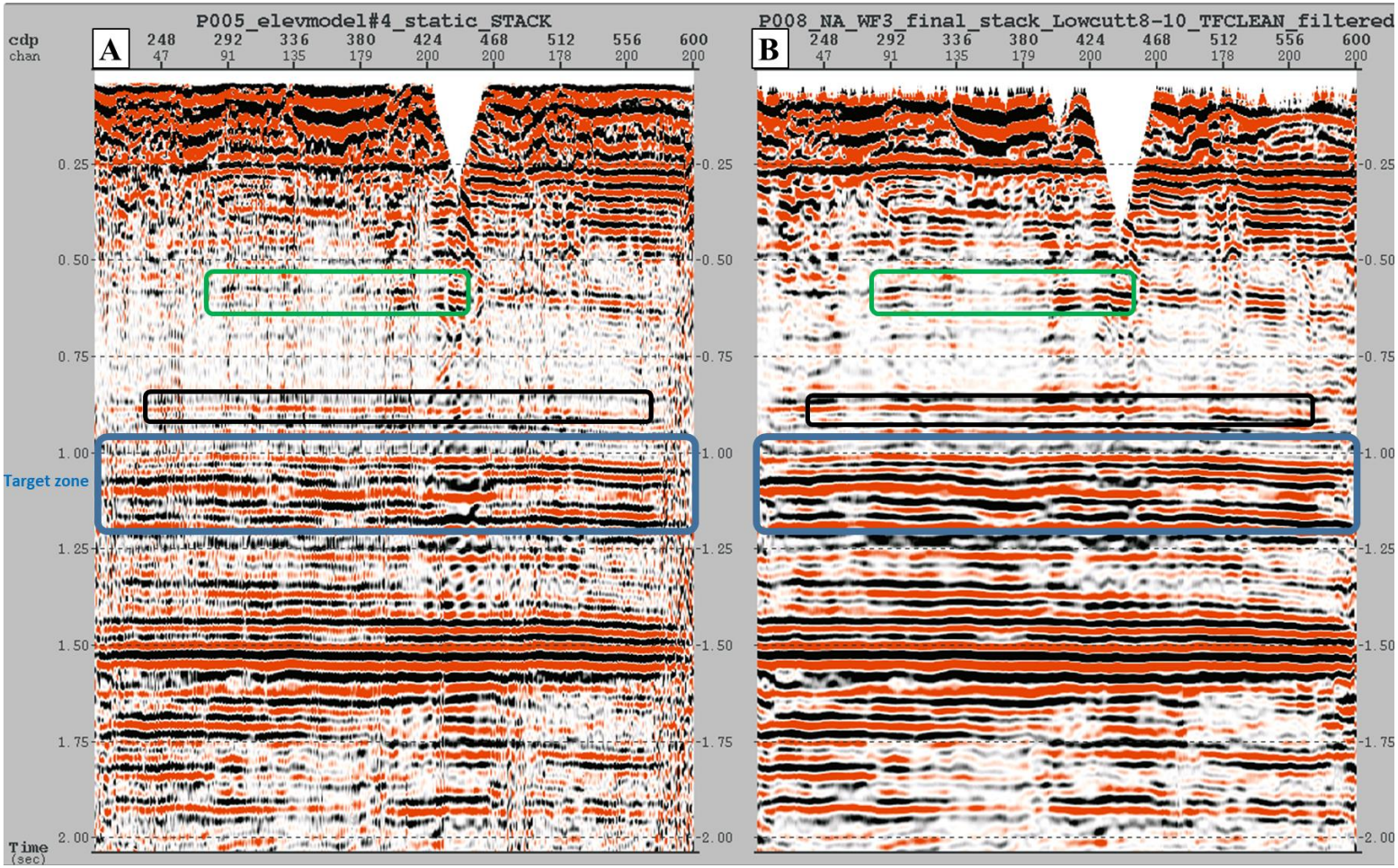

Figure 2.21. The stacked seismic section. A) Before the noise attenuation processing. B) After the noise attenuation processing. The outlined areas indicate the significant improvements.

The reflectivity coefficient series is assumed to be random and stationary and has a constant amplitude spectrum in the frequency domain. The seismic wavelet, on the other hand, is assumed to have an amplitude spectrum that changes slowly and smoothly within the frequency range. Therefore, the amplitude spectrum can be estimated by smoothing the spectrum of the input trace. The phase information of the seismic wavelet is used to design the minimum phase operator for the deconvolution filter.

The surface consistent convolutional model of the seismic trace (Taner and Koehler, 1981) is given by Equation (3):

$$x_{ij}(t) = \ s_i(t) \ * \ r_j(t) \ * h_k(t) * e_l(t) \ , \tag{3}$$

where $x_{ij}(t)$ is the seismic trace at source location *i* and receiver location *j*, $s_i(t)$ is the source response at location *i*, $r_j(t)$ is the receiver response at location *j*, $h_k(t)$ is the offset response at position *k,* and $e_l(t)$ is the reflectivity function at common midpoint *l*. Hence, the log of the Fourier transform is given by Equation (4):

$$\ln X_{ij}(f) = \ \ln S_i(f) + \ln R_j(f) + \ \ln H_k(f) + \ \ln E_l(f) \ , \tag{4}$$

The convolutional components are determined by least-square error minimization. Subsequently, a designed inverse filter based on undesirable components is applied to the data. The surface consistent components (i.e., source and receiver) capture the effect of acquisition variations and near surface effects. Nonetheless, the offset and common midpoint terms are required in the decomposition of the input signal to separate the effect of residual noise and nonwhite reflectivity from the source and receiver components (Cary and Lorentz, 1993).

The frequency domain deconvolution (DECONF) module was used to apply a bandlimited spiking deconvolution to the data. The deconvolution operator was designed

and applied to each seismic trace as a trace-by-trace filter. The results obtained from DECONF application are shown in Figure 2.22. The vertical resolution and clarity of the reflection events are improved significantly at the target zone.

The surface consistent deconvolution was applied to the data in two steps. First, the surface consistent autocorrelation analysis (SURFAN) module was used to compute the log power spectra of the seismic traces, reduce the accumulated log spectra to surface consistent components, and store the autocorrelation information. Second, the surface consistent deconvolution (SURFDEC) module was utilized to design convolution operators and apply them to the seismic data. The operators were designed based on the autocorrelations computed by SURFAN. The data was decomposed into four components (i.e., source, receiver, offset, and CMP) and then deconvolved by the source and receiver operators (Figure 2.23). As a result, the source and receiver variations due to the acquisition and near surface effects were removed from the data, and reflection events were sharpened.

The surface consistent deconvolution contributed more to removing the seismic wavelet, increasing temporal resolution, and enhancing the reflection events continuity than the spiking deconvolution (Figure 2.24).

The comparison of both convolution methods was performed on the stacked seismic section (Figures 2.25 and 2.26). Several improvements in the stacked section obtained from the surface consistent deconvolution are highlighted. The stacked seismic section shows better short-term multiples suppression, higher signal-to-noise ratio, and sharper reflection events.

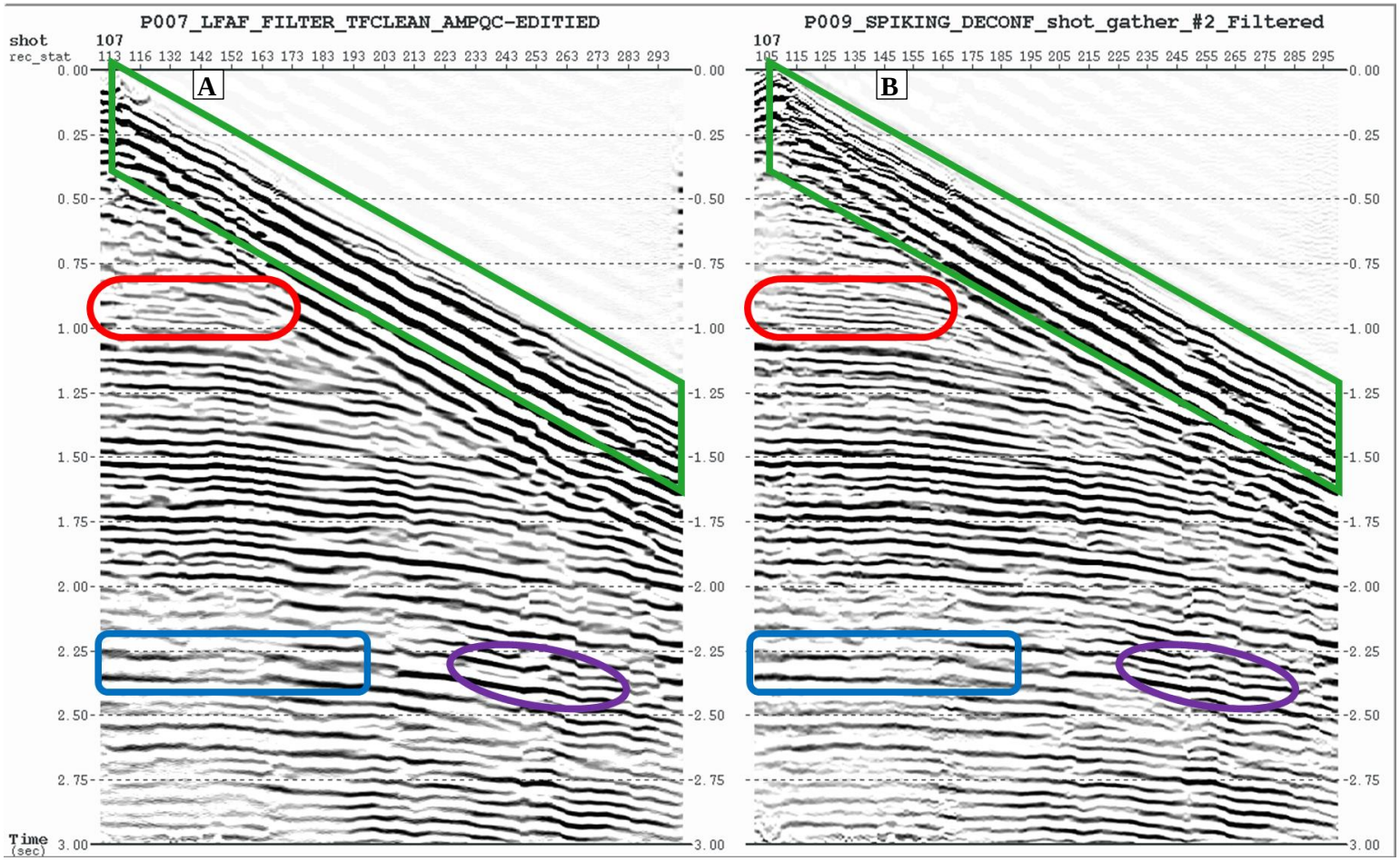

Figure 2.22. Shot gather 107. A) Before the application of the spiking deconvolution. B) After the application of the spiking deconvolution. The outlined areas emphasize the significant improvements obtained from the spiking deconvolution.

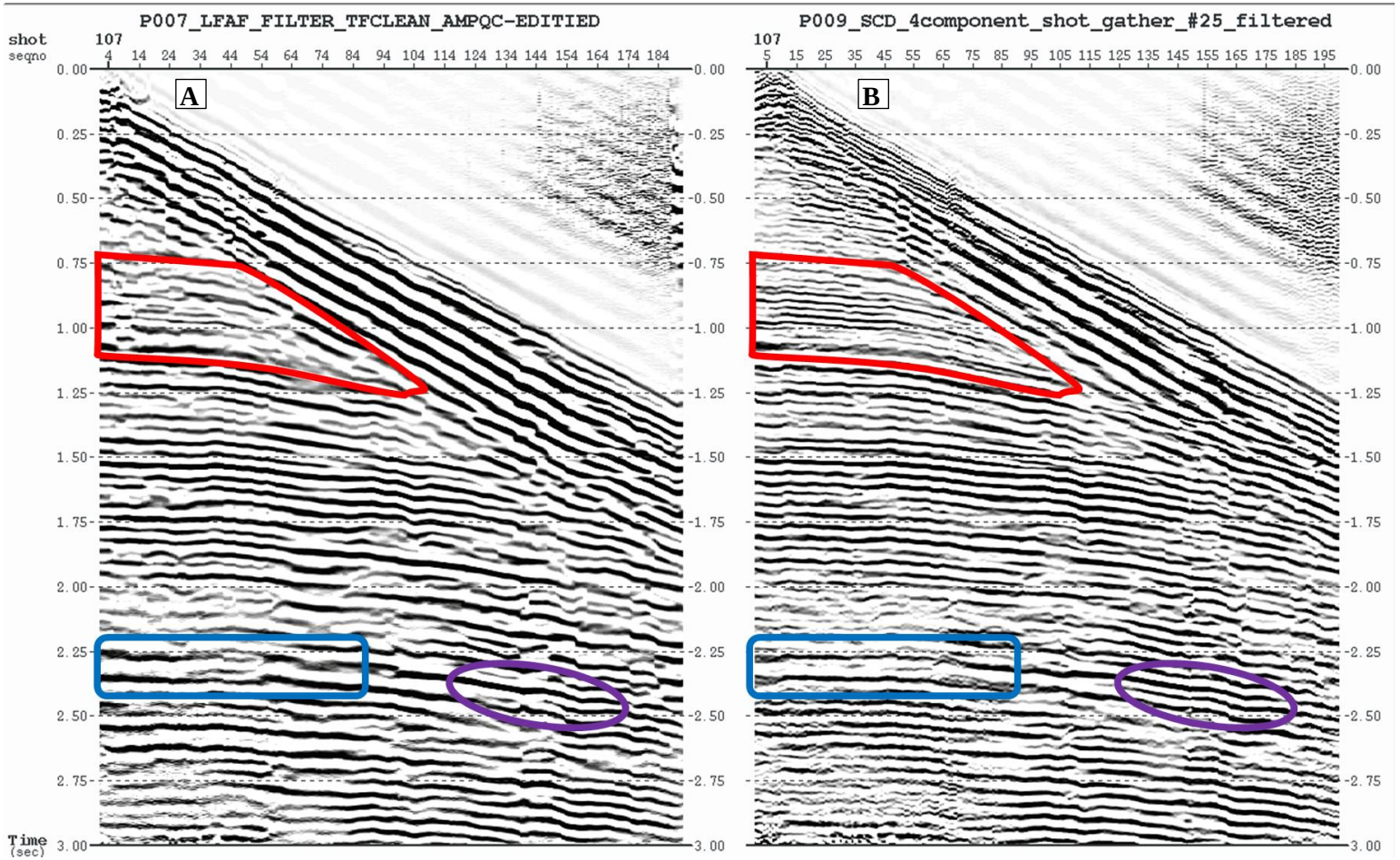

Figure 2.23. Shot gather 107. A) Before the application of the surface consistent deconvolution. B) After the application of the surface consistent deconvolution. The outlined areas underline the enhanced reflections obtained from the surface consistent deconvolution.

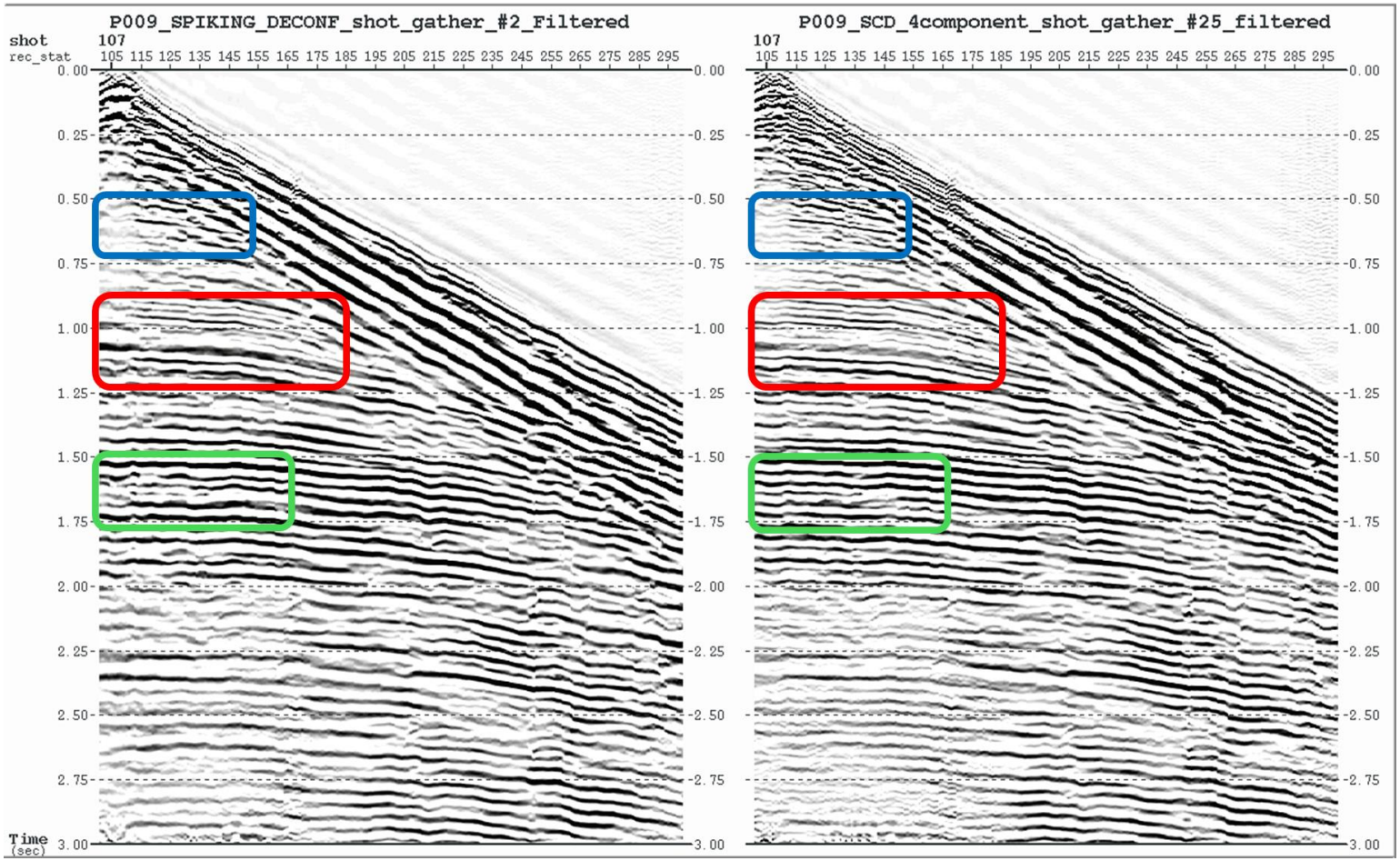

Figure 2.24. Shot gather 107. A) After the spiking deconvolution. B) After the surface consistent deconvolution. The outlined areas indicate relative improvements of the surface consistent deconvolution over the spiking deconvolution.

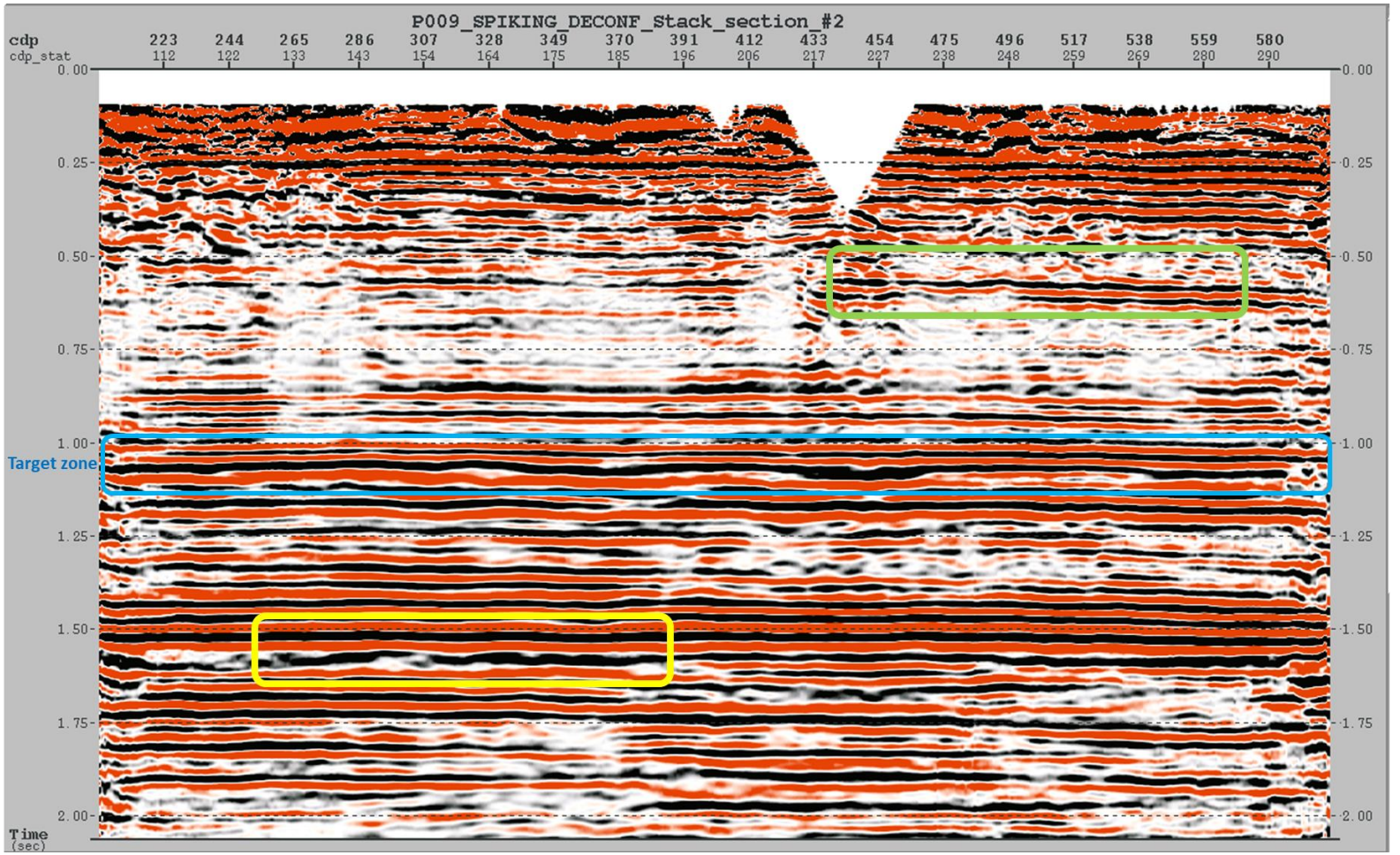

Figure 2.25. The stacked seismic section after applying trace-by-trace spiking deconvolution. The outlined areas highlight the significant changes obtained from the spiking deconvolution.

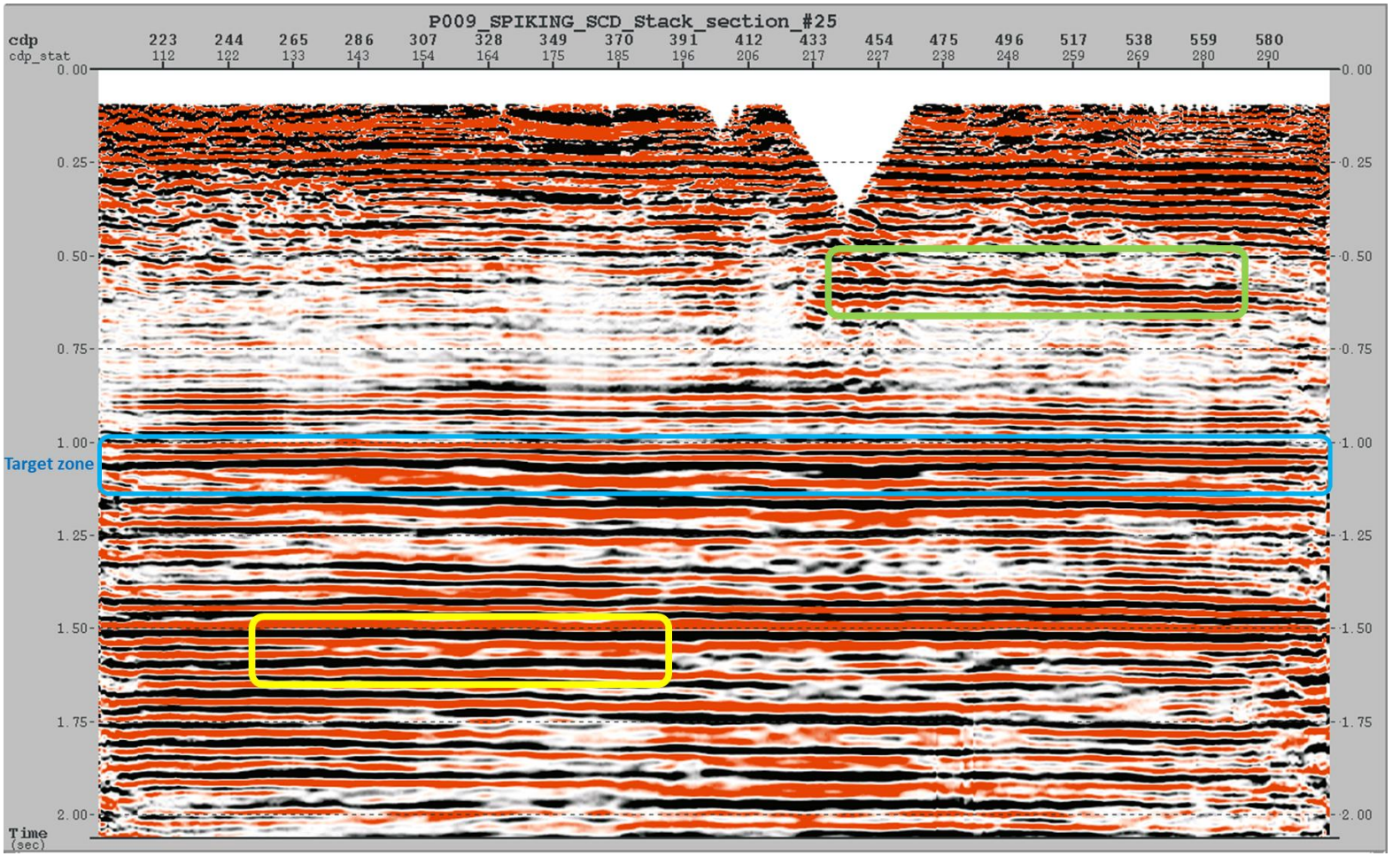

Figure 2.26. The stacked seismic section after applying four-component surface consistent deconvolution. The vertical resolution and continuity of the reflections increased considerably after the surface consistent deconvolution.

The spectral analyses of the deconvolution methods were performed on the prestack and poststack data to investigate the frequency bandwidth recovery (Figures 2.27 and 2.28). The data obtained from surface consistent deconvolution has a wider amplitude spectrum. Nonetheless, high-frequency random noise can affect the spectral analysis of the prestack data. Therefore, the spectral analysis performed on the stacked section, which contains less random noise, is more reliable and diagnostic. The spectral analysis was also applied to the stacked sections for both convolution methods and, the obtained amplitude spectra are shown in Figures 2.29 and 2.30.

The surface consistent deconvolution method provided better results than the trace-by-trace spiking deconvolution. The main advantages of this method are noise reduction, preserved relative amplitudes, and increased temporal resolution. Therefore, the data obtained from the surface consistent deconvolution were chosen for further processing steps.

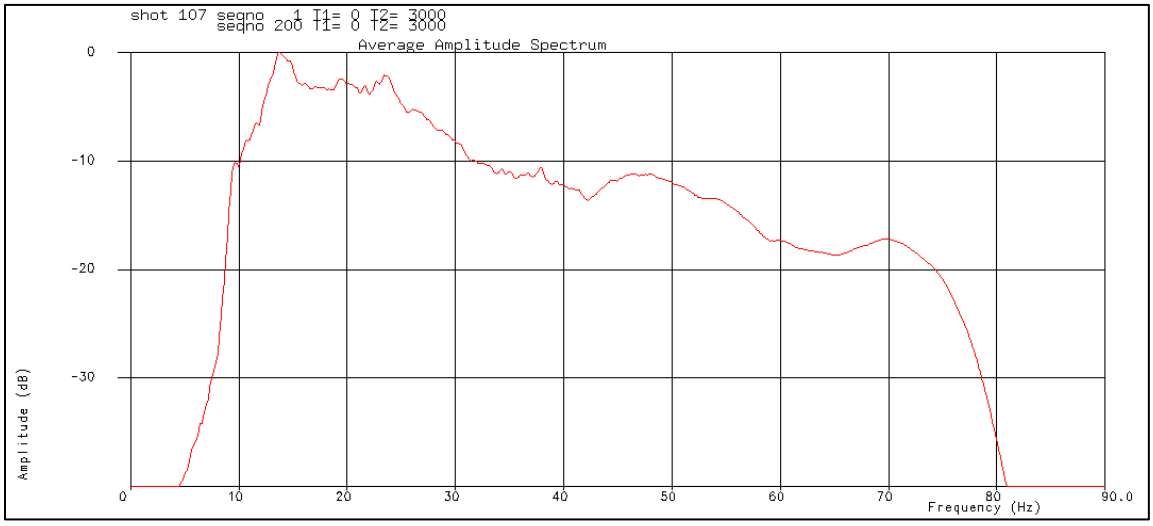

Figure 2.27. The average amplitude spectrum of shot gather 107 after the spiking deconvolution. Amplitudes at higher frequencies were slightly recovered.

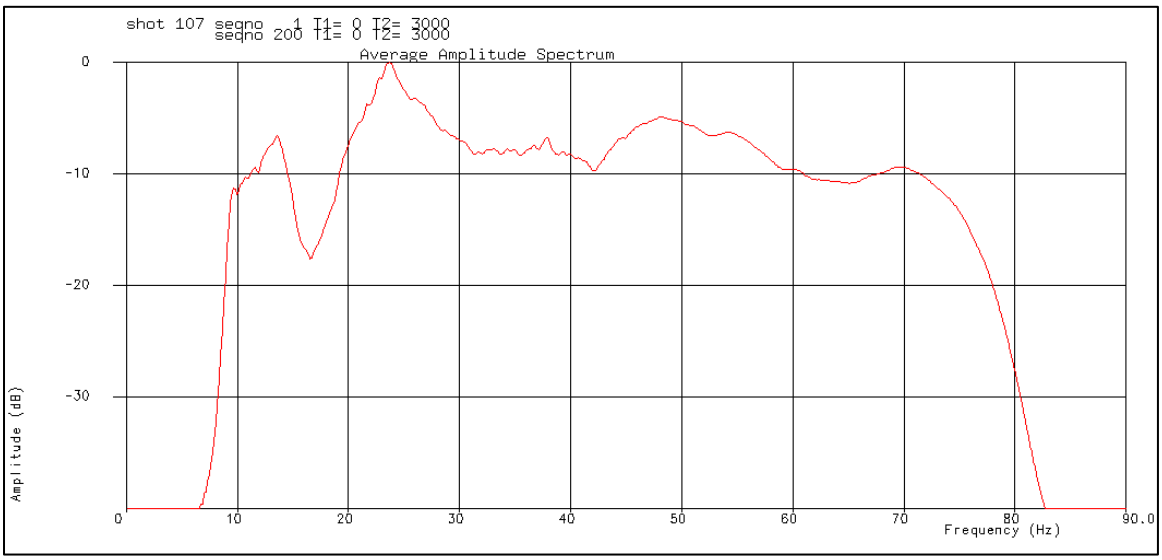

Figure 2.28. The average amplitude spectrum of shot gather 107 after the surface consistent deconvolution. High-frequency amplitudes were recovered considerably.

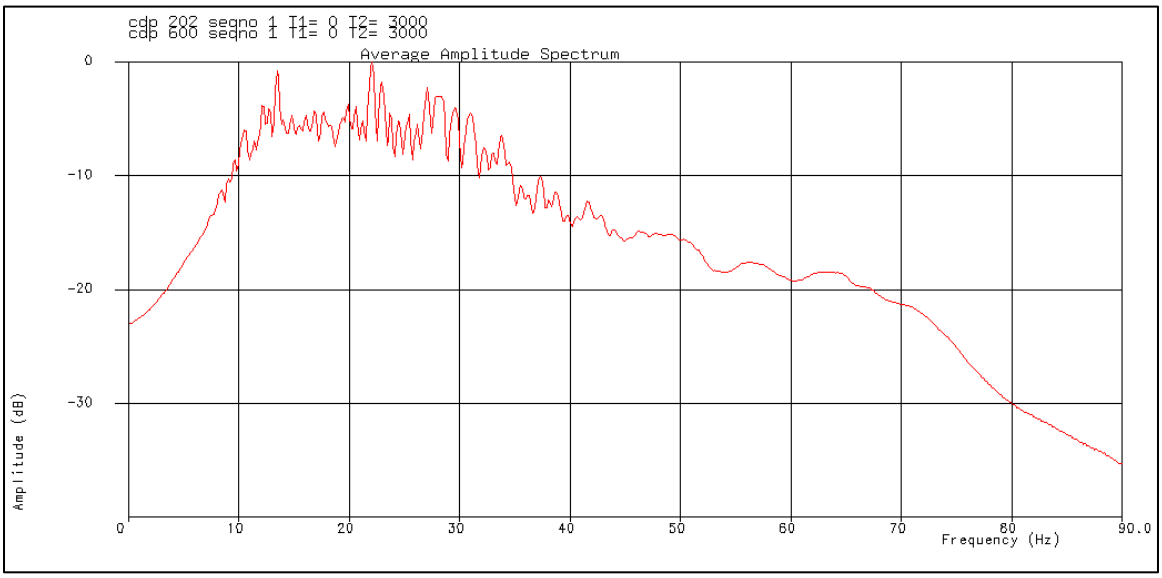

Figure 2.29. The average amplitude spectrum of the stacked section obtained from the spiking deconvolution. The dominant frequency of the stacked seismic data is around 22 Hz.

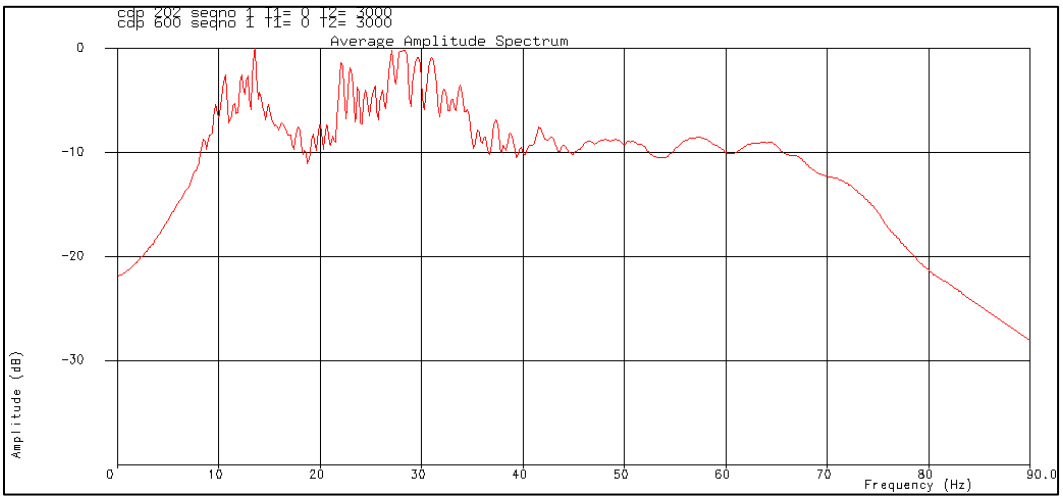

Figure 2.30. The average amplitude spectrum of the stacked section obtained from the surface consistent deconvolution. The stacked section has a broader frequency bandwidth and a higher dominant frequency of 28 Hz.

2.8. SURFACE CONSISTENT AMPLITUDE BALANCING

Surface consistent amplitude balancing is a crucial processing step to prepare prestack land data for AVO analysis and seismic lithology discrimination. This method is commonly used after the application of surface consistent deconvolution (Cary and Nagarajappa, 2013). Since amplitude spectra of the data were corrected for the acquisition and near surface variations, the remaining surface consistent effects are characterized as amplitude scalars in the time domain. The objective of this processing step is to apply the inverse of the computed scalars.

The surface consistent amplitude balancing analysis (BALAN) module was used to compute the root-mean-square (RMS) amplitudes of each seismic trace within an analysis window. A basic assumption of BALAN is that the computed amplitudes in the designed gate represent the true character of the seismic trace. Therefore, the analysis window was designed on high signal-to-noise ratio zone that includes the target reflector.

The log of the computed RMS amplitudes of each seismic trace was stored for the following application.

The surface consistent amplitude balancing solution (BALSOL) module was used to reduce the computed RMS amplitudes to surface consistency. BALSOL decompose the trace amplitude information by least-squares error minimization into four components, i.e., source, receiver, offset, and CMP. The surface consistent solution obtained from BALSOL was written in the seismic database. Figure 2.31 shows the source and receiver amplitude scalars obtained from BALSOL.

The surface consistent amplitude balancing application (BALAPP) module was used to apply the amplitude scalars to the data. The source and receiver corresponding scalars (i.e., surface consistent scalars) were used to balance each seismic trace. The obtained results from BALAPP were examined and validated (Figure 2.32). The spatial amplitude variations associated with different source and receiver stations were removed. The comparison of the stacked sections before and after the application of BALAN, BALSOL, and BALAPP are shown in Figures 2.33 and 2.34. The observed amplitude vertical banding of the data is corrected, and the coherency of the reflections is improved.

2.9. VELOCITY ANALYSIS AND NORMAL MOVEOUT CORRECTION

Velocity analysis is a vital step in seismic data processing. Seismic velocities greatly influence subsequent processing steps such as NMO correction and stacking, interval-velocity estimation, prestack time migration, and time-to-depth conversion. Therefore, determining the correct seismic velocity requires profound examination of the data.

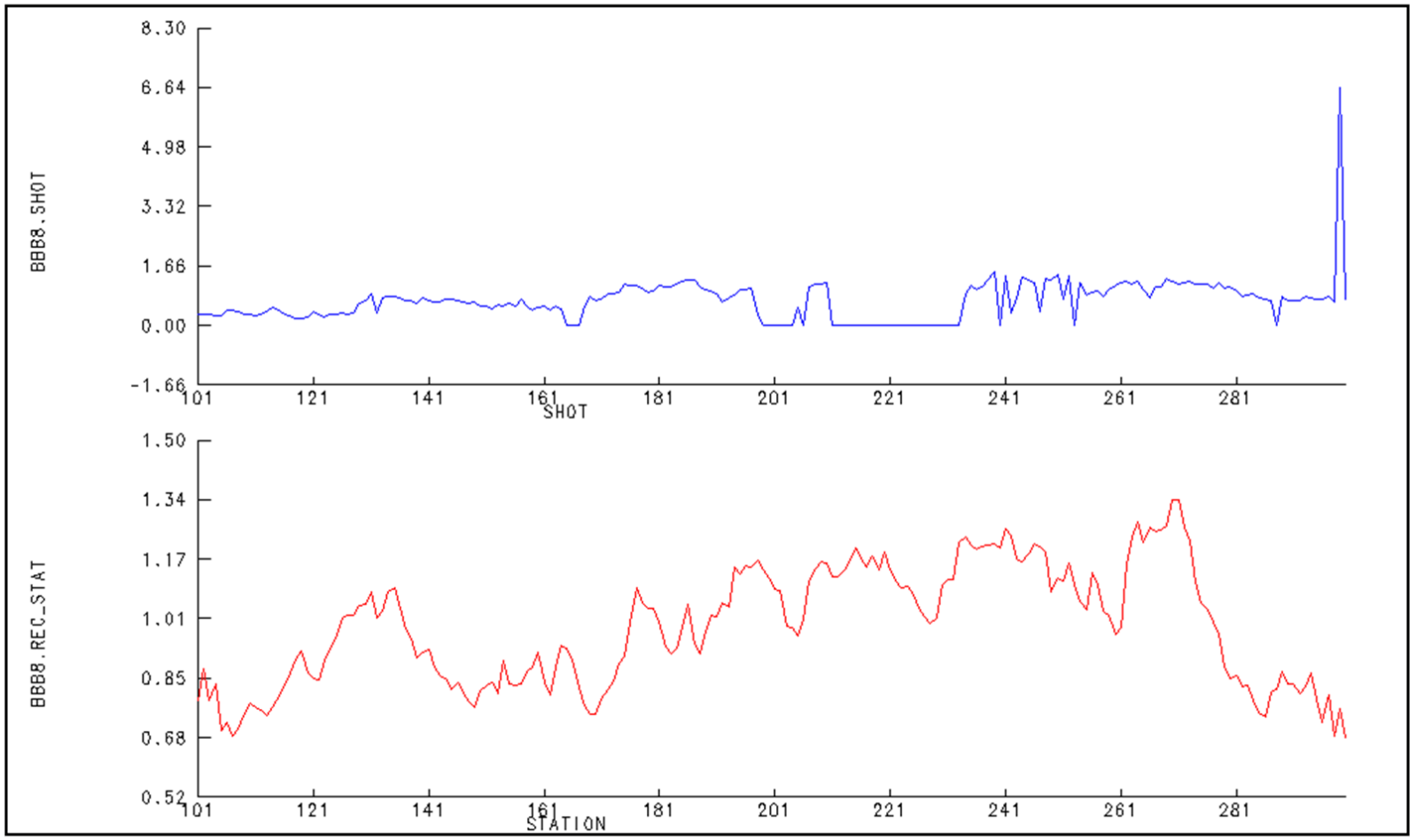

Figure 2.31. Amplitude scalars obtained from applying BALAN, BALSOL and BALAPP. The top and bottom profiles display scalars associated with source and receiver stations, respectively.

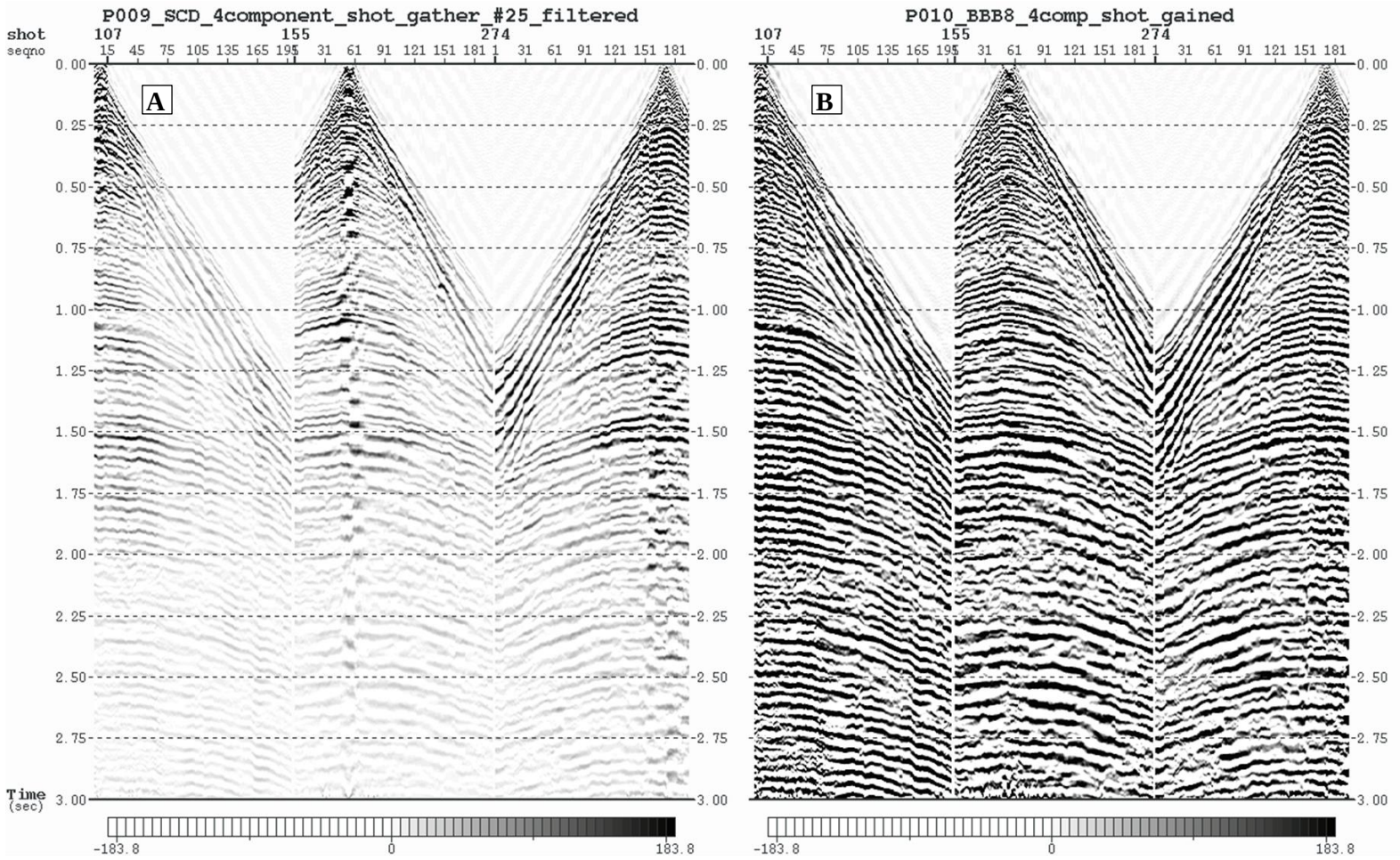

Figure 2.32. Shot gathers 107, 155, and 274. A) Before applying the surface consistent amplitude correction. B) After applying the surface consistent amplitude correction.

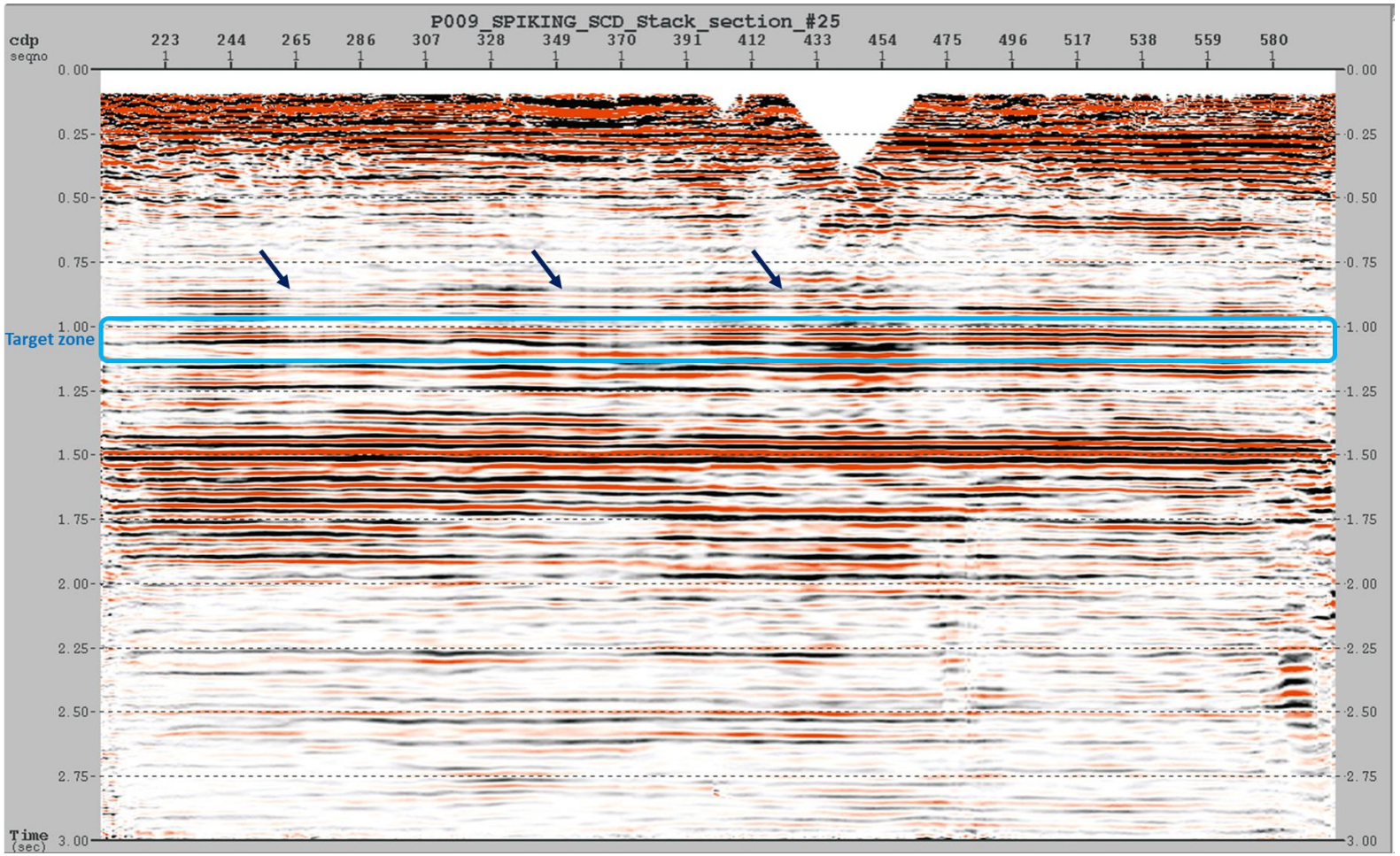

Figure 2.33. The stacked seismic section before applying the surface consistent amplitude correction. The vertical banding of high and low amplitudes is indicated.

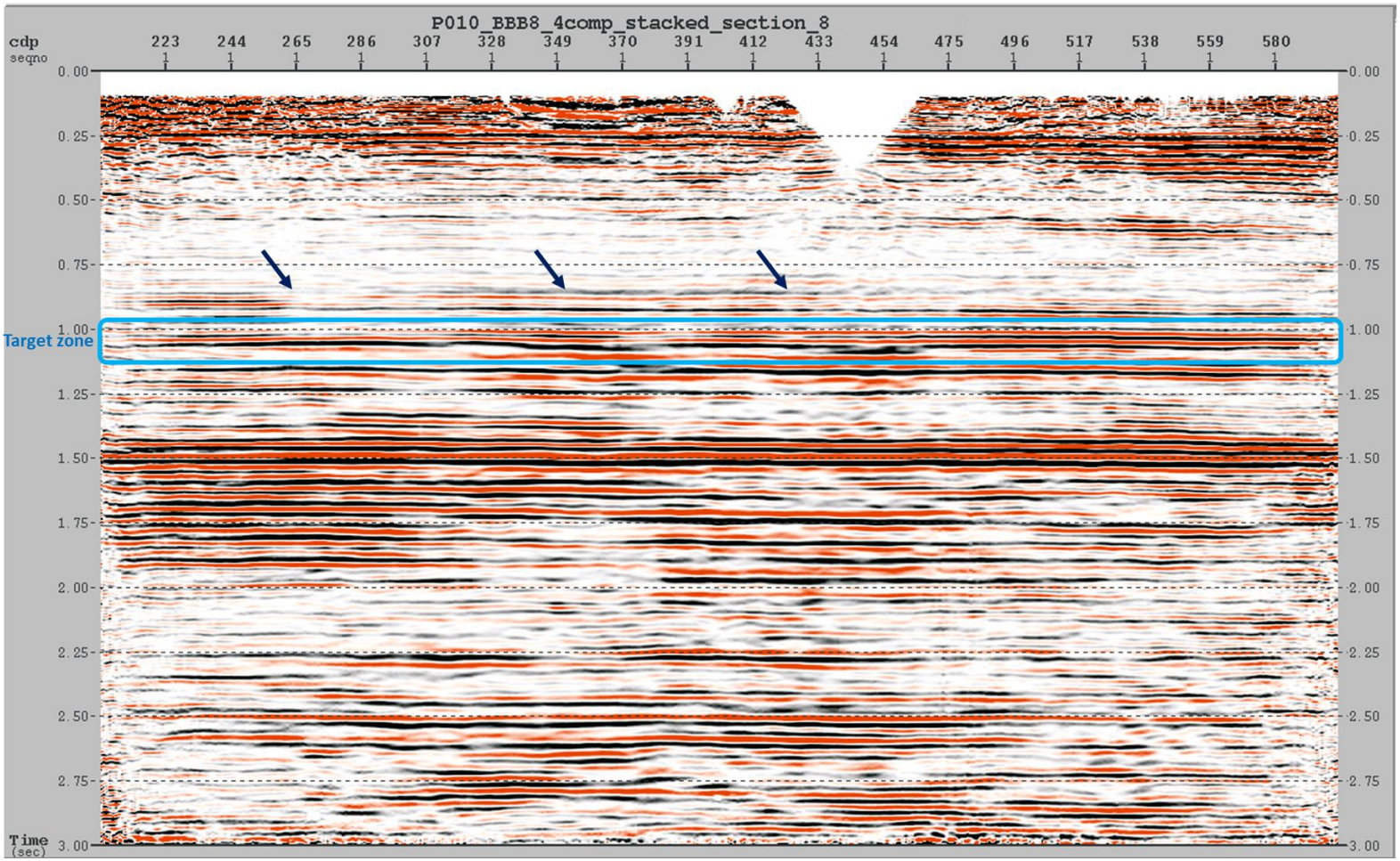

Figure 2.34. The stacked seismic section obtained from applying the surface consistent amplitude correction. The previously detected vertical amplitude banding is removed.

Seismic velocity types include interval, average, RMS, and stacking velocity. The interval velocity (i.e., the velocity in a single layer) is used for time-to-depth conversions. The stacking velocity, on the other hand, corrects for the normal moveout of seismic reflections.

The seismic velocity varies based on the density and elastic moduli of the rocks. In sedimentary rocks, porosity can greatly affect the elastic moduli and, hence, alters the rock velocity. Velocity generally increases with depth because of the increased overburden pressure.

The quality and effectiveness of velocity analysis depend on several factors. The maximum offset, signal-to-noise ratios, recording time, static correction, frequency bandwidth, and the structure of the subsurface contribute to the result obtained from velocity analysis.

The resulting velocities from the analysis consist of time and rms velocity pairs called vertical velocity functions. The number of velocity functions from the analysis is decided based on the complexity of the subsurface structure and the lateral velocity variations. Furthermore, the velocity field is generated by the spatial and temporal interpolation of the vertical velocity functions.

The velocity analysis of seismic data includes different techniques such as vertical velocity semblance, constant velocity stacks (CVS), function velocity stacks (FVS). The vertical velocity semblance method calculates amplitude coherency along hyperbolic trajectory within CMP gathers using different values of zero-offset time and velocity (Neidell and Taner, 1971). The amplitude coherency is maximized at the correct zero-offset time and velocity for each seismic reflection. In addition, this technique helps in

identifying seismic multiples that are associated with relatively low velocities. On the other hand, the CVS technique is based on stacking a group of CMP gathers using a range of constant velocities. The resulting stacks are examined to find the best stack response based on reflection continuity.

The velocity analysis implemented in this study was done by integrating both vertical velocity semblance and CVS techniques (Figures 2.35 and 2.36). The correct NMO velocities of the seismic reflections were determined from the vertical velocity semblance. Subsequently, CVS technique was used to refine the selected NMO velocities to improve the continuity of reflection events. The resulting NMO velocities were interpolated to obtain the stacking velocity field (i.e., velocity model) (Figure 2.37). The velocity model has a higher uncertainty at the very beginning and end of the seismic line. Nonetheless, the stacking velocity field is relatively smooth, and velocity anomalies were not observed.

The obtained velocity field was used to apply NMO correction to all CMP gathers (Figures 2.38 and 2.39). The primary reflection events were flattened by applying the correct stacking velocity. Subsequently, a stretch mute was performed to remove the undesirable effect of NMO correction on shallower reflections at far offsets (Figure 2.40). The separation between primary and multiple reflections is a function of velocity difference and offset. The area under 1.5 seconds exhibits multiples that have an undercorrected NMO pattern due to their relatively high moveout. Multiples recorded in CMP gathers with high-fold coverage and relatively large offset are discriminated by velocity and, therefore, attenuated by the process of CMP stacking. On the other hand,

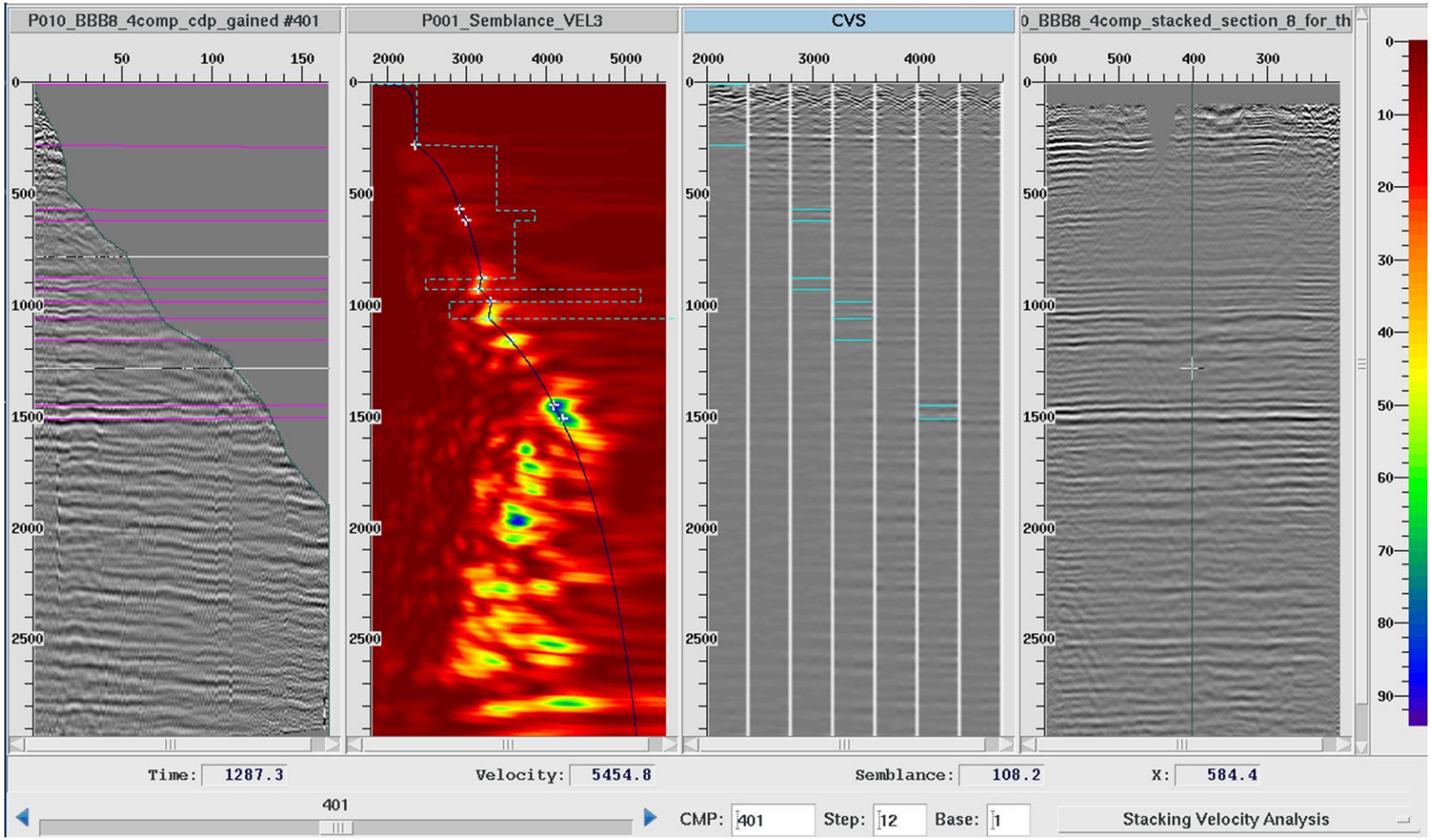

Figure 2.35. The velocity navigator tool used for velocity analysis in this study.

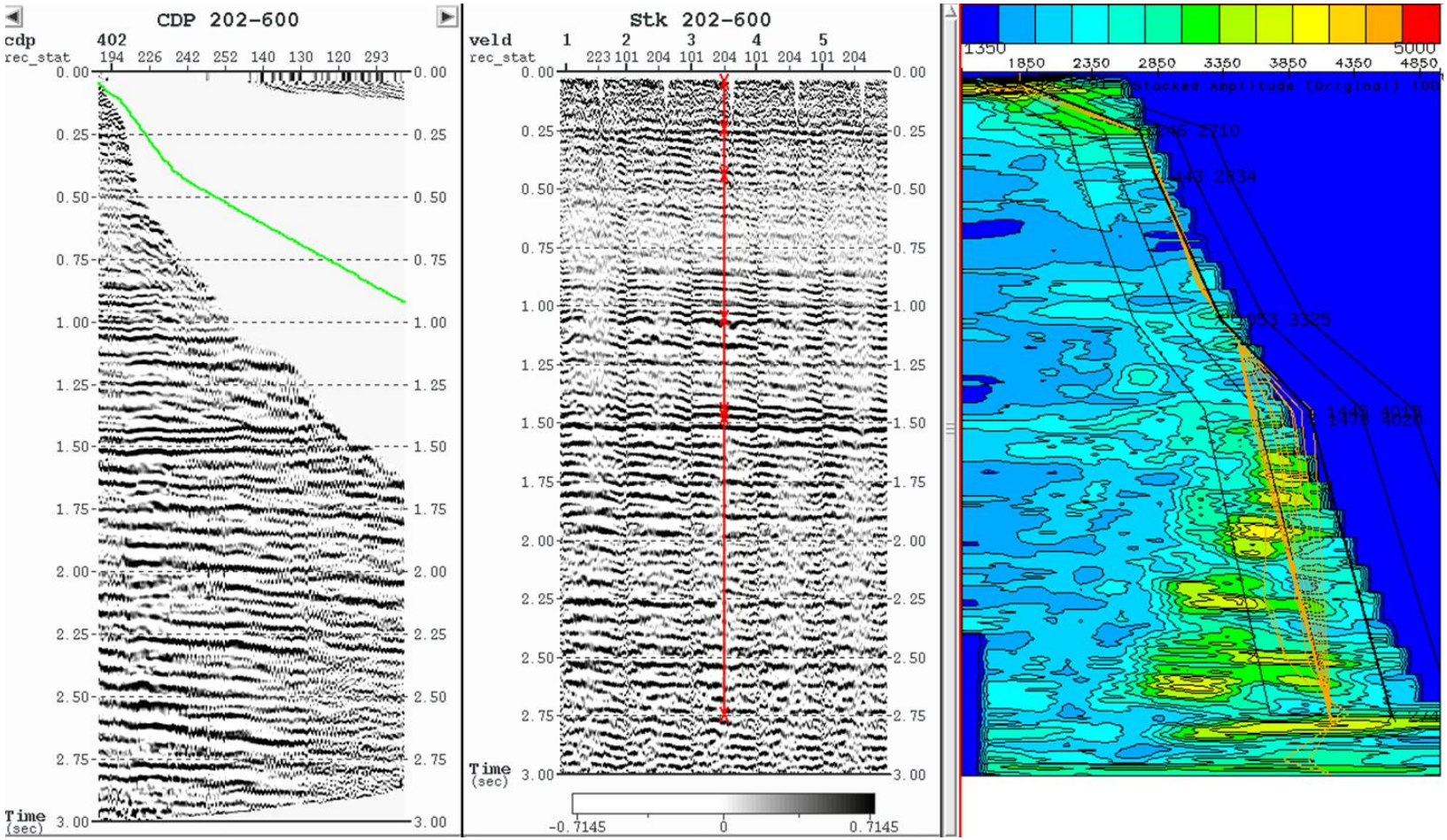

Figure 2.36. The interactive velocity analysis tool (VELDEF) used to refine the determined velocities.

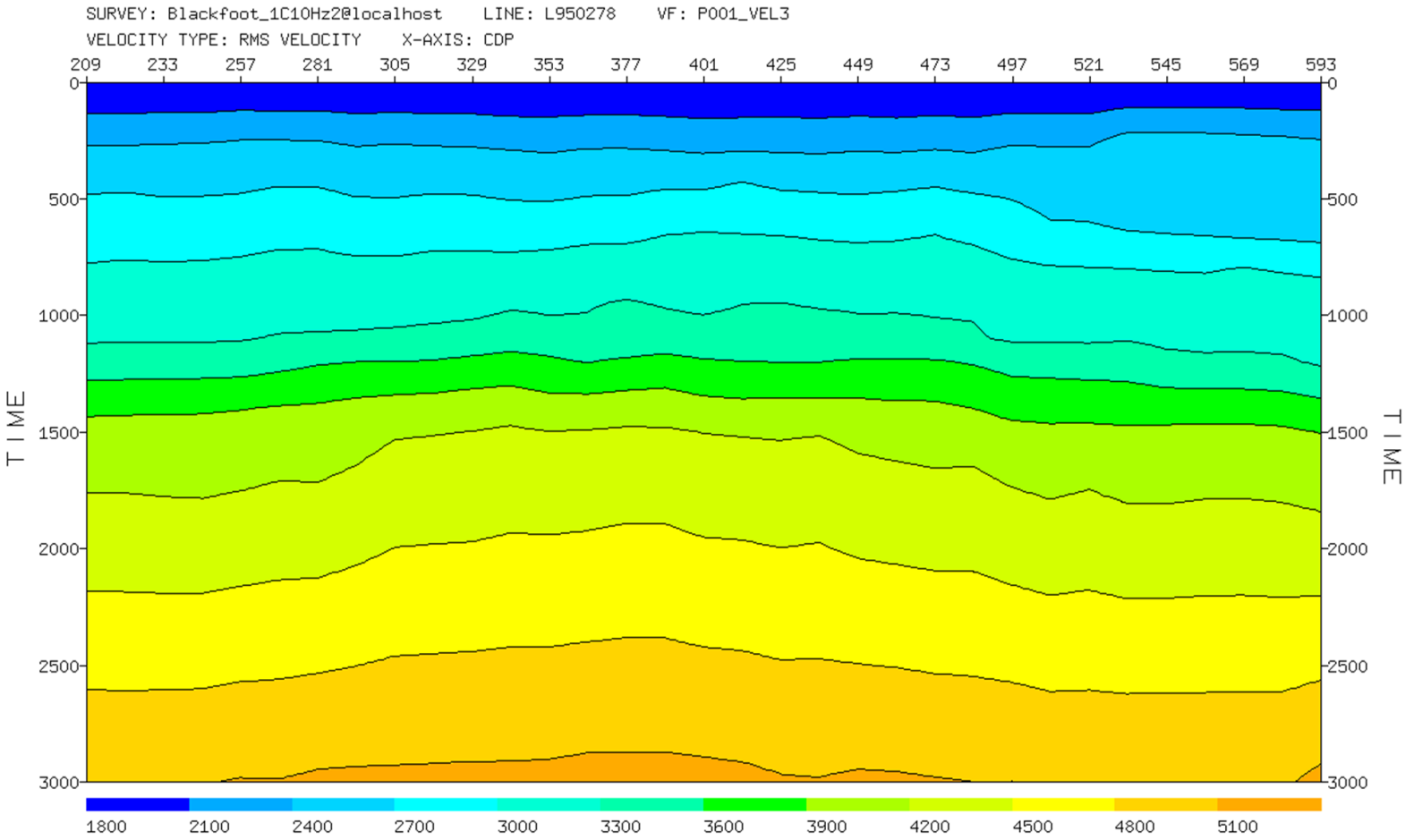

Figure 2.37. The obtained velocity field showing computed stacking velocity of the seismic profile.

the CMP stacking is less effective in attenuating multiples recorded near the beginning and end of the seismic line due to low-fold coverage.

2.10. RESIDUAL STATIC CORRECTION

Seismic traces are affected by the near surface layers in terms of relative time delay, amplitude distortion, and phase change (Taner et al., 1974). The estimation and correction of these effects are essential in processing land seismic data. The final seismic imaging of the subsurface is directly influenced by the process of correcting near surface effects.

The seismic wave propagation through near surface anomalies results in misalignment of individual traces within CMP gathers. These misalignments persist throughout the stacking process and adversely affect the quality of stacked seismic sections (Moser and Jovanovich, 1984). Therefore, residual static corrections are computed and applied to the CMP gathers before the stacking process.

The lateral velocity variations and thickness of the near surface layers are best approximated by the surface-consistent approach. In this approach, each source and receiver position has a consistent near surface effect on seismic traces associated with that source or receiver (Ronen and Claerbout, 1985). The effective removal of near surface effects increases the coherency of reflections after stacking.

Surface consistent residual statics, however, are computed based on assumptions that may not be entirely true (Henley, 2012). The first assumption is surface-consistency where a specified surface location is associated with one constant time delay, irrespective of the wave path. The first assumption is valid for most seismic data as the weathering

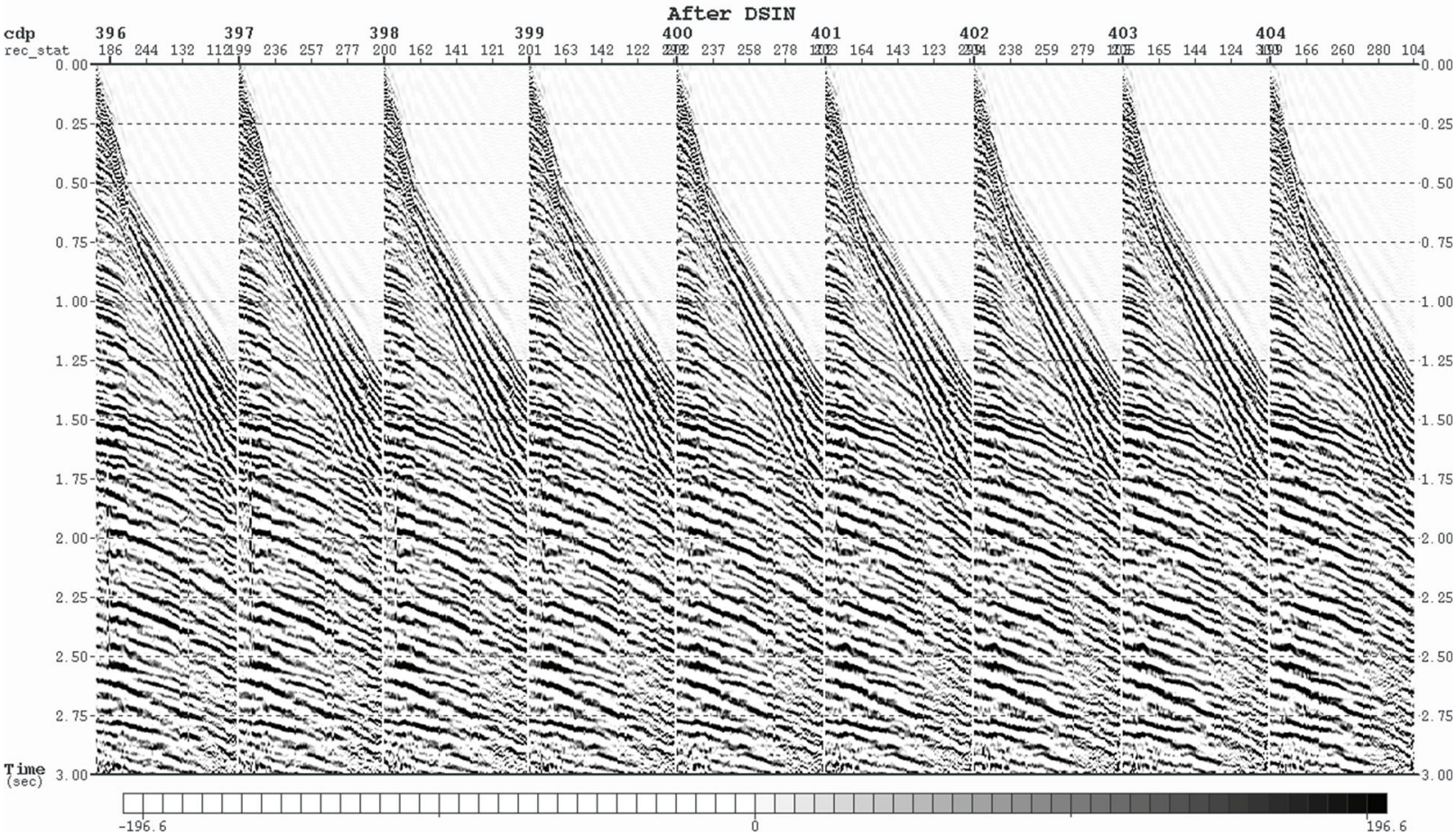

Figure 2.38. CMP gathers 396 to 404 before applying the NMO correction.

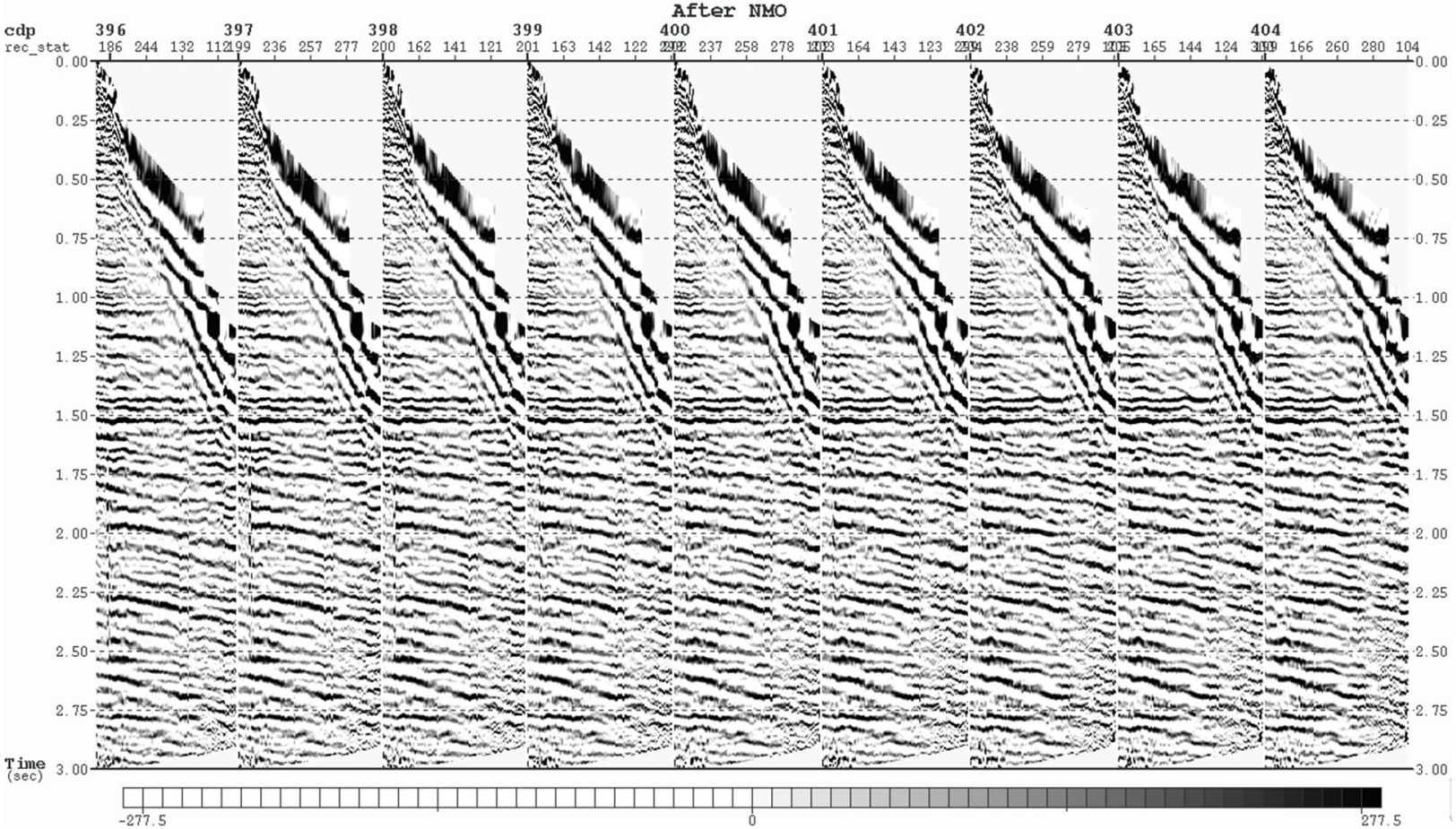

Figure 2.39. CMP gathers 396 to 404 after applying the NMO correction.

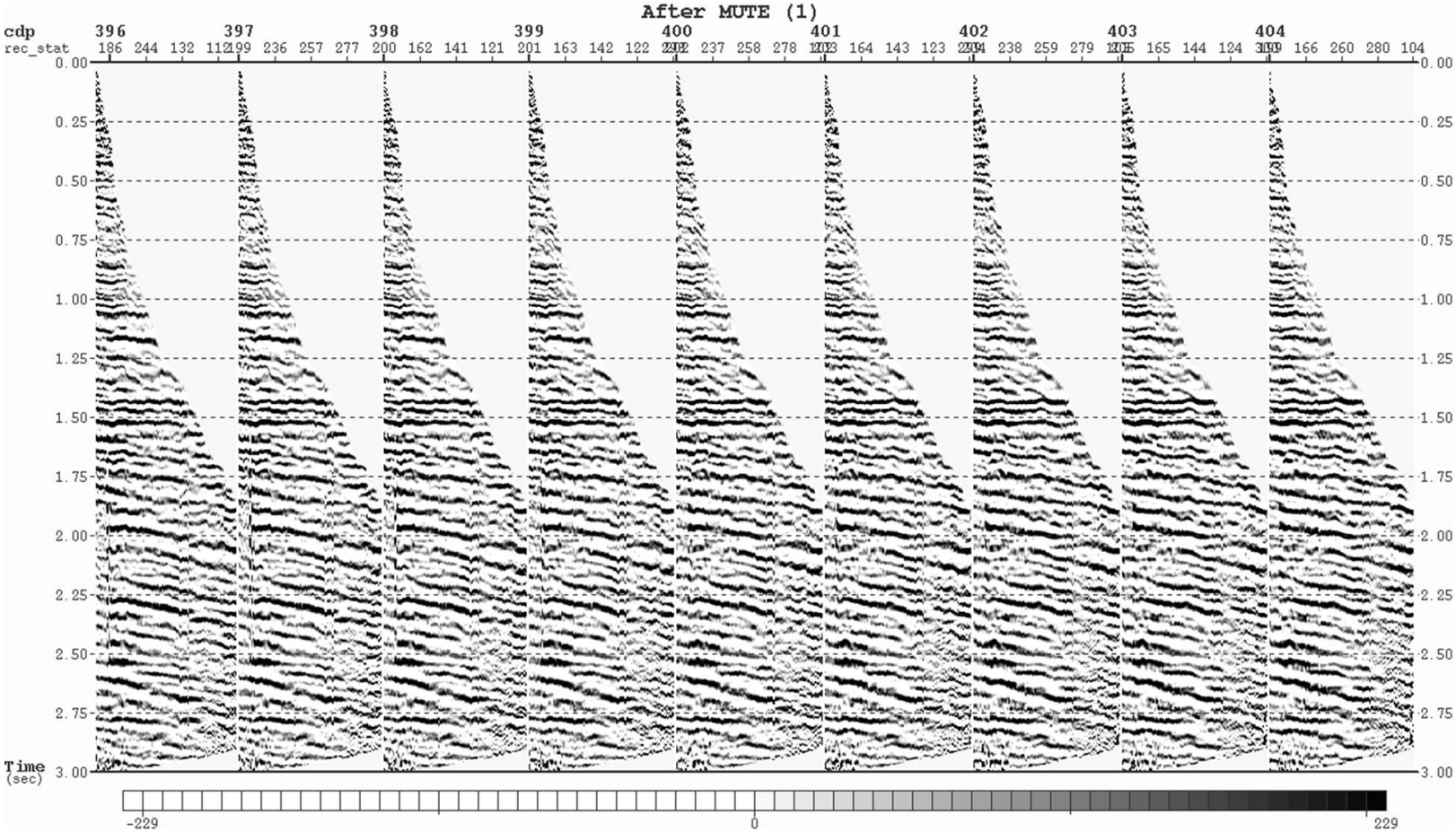

Figure 2.40. CMP gathers 396 to 404 after applying the stretch mute.

layer is commonly associated with low velocity which bends the wave almost vertically based on Snell's law. Nonetheless, the first assumption is violated when the weathered layer has a higher velocity than that of the underlying layer. As a result, reflections are traveling through different ray paths within the weathering layer, as illustrated in Figure 2.41.

The second assumption is the stationarity of the residual statics (i.e., waves reflecting from deep subsurface interfaces travel along the same path within the weathering layer with respect to shallow reflections). In other words, residual static correction is constant in time where all reflections recorded in a seismic trace are affected by the same time delay.

Two types of surface consistent residual statics algorithms were tested in this study. Both techniques compute residual statics based on the cross-correlation of each input trace and a reference pilot trace. The resulting lag values from the cross-correlation are subsequently reduced to surface consistency and applied to seismic traces.

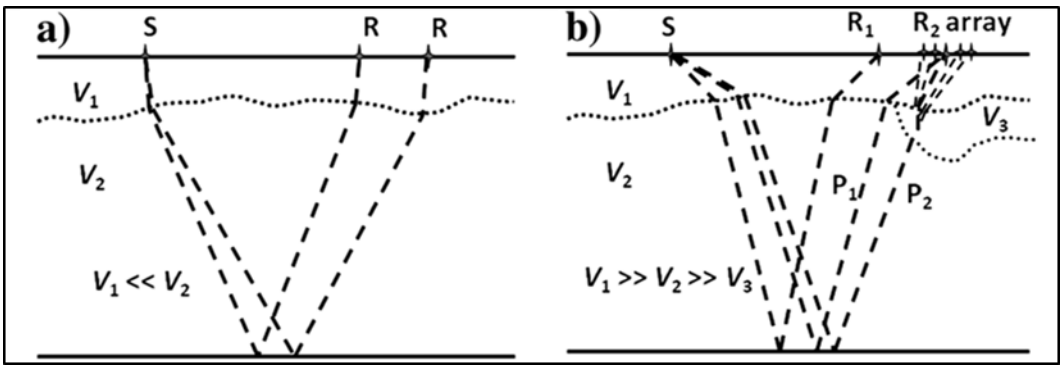

Figure 2.41. The ray path of reflected seismic waves. a) The velocity of the shallower layer is much smaller than the underlying velocity. b) The velocity of the shallower layer is greater than the underlying velocity, where surface consistency assumption is violated (Henley, 2012).

The surface consistent residual statics generation (EPSTX) module was used to compute residual statics. Within the designed analysis gate, the cross-correlation of input traces and their CMP pilot trace are computed and accumulated for all source and receiver stations. The EPSTX application selects the largest lag of each accumulated correlation to generate the surface consistent residual statics. The stacked seismic sections before and after the application of the EPSTX module are shown in Figures 2.42 and 2.43. The surface consistent residual statics applied to the data improved the continuity of the seismic reflections and increased the vertical resolution. Significant improvements in certain areas of the stacked seismic section were highlighted.

The second approach in computing surface consistent residual statics was used and compared to the EPSTX module. This approach was performed in two stages. First, the automatic residual statics analysis (STATPIK) module was applied to the data. This application computes a large number of correlations for each group of input traces (i.e., CMP gather). The resulting lag values are checked for consistency. The pilot trace is constructed for each group using the time lag values that pass the consistency check. Then, each trace in the group is correlated with its associated pilot to obtain relative time-shifts. Second, the resulting time-shift values are reduced to surface consistency by the automatic residual statics generation (STATANL) module. In this application, there are two methods for reducing time-shift values to surface consistency (i.e., median-based reduction and standard least-squares reduction). The median-based reduction method is more suitable for low signal-to-noise ratio and, hence, was selected. Figure 2.44 shows the stacked seismic section after applying the surface consistent residual statics obtained from the STATANL module. The second approach provides better imaging of the target

zone at a depth of 1100 ms. Furthermore, the outlined areas indicate further improvements over the EPSTX module. Therefore, this approach was selected to compute the surface consistent residual statics.

The surface consistent residual statics were applied to the data in two passes (Figures 2.45 and 2.46). The velocity analysis and NMO correction were applied before each residual statics to improve the obtained results. Each residual statics pass contains ten iterations to ensure the convergence of the solution.

2.11. MIGRATION

Migration is the last step in the seismic data processing workflow. The importance of this step lies within its ability to move recorded reflections to their true locations. In addition, migration eliminates diffractions and increases both temporal and spatial resolution. The algorithms of migration are implemented in various methods and operated in different domains. For instance, the prestack and poststack migration algorithms are developed for CMP gathers and stacked data, respectively. The prestack algorithm is relatively more accurate as it uses prestack information. Migration can be performed in the depth domain to image complex geological structures. However, this technique is sensitive to the velocity model of the subsurface and requires the integration of stacking velocities, well logs, and tomography modeling.

The migration algorithms used in this study require a flat reference datum. Hence, the seismic data and the velocity model were moved from the floating datum to the final flat datum at elevation 900 m above sea level. The stacked seismic section referenced to the flat datum is shown in Figure 2.47.

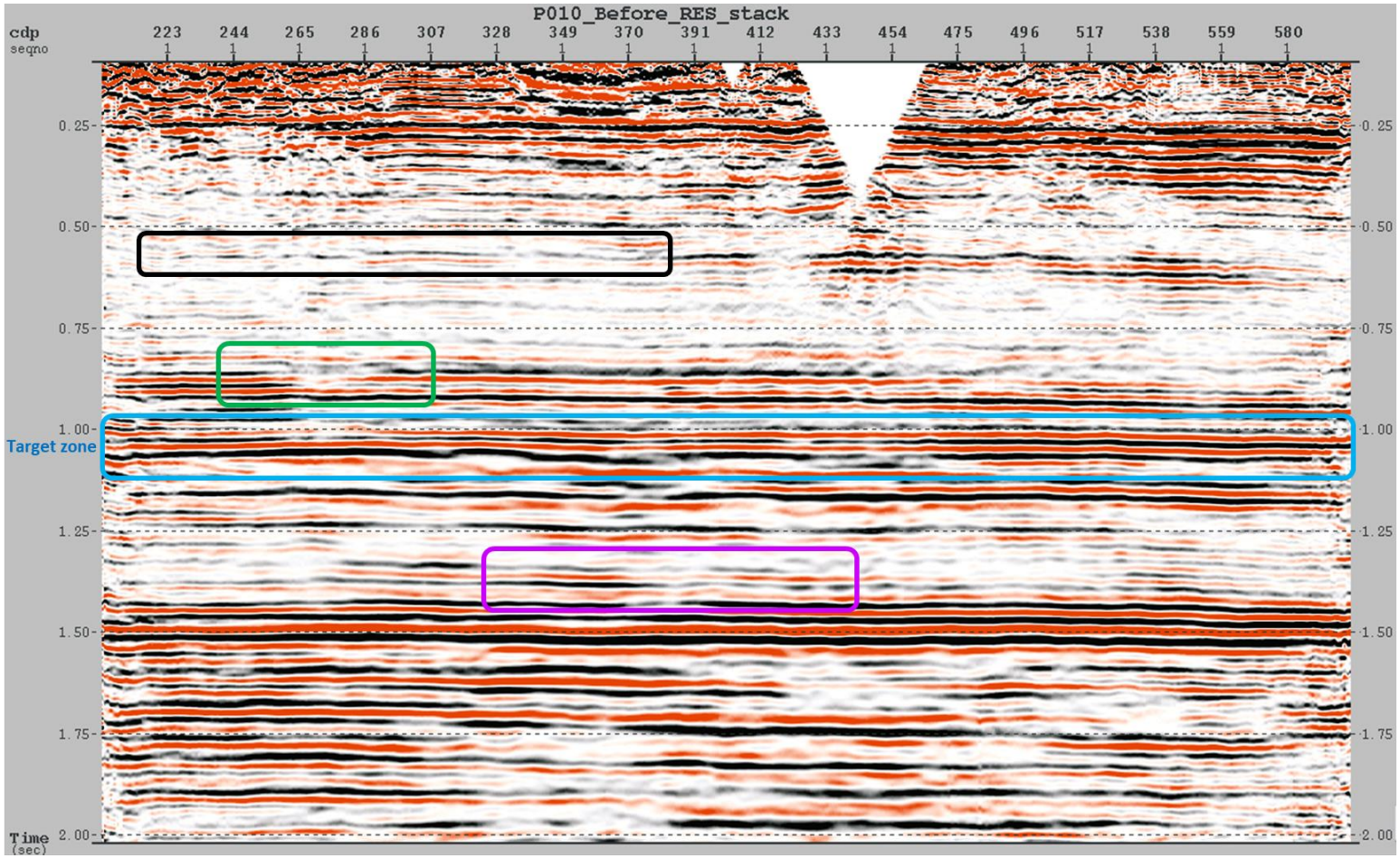

Figure 2.42. The stacked seismic section before applying the surface consistent residual statics.

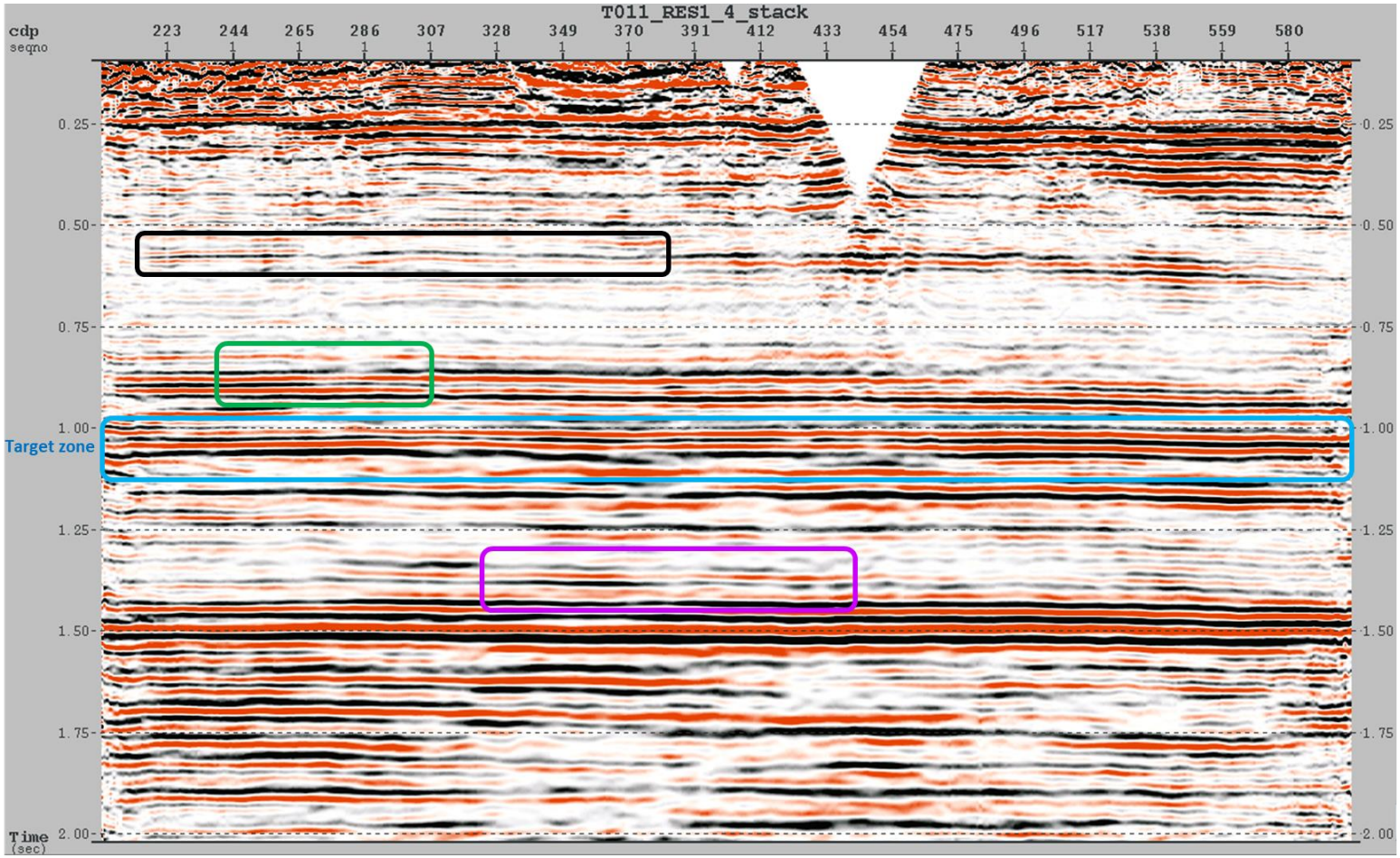

Figure 2.43. The stacked seismic section after applying the surface consistent residual statics obtained from the EPSTX module. The outlined areas indicate the significant improvements.

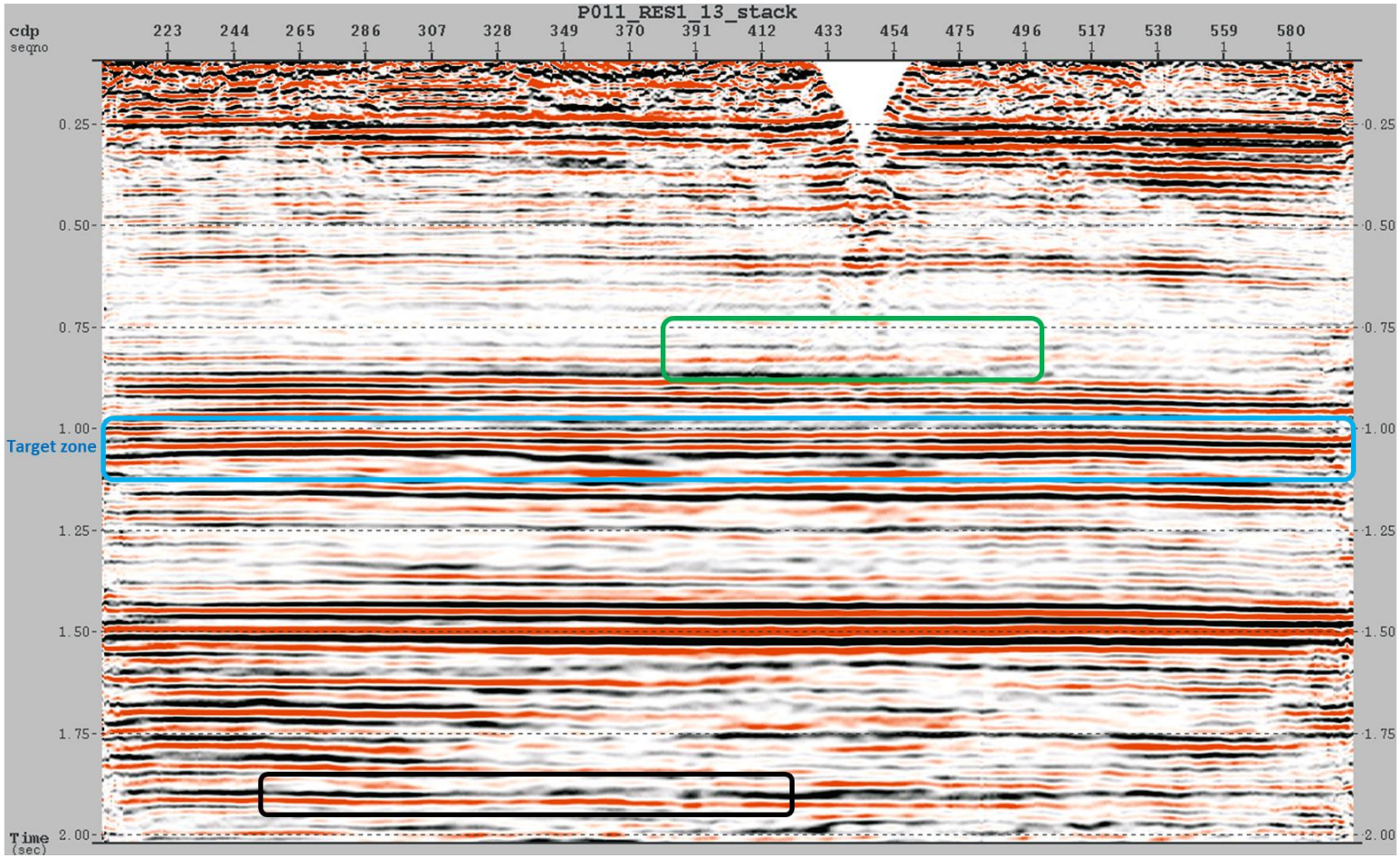

Figure 2.44. The stacked seismic section after applying the surface consistent residual statics obtained from the second approach. The outlined areas highlight the relative improvements of this approach over the first one.

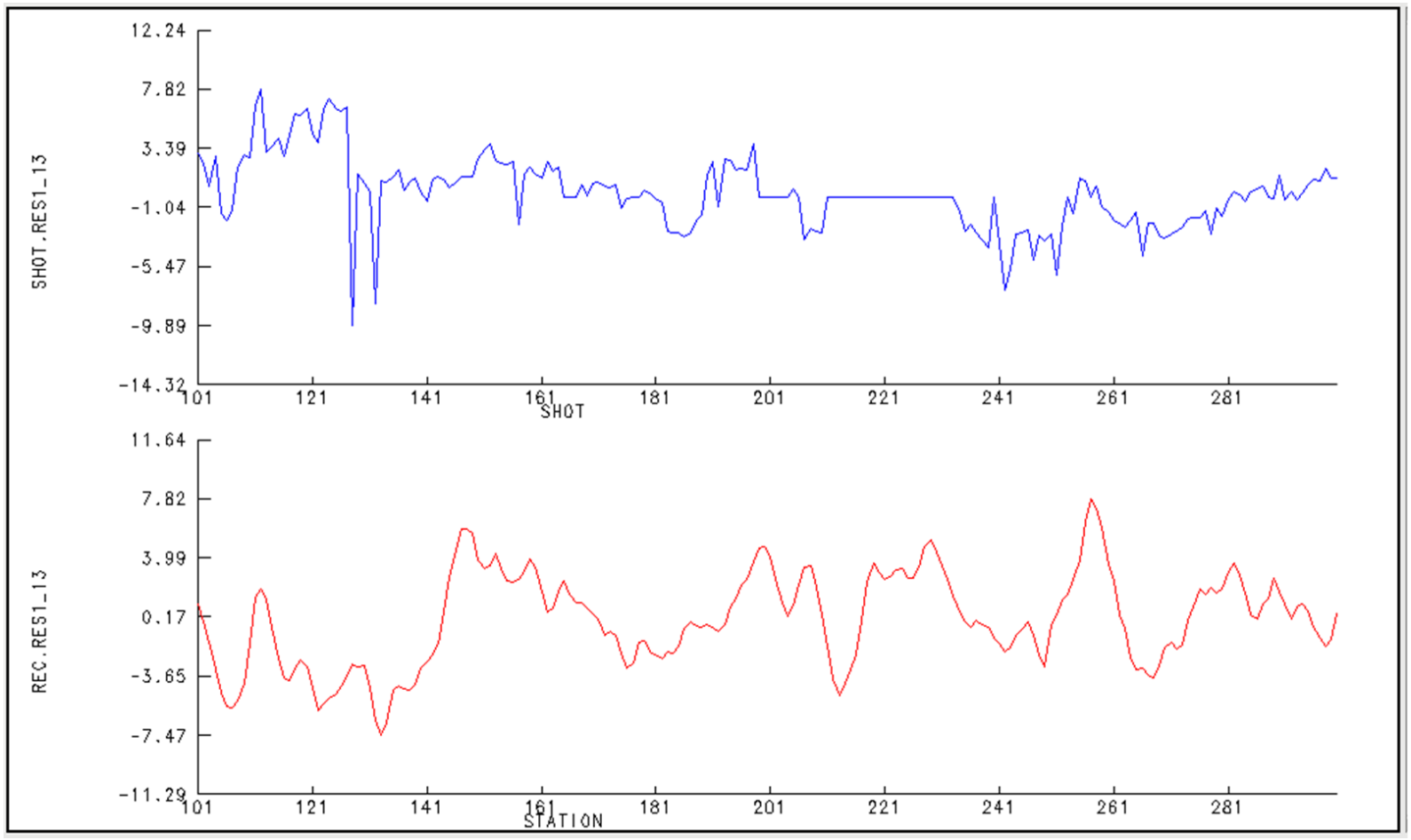

Figure 2.45. The first pass computed residual static correction for the source (top) and receiver (bottom) stations.

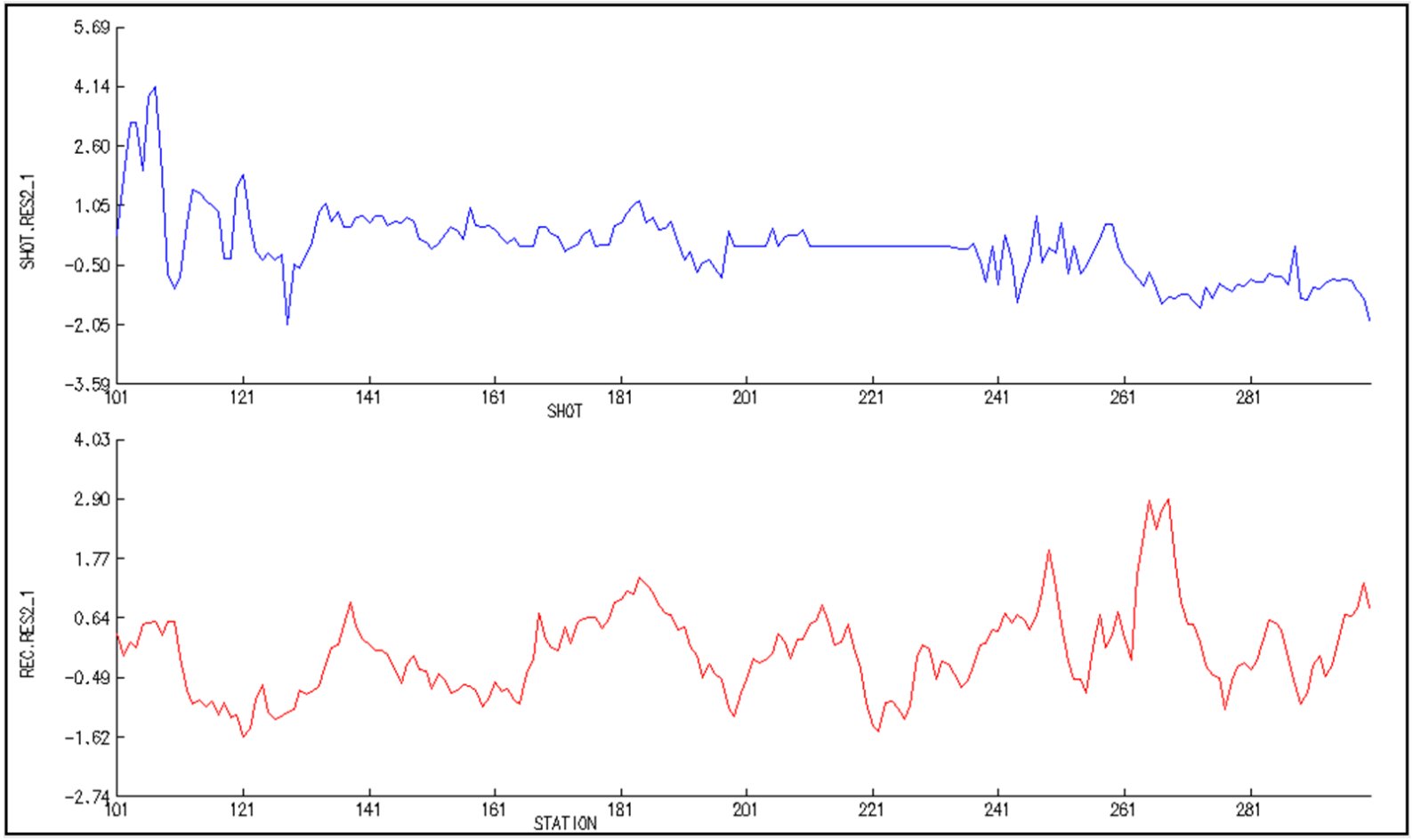

Figure 2.46. The second pass computed residual static correction for the source (top) and receiver (bottom) stations.

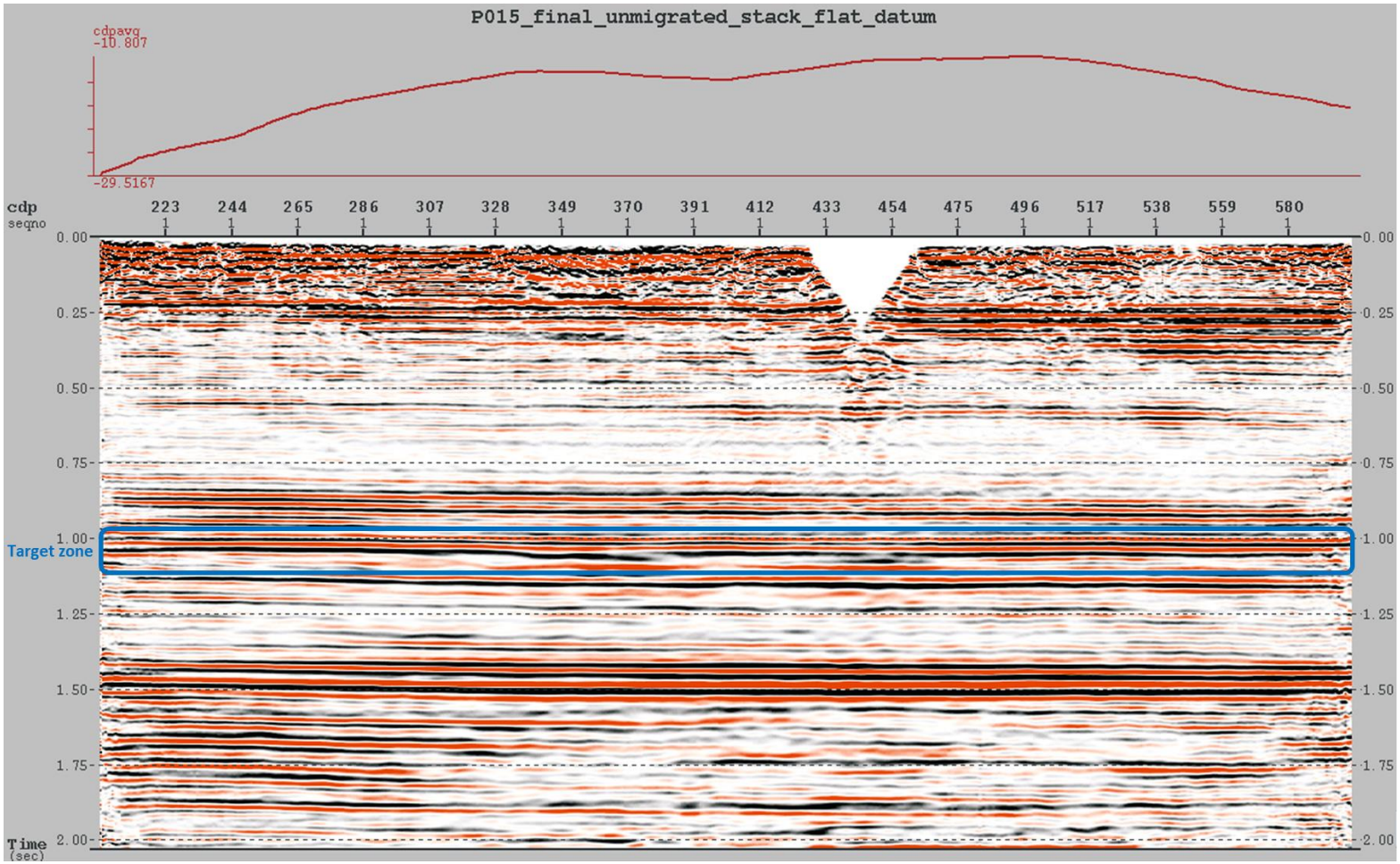

Figure 2.47. The unmigrated stacked seismic section referenced to the flat datum at the elevation 900 m above sea level.

In this study, prestack and poststack time migration methods were tested to obtain the migrated section that best image the subsurface. Two techniques were selected based on computational resources, geological complexity, and velocity field accuracy.

The space-time Kirchhoff migration (MIGTX) module was used to obtain prestack and poststack time migrated seismic sections. The imaging operator of this technique is based on the Kirchhoff migration algorithm described in Stolt and Benson (1986).

The poststack time migrated section was obtained after optimizing the maximum dip limit (Figure 2.48). The input data for this method are the stacked seismic traces and the velocity field. The changes in structure due to migration were small since most of the reflection events in the stacked section are considerably flat. At the target zone, a better seismic imaging of the channel fill deposits was obtained. The base of the channel is more interpretable and located near CMP 350.

On the other hand, prestack time migration algorithm has more requirements and restrictions on the data. The algorithm requires regularized offsets and CMP gathers to have the same number of traces. Therefore, the uniform geometry grouping (UNIFORM) module was used to regularize offsets and add dead traces to CMP gathers that have less than 200 traces. The added traces were removed after the migration process. The resulting CMP gathers were migrated and corrected for NMO simultaneously by the MIGTX module. Subsequently, the data were stacked to obtain the migrated seismic section (Figure 2.49). The obtained seismic section is similar to the poststack migrated section in terms of structure and the imaging of the incised valley at the target reservoir.

Nonetheless, prestack time migration provided higher signal-to-noise ratios and better reflection coherency (Figure 2.50).

The legacy prestack time migrated section provided by CREWES was imported in order to assess the quality of the processing in this study. The obtained stack from the Kirchhoff prestack time migration and the legacy stack were compared and analyzed (Figures 2.51 and 2.52). The legacy stack provides an overall better vertical resolution than the prestack time migrated section processed in this study. However, reflection continuity and signal-to-noise ratios are better in the seismic section obtained in this study. The spectral analyses of both seismic sections indicate that the legacy stack has a wider frequency bandwidth. The computed average amplitude spectrum of the legacy data extends to 120 Hz at a given threshold of -20 dB (Figure 2.53). Most of the higher frequency amplitudes represent random noise. On the other hand, the amplitude spectrum of the seismic section obtained in this study extends only to 78 Hz at the same given threshold (Figure 2.54). At the target zone, both sections provide good imaging of the subsurface strata. However, the seismic section obtained in this study provides a better image of the incised valley channel fill deposits (Figure 2.55). The resulting stacked section was exported in SEGY format to conduct seismic interpretation.

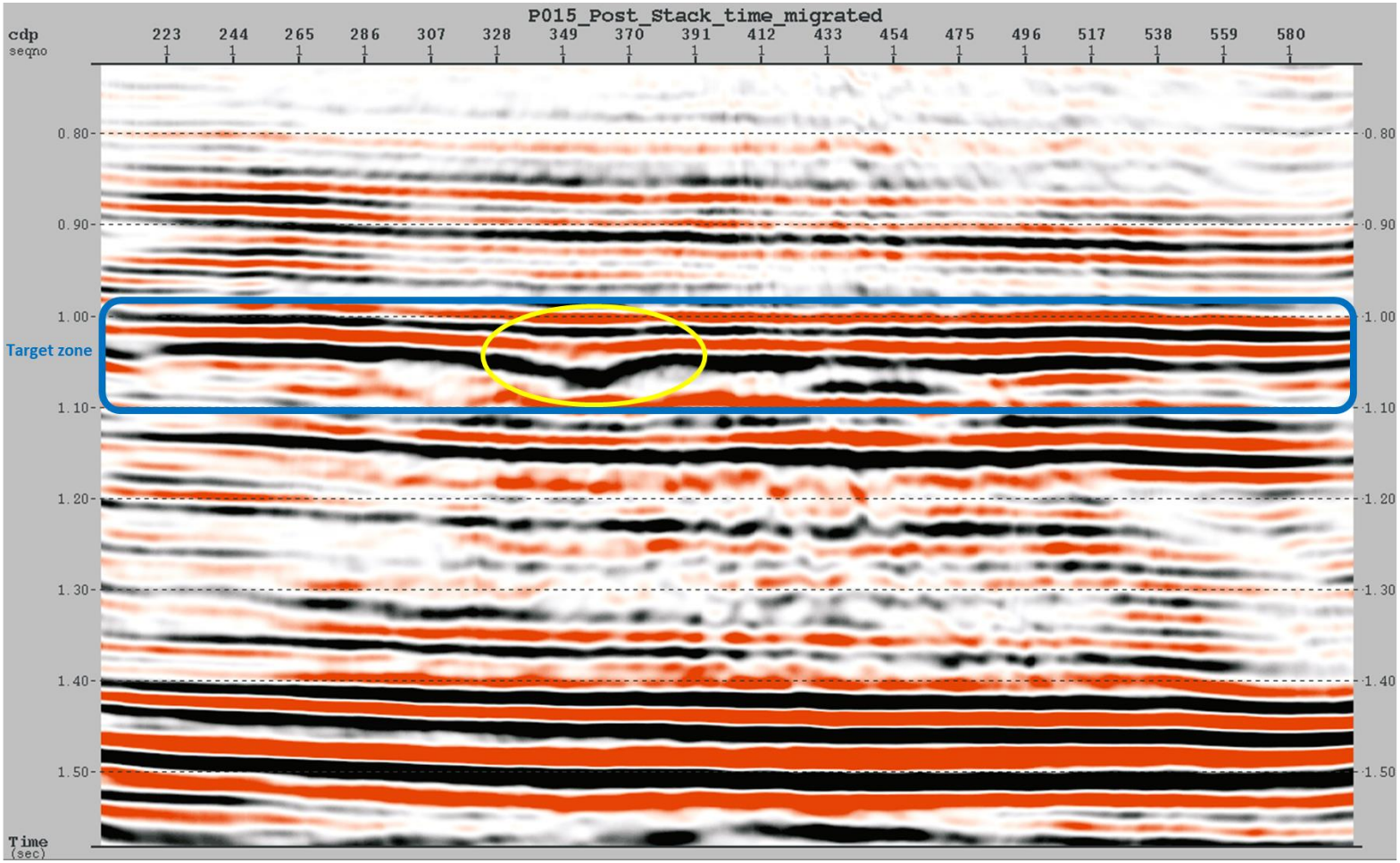

Figure 2.48. The stacked seismic section after the Kirchhoff poststack time migration.

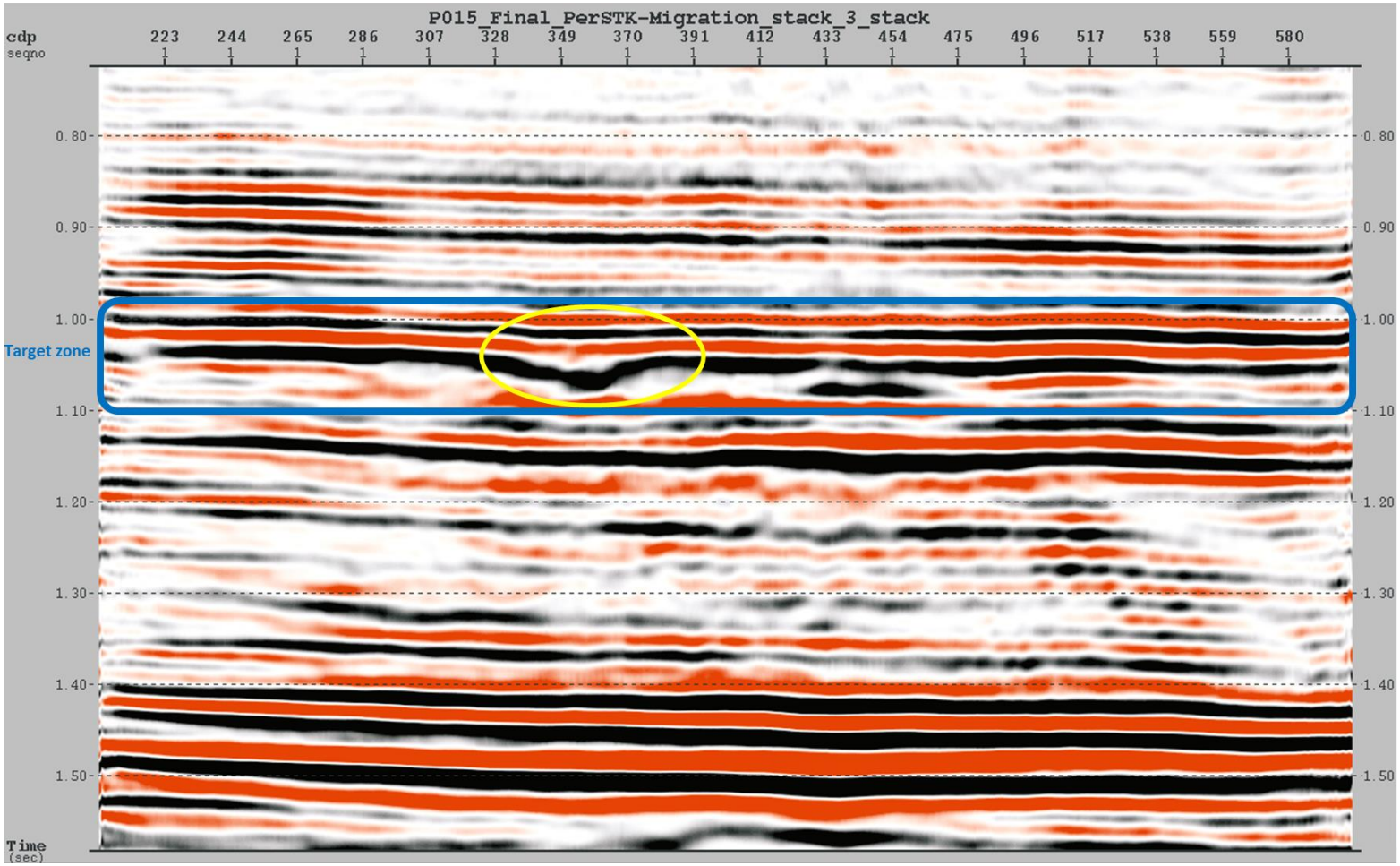

Figure 2.49. The stacked seismic section after the Kirchhoff prestack time migration.

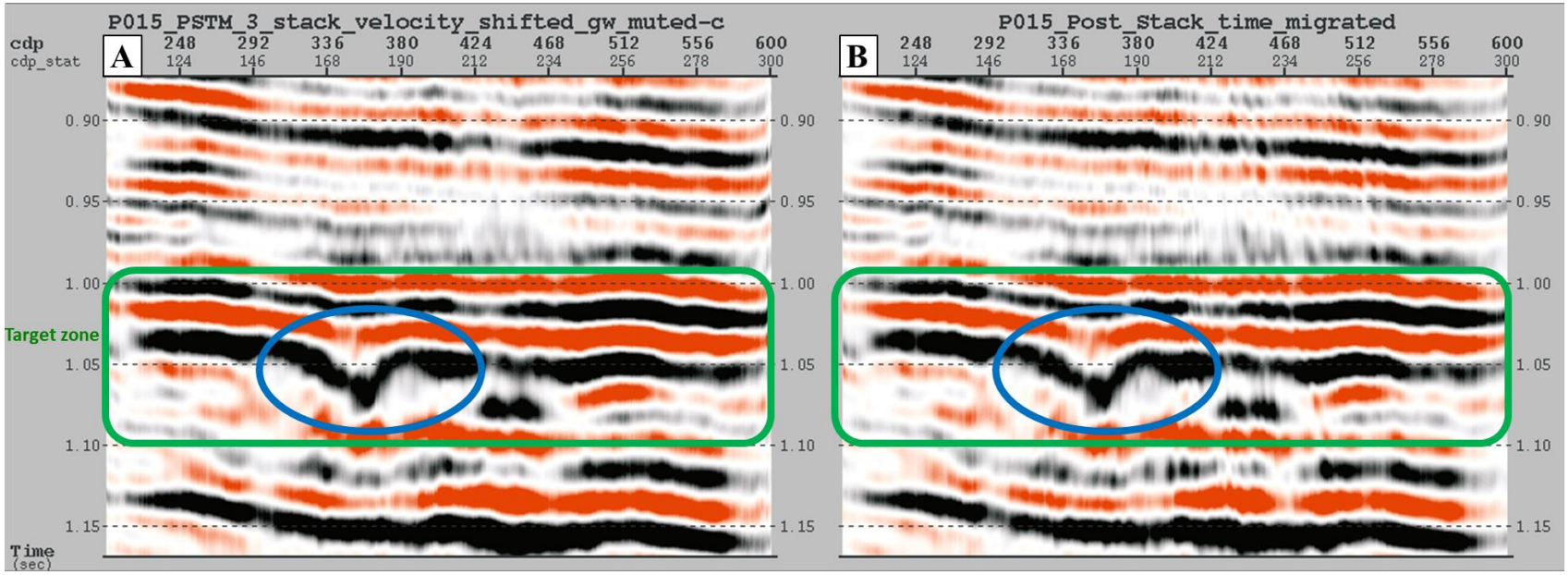

Figure 2.50. Enlarged target zone. A) After prestack time migration. B) After poststack time migration. The circle outlines the incised valley.

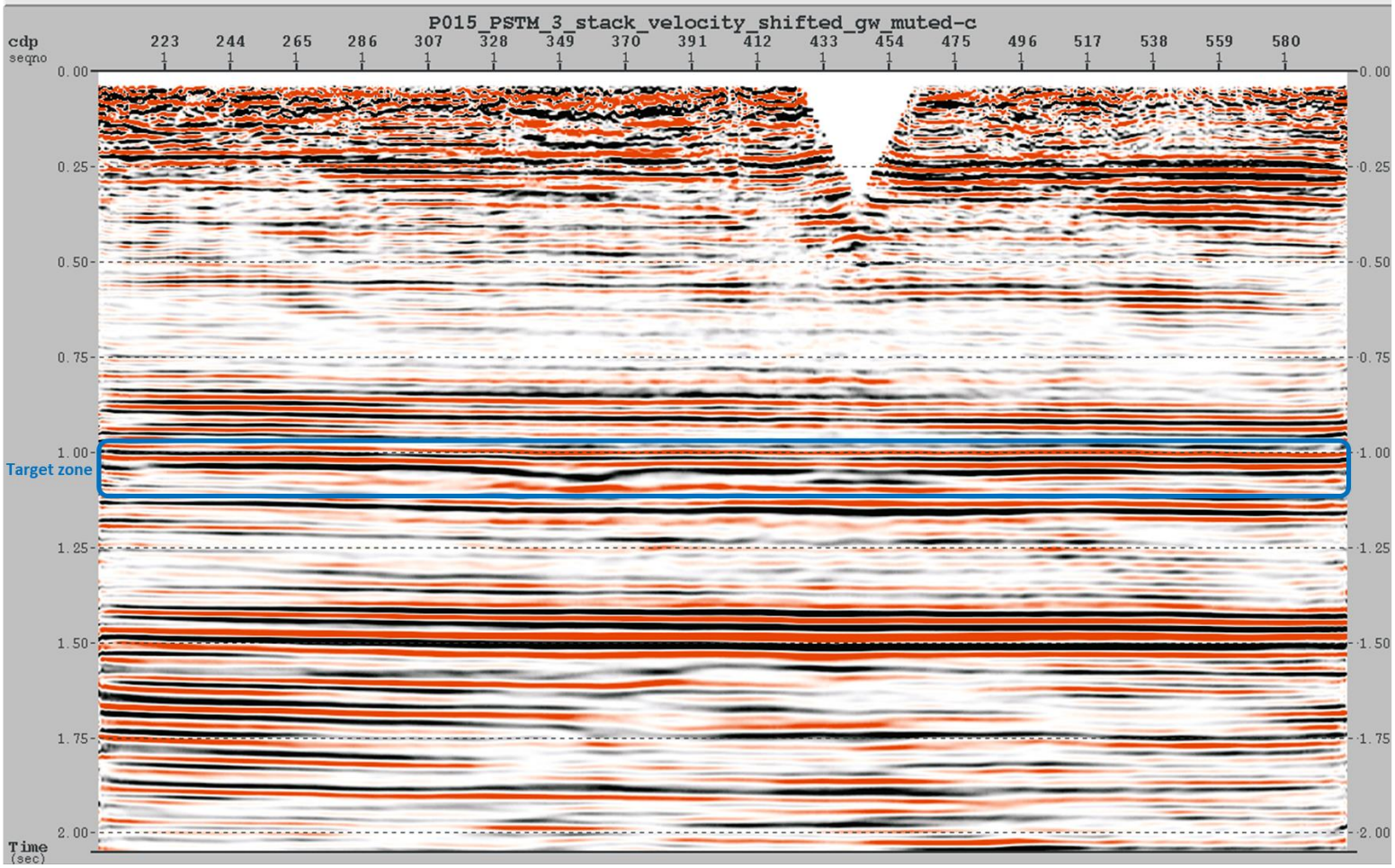

Figure 2.51. The stacked seismic section after the Kirchhoff prestack time migration.

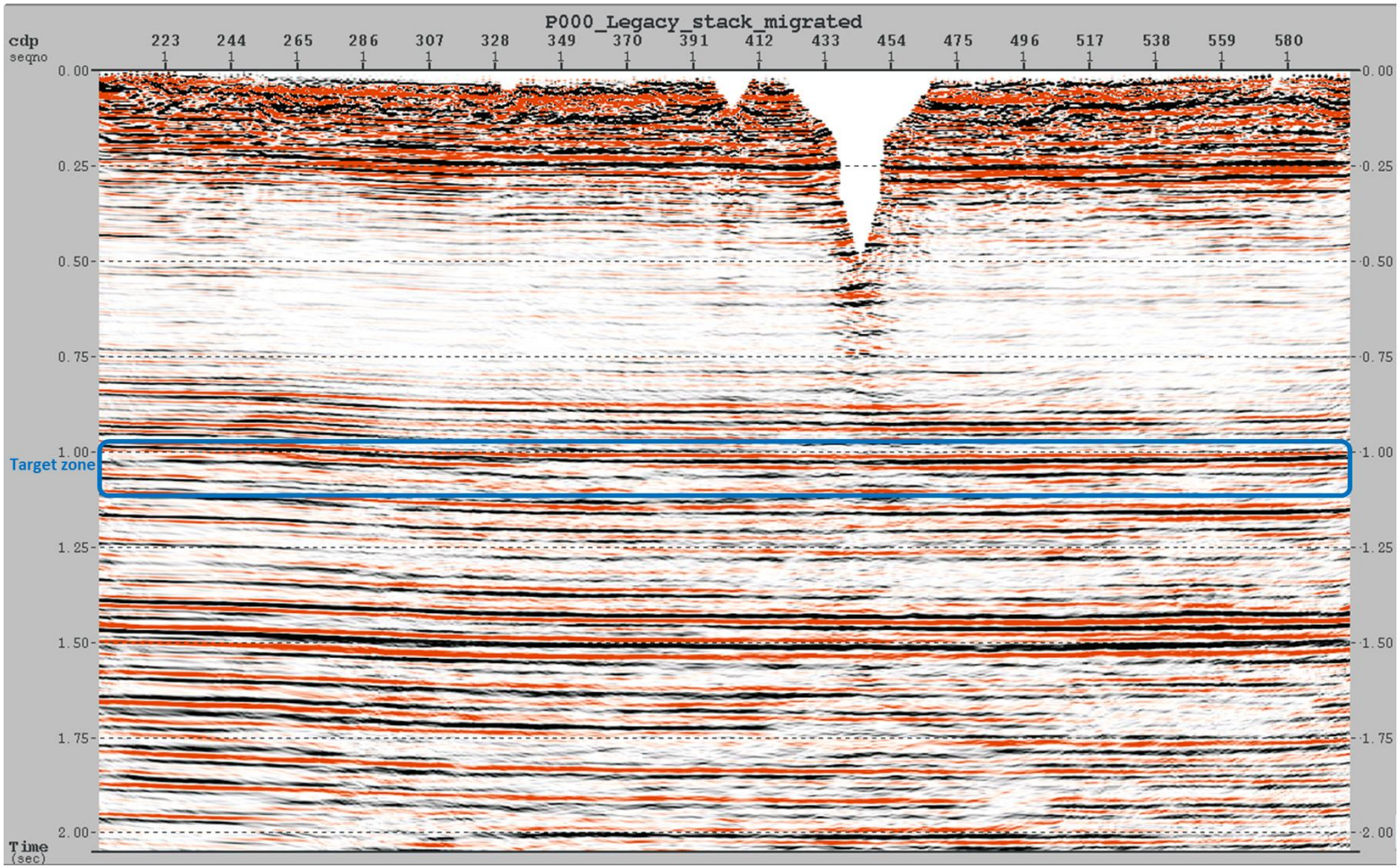

Figure 2.52. The stacked seismic section of the legacy data.

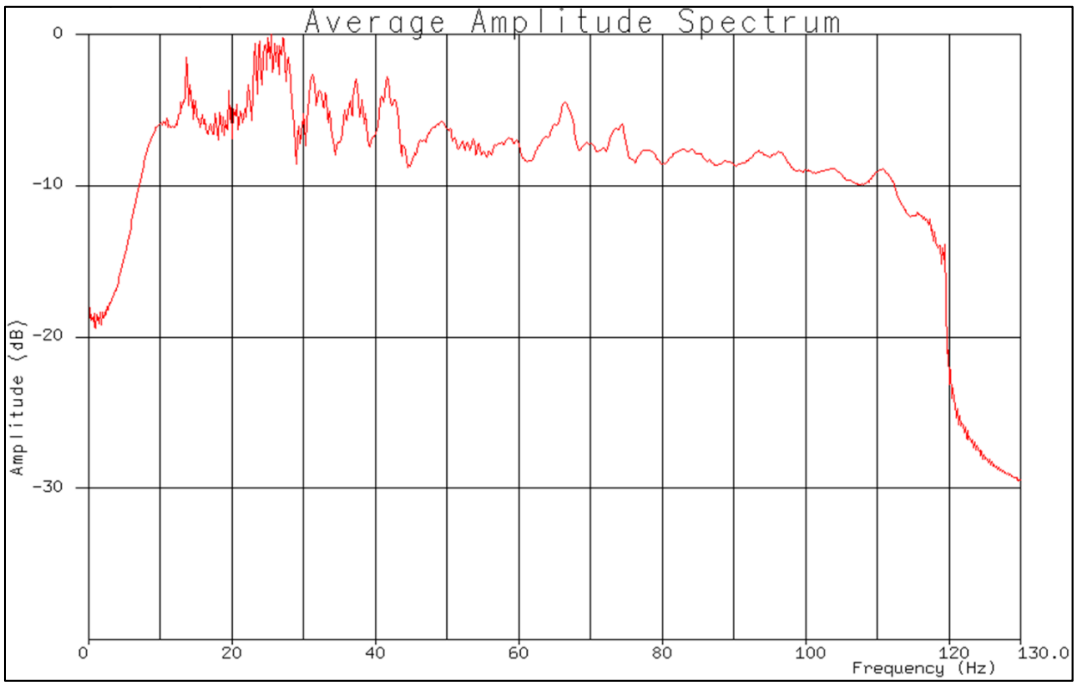

Figure 2.53. The average amplitude spectrum of the stacked section obtained from the legacy data.

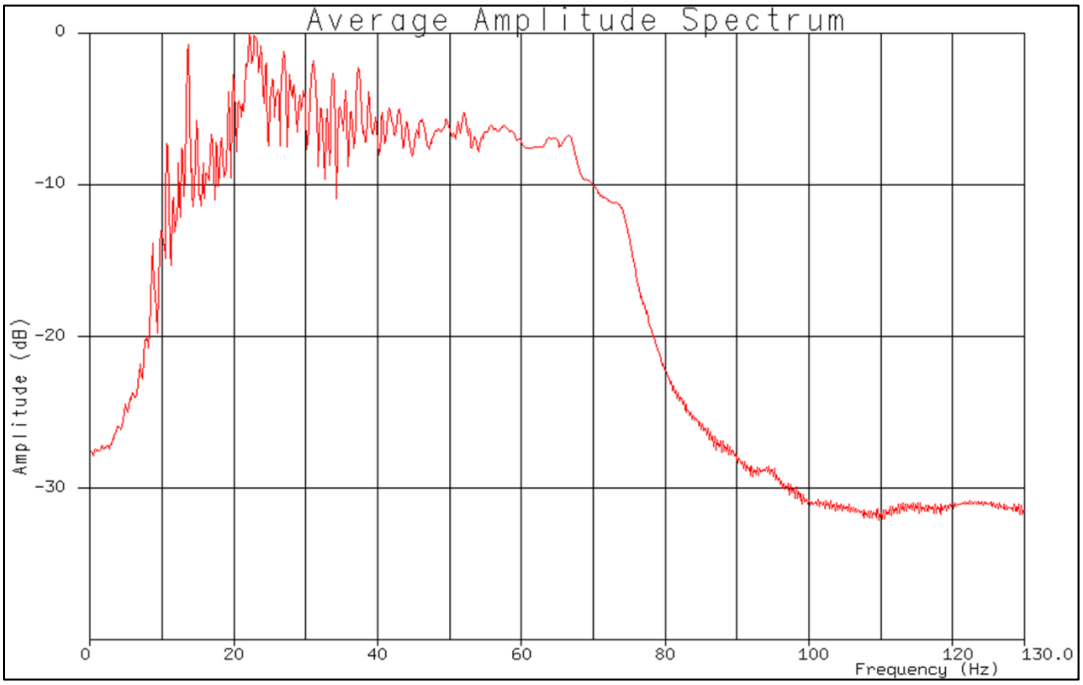

Figure 2.54. The average amplitude spectrum of the stacked section obtained from the Kirchhoff prestack time migration.

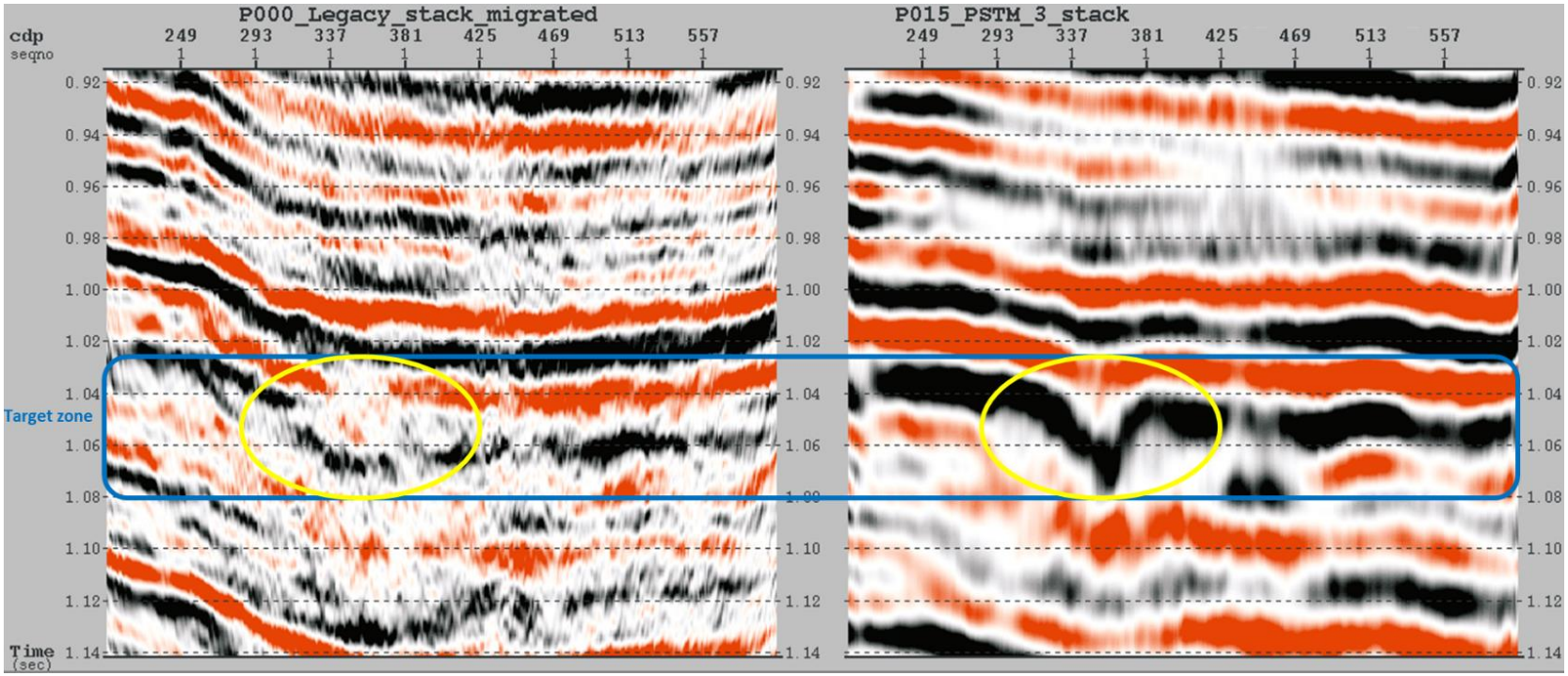

Figure 2.55. Enlarged target zone. A) Prestack time migrated section from the legacy data. B) Prestack time migrated section obtained in this study. The outlined area indicates the incised valley.

3. SEISMIC INTERPRETATION

This research is focused on seismic processing. A simple seismic interpretation was performed using the interpretation software of the IHS Markit Kingdom. The SEGY file of the final stacked seismic section was loaded into the interpretation software. Log data from Well 14-09, including gamma ray, density, porosity, sonic, and resistivity, were utilized to generate synthetic seismogram and establish seismic-to-well tie. Four key seismic horizons were selected based on their strong reflection amplitudes and coherency. The key horizons were identified and picked on the stacked seismic section.

Well 14-09, which intersects the seismic profile at CMP 312, provides valuable information of the subsurface. The surface elevation of the well is 927 m above sea level. All available logs start from 200 m measure depth (MD) to 1600 m which are equivalent to 727 m above sea level to 673 below sea level. The imported formation tops include Viking, Blairmore, Glauconitic, and Mississippian markers (Figure 3.1).

Sonic and density logs from Well 14-09 were used to computed the acoustic impedance and the reflection coefficients. The Walden-white deterministic wavelet extraction algorithm was used to obtain the extracted seismic wavelet from seismic traces within 50 ft of the well (Walden and White, 1984). The dominant frequency of the wavelet is around 25 Hz (Figure 3.2.). By convolving reflection coefficients with the extracted wavelet, the synthetic seismogram was obtained (Figure 3.3). All seismic traces within a radius of 100 meters were extracted. The computed coefficient from the correlation of the extracted traces and synthetic seismogram is 0.944, which indicates an excellent correlation. The obtained T/D chart is shown in Figure 3.4. The four key seismic horizons were identified and picked on the seismic section using the synthetic

seismogram (Figure 3.5). At the target zone, edges of the incised valley channel fill deposits were mapped clearly (Figure 3.6).

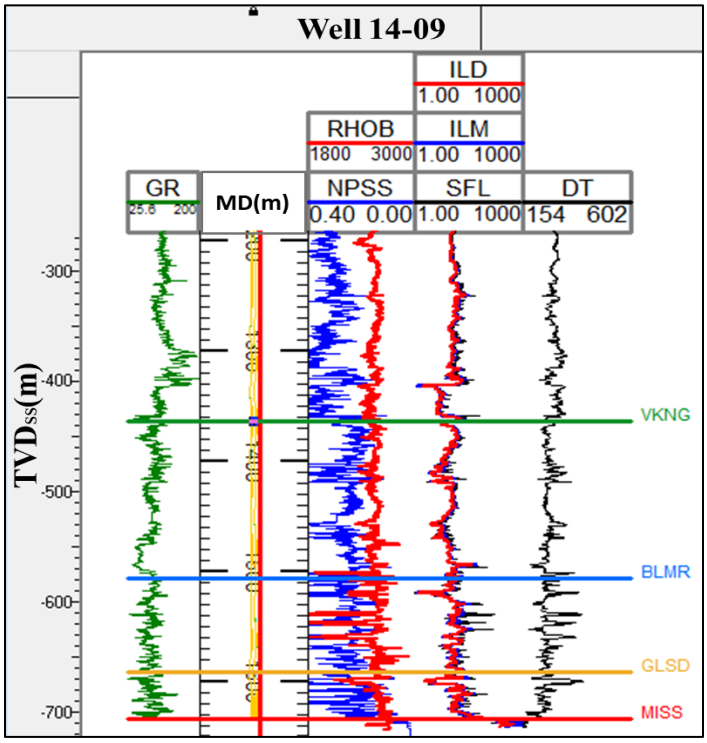

Figure 3.1. Log data and formation tops from Well 14-09.

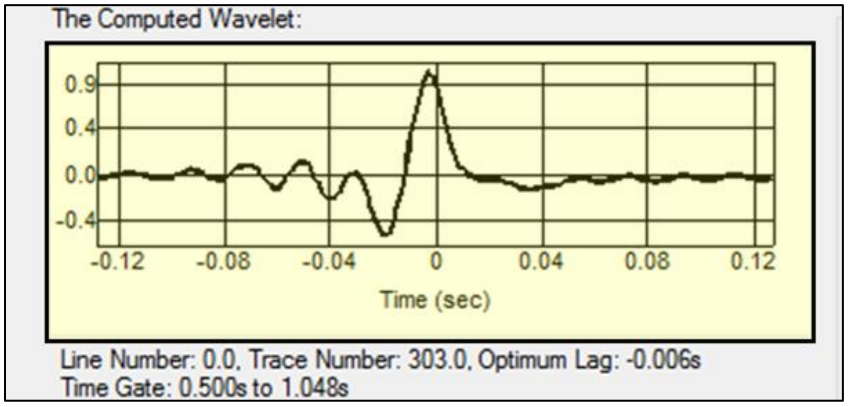

Figure 3.2. Extracted seismic wavelet from seismic traces within 50 ft of Well 14-09.

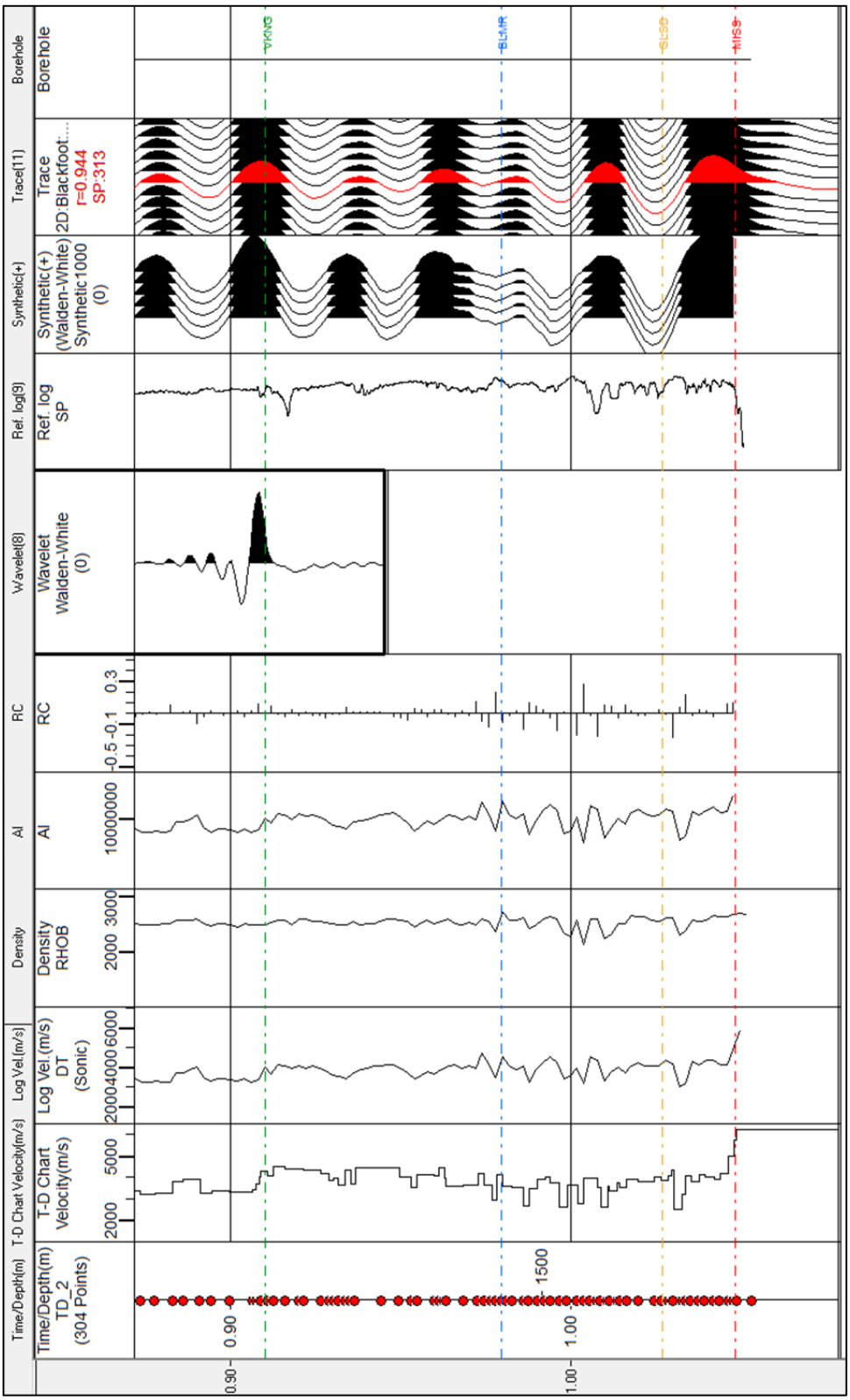

Figure 3.3. Synthetic seismogram of Well 14-09. A Good correlation is indicated between the synthetic seismogram and the extracted seismic traces.

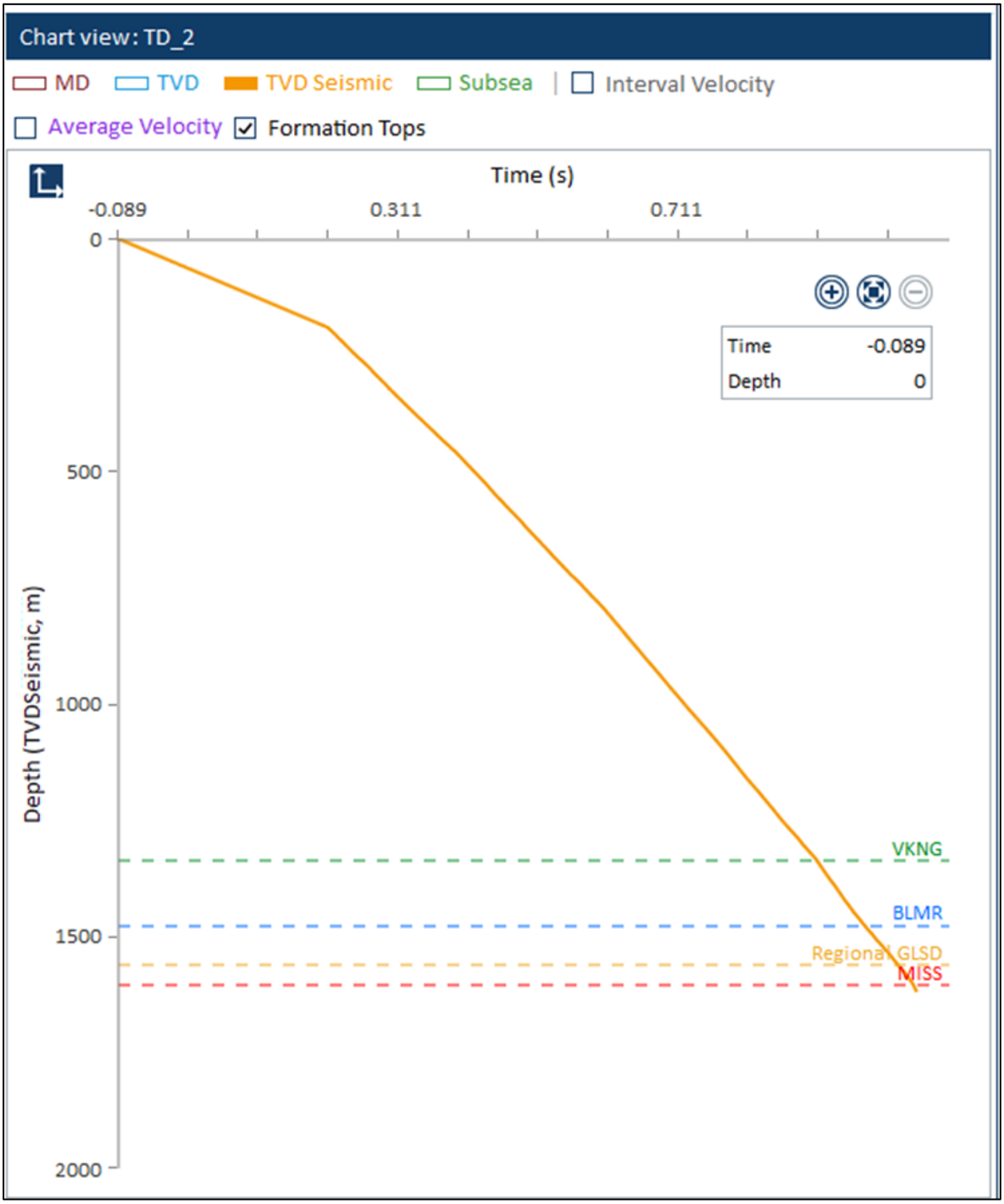

Figure 3.4. The obtained T/D chart from the seismic-to-well tie.

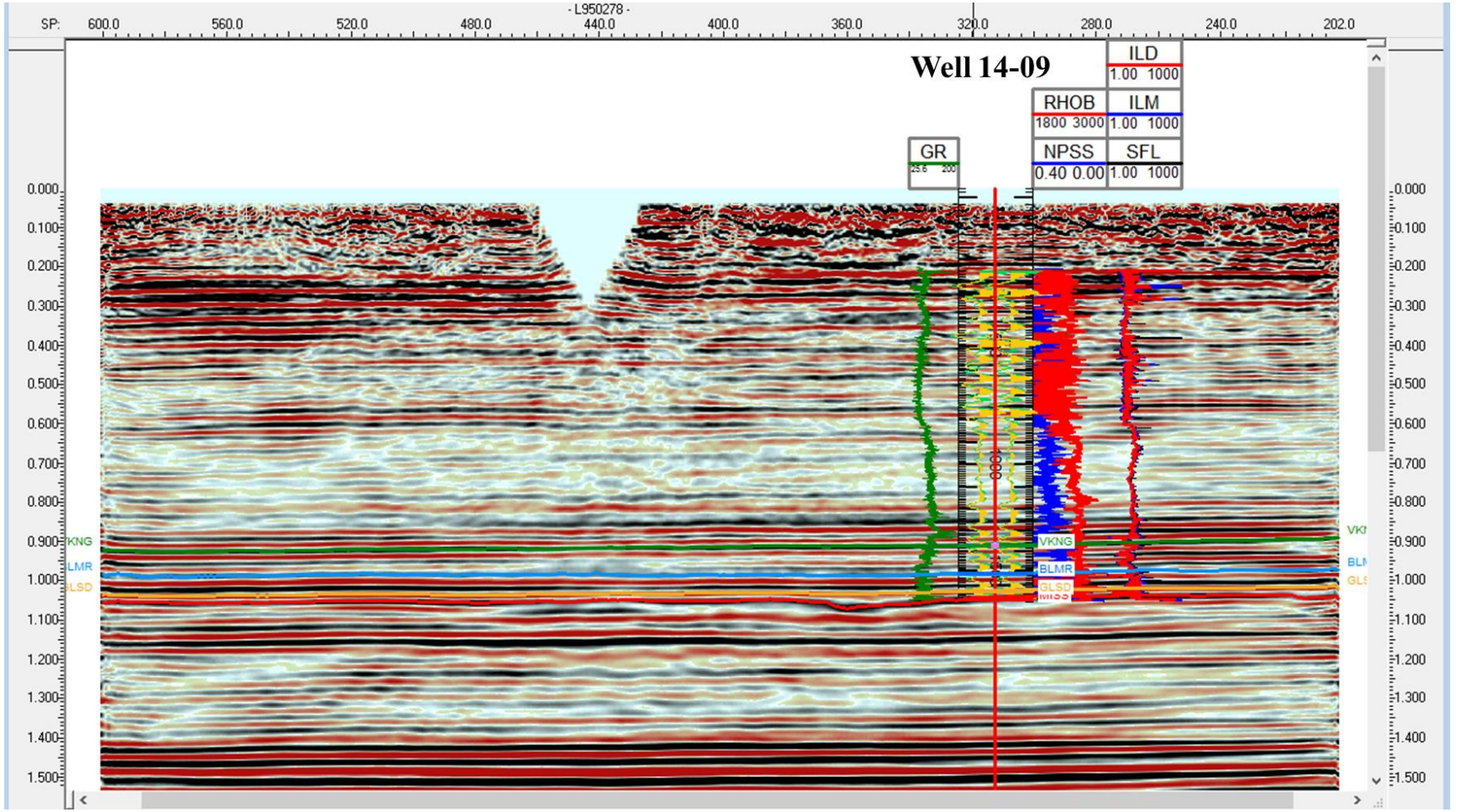

Figure 3.5. Well 14-09 superimposed on the stacked seismic section.

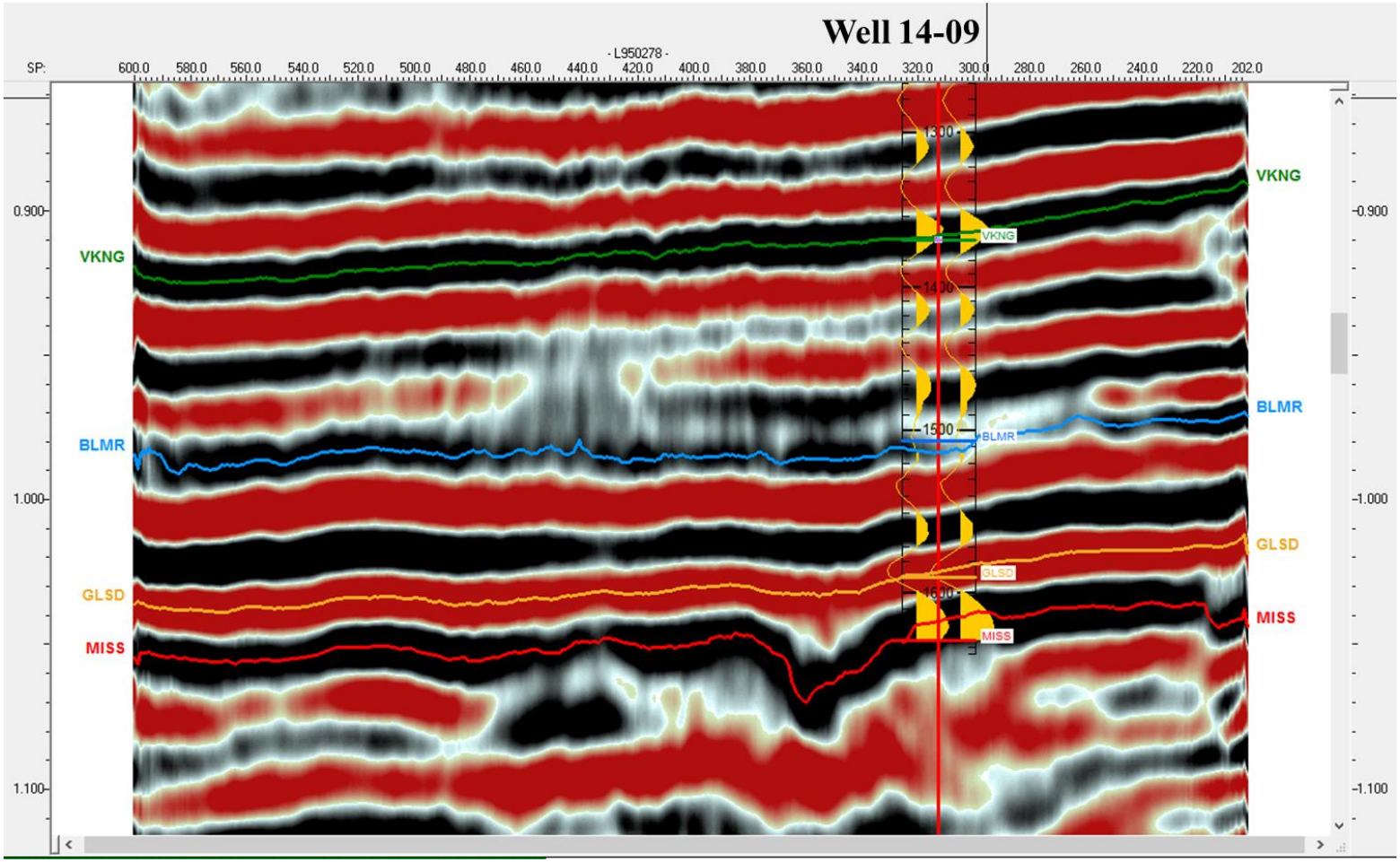

Figure 3.6. Interpreted seismic section at the target zone.

4. CONCLUSIONS

The single-component 10 Hz geophone data were reprocessed to increase vertical resolution and provide a better seismic image of the incised valley channel fill deposits of the Glauconitic Formation. The reprocessing of the data implements amplitude-preserved seismic processing followed by the Kirchhoff prestack time migration. The resulting common image gathers obtained from the Kirchhoff prestack time migration can be used in further AVO analysis and lithology discrimination of the target zone. The focus of the reprocessing is targeted at a time interval from 1000 ms to 1500 ms. Log data from Well 14-09 were used to conduct seismic interpretation to assess the quality of the final stacked seismic section. In addition, results from the legacy data were compared to the data in this study.

The offset-dependent spherical divergence correction was applied to the data in order to compensate for amplitudes decay in the time and offset domains. The effects of the source and receiver elevation variations were efficiently removed by applying the elevation statics.

Noise attenuation processing was performed by applying the LFAF module, bandpass filtering, and TFCLEAN module. Linear noise such as ground roll and air blast noise were filtered using the LFAF module. Bandpass filtering significantly removed residual noise below 10 Hz and the high-frequency random noise. The TFCLEAN module suppressed random noise that lies in the same frequency range as the signal. As a result, higher signal-to-noise ratios were obtained and the coherency of reflection events was improved.

Bandlimited spiking (trace-by-trace) and surface consistent deconvolutions were applied to the data to increase the vertical resolution of the data. The surface consistent deconvolution showed better results on the seismic section. The surface consistent deconvolution increased the dominant frequency of the stacked seismic section from 22 Hz to 28 Hz.

Surface consistent amplitude balancing algorithm was used to compensate for amplitude variations in the time domain due to the data acquisition. The application of the computed surface consistent amplitude scalars significantly reduced the amplitude vertical banding observed in the stacked seismic section.

Velocity analysis in this study was performed by integrating vertical velocity semblance and CVS techniques. The resulting stacking velocities were used to apply NMO correction to the CMP gathers. As a result, primary reflection events were flattened to maximize the CMP stacking power. On the other hand, multiples at later traveltime were attenuated in the stacking processes by velocity discrimination.

Two surface consistent residual statics algorithms (i.e., EPSTX and STATANL) were tested on the data to compute the short-wavelength statics. The STATANL approach provided better imaging of the target zone and was applied to the data in two passes. In order to achieve better results, velocity analysis and NMO correction were applied before each residual static correction.

The Kirchhoff prestack and poststack time migration methods were tested to obtain the migrated section that best image the subsurface. The results from both migration algorithms were similar in terms of structure and the imaging of the incised

valley at the target reservoir. However, prestack time migration provided higher signal-to-noise ratios and better reflections coherency.

The obtained stacked seismic section after the Kirchhoff prestack time migration processing and the legacy poststack seismic data provided by CREWES were compared in order to assess the quality of the processing of this study. While the legacy stack provides an overall better temporal resolution and wider frequency bandwidth, the prestack time migrated processed in this study has better reflection continuity and higher signal-to-noise ratios. At the target zone, the incised valley of the Glauconitic Formation is better imaged by the prestack time migrated section obtain in this study.

A simple seismic interpretation was conducted using the interpretation software of the IHS Markit Kingdom. In order to generate synthetic seismogram and establish seismic-to-well tie, log data from Well 14-09 were utilized. Four key seismic horizons, including the target reservoir, were identified and picked on the seismic section to assess the quality of the processed seismic data.

BIBLIOGRAPHY

Arya, V. K., and H. D. Holden, 1978, Deconvolution of Seismic Data - An Overview: IEEE Transactions on Geoscience Electronics, **16**, no. 2, 95-98.

Barry, K. M., D. A. Cavers, and C. W. Kneale, 1975, Recommended standards for digital tape formats: Geophysics, **40**, 344–352.

Cary, P. W., and G. A. Lorentz, 1993, Four-component surface-consistent deconvolution: Geophysics, **58**, 383-392.

Cary, P. W., and N. Nagarajappa, 2013, Questioning the Basics of Surface-Consistent Scaling: SEG, Expanded Abstracts, 418-422.

Connolly, C. A., L. M. Walter, H. Baadsgaard, and F. J. Longstaffe, 1990, Origin and evolution of formation waters, Alberta Basin, Western Canada sedimentary Basin. I. Chemistry: Applied Geochemistry, **5**, no. 4, 375–395.

Dufour, J., J. Squires, W. N. Goodway, A. Edmunds, and I. Shook, 2002, Integrated geological and geophysical interpretation case study, and Lamé rock parameter extractions using AVO analysis on the Blackfoot 3C-3D seismic data, southern Alberta, Canada: Geophysics, **67**, 27-37.

Gallant, E. V., R. R. Stewart, M. B. Bertram, and D. C. Lawton, 1995, Acquisition of the Blackfoot broad-band seismic survey: CREWES Research Report, **7**, no. 36, 1-9.

Goupillaud, P., A. Grossmann, and J. Morlet, 1983, Cycle-octave representation for instantaneous frequency spectra: SEG, Expanded Abstracts, 613-615.

Hatherly, P., M. Urosevic, A. Lambourne, and B. J. Evans, 1994, A simple approach to calculating refraction statics corrections: Geophysics, **59**, 156–160.

Henley, D. C., 2012, Interferometric application to static corrections: Geophysics, **77**, no. 1, Q1–Q13.

Hopkins, J., and R. Meyer, 2001, Lithology of Paleovalley-Fills from Petrophysical Data: Mannville Group, Lower Cretaceous, Southern Alberta, Canada: Petrophysics, **42**, no. 5, 444-456.

Lu, H., and R. Maier, 2009, Revisiting the Blackfoot 3C-2D broad-band seismic data: CREWES Research Report, **21**, no. 52, 1-9.

Machel, H. G., M. L. Borrero, E. Dembicki, H. Huebscher, L. Ping, and Y. Zhao, 2012, The Grosmont: the world's largest unconventional oil reservoir hosted in carbonate rocks: Geological Society, **370**, no. 1, 49-81.

Maier, R., K. W. H. Hall, and H. Lu, 2009, The CREWES data library: CREWES Project Research Report, **21**, no. 56, 1-3.

Mawdsley, M. J., A. L. Earner, and B. A. Zaitlin, 1996, Exploration for incised valley channel sandstones of the Lower Cretaceous (Alberta, Canada) using 3D seismic: risks and opportunities: SEG, Expanded Abstracts, 295-298.

Miller, S. L., E. Aydemir, and G. F. Margrave, 1995, Preliminary interpretation of P- P and P-S seismic data from the Blackfoot broad-band survey: CREWES Project Research Report, **7**, no. 42, 1-18.

Moser, A. R., and D. B. Jovanovich, 1984, 3-D residual statics: SEG, Expanded Abstracts, 425-429.

Neidell, N. S., and M. T. Taner, 1971, Semblance and other coherency measures for multichannel data: Geophysics, **36**, 482-497.

Newman, P., 1973, Divergence effects in a layered earth: Geophysics, **38**, 481-488.

Oppenheim, A.V., and R.W. Schafer, 1989, Discrete-Time Signal Processing: Prentice Hall.

Robinson, E.A., and S. Treitel, 1980, Geophysical Signal Analysis: Prentice Hall.

Ronen, J., and J. F. Claerbout, 1985, Surface-consistent residual statics estimation by stack-power maximization: Geophysics, **50**, 2759-2767.

Stewart, R. R., 1995, The Blackfoot broad-band 3-C seismic survey: Introduction: CREWES Research Report, **7**, no. 35, 1-2

Stolt, R.H., and A.K. Benson, 1986, Seismic migration: Geophysical Press Ltd.

Taner, M. T., and F. Koehler, 1981, Surface consistent corrections: Geophysics, **46**, 17-22.

Taner, M. T., F. Koehler, and K. A. Alhilali, 1974, Estimation and correction of near-surface time anomalies: Geophysics, **39**, 441-463.

Taner, M. T., F. Koehler, and R. E. Sheriff, 1979, Complex seismic trace analysis: Geophysics, **44**, 1041-1063.

Ursin, B., 1990, Offset-dependent geometrical spreading in a layered medium: Geophysics, **55**, 492-496.

Walden, A. T., and R. E. White, 1984, On errors of fit and accuracy in matching synthetic seismograms and seismic traces: Geophysical Prospecting, **32**, no. 5, 871–891.

Wang, D. Y., and D. W. McCowan, 1989, Spherical divergence correction for seismic reflection data using slant stacks: Geophysics, **54**. 563-569.

Wright, G. N., M. E. McMechan, D. E. Potter, G. Mossop, and I. Shetsen, 1994, Structure and architecture of the Western Canada sedimentary Basin: Geological Atlas of the Western Canada sedimentary Basin, **4**, 25-40.

Yilmaz, O., 2001, Seismic data analysis: Processing, inversion, and interpretation of seismic data: Society of Exploration Geophysicists.

Zailtlin, B., R. W. Dalrymple, R. Boyd, D. Leckie, and J. MacEachern, 1995, The stratigraphic organization of incised valley systems: Implications to hydrocarbon exploration and production: Canadian Society of Petroleum Geologists.

VITA

Bader Mohammed A Algarni was born in Dhahran, Saudi Arabia. He graduated from The University of Leeds with a bachelor degree in geophysical sciences in 2012. He joined the Saudi Aramco in 2012. He was awarded a scholarship from the Saudi Arabian Oil company to pursue a master's degree in the field of seismic data processing in 2016. In August 2017, he began the master's program in the department of Geosciences and Geological and Petroleum Engineering at Missouri University of Science and Technology. He received the MS degree in Geology and Geophysics from Missouri University of Science and Technology in May 2019.